The Behaviour of Silica Nanoparticles in Multi-Phase Ionic Solutions: Enhanced Oil Recovery Implications

By

©Saeed Jafari Daghlian Sofla

A thesis submitted to the school of Graduate Studies in partial fulfilment of the requirements for the degree of

Doctor of Philosophy

Faculty of Engineering and Applied Science
Memorial University of Newfoundland

May, 2019

St. John's, Newfoundland
Canada

Abstract

Conventional oil production methods produce approximately one-third of the initial oil in place from a reservoir, on average. The remaining oil is a large attractive target for Enhanced Oil Recovery (EOR) techniques. Recently, the potential of using nanoparticles in EOR methods has been explored with some promising results from preliminary evaluations. However, the application of nanoparticles in real oil reservoirs is limited by knowledge gaps. The stability of nanoparticles in the injection or formation water containing diverse types and concentrations of ions is a challenge. It is still unknown whether and under which conditions nanoparticles can self-assemble at the oil-water interface and alter the oil-water interfacial properties. The wettability alteration capacity of nanoparticles usually investigated by contact angle measurements is affected by subtle experimental artefacts; hence, the result of conventional contact angle measurements may not be reliable to evaluate the effect of nanoparticles on the wettability of substrates. Moreover, the mechanism of wettability alteration by nanoparticles is not clear yet.

The stability of nanoparticles in the aqueous phase is the primary challenge to using nanoparticles in reservoir conditions. Nanoparticles are extremely unstable in high salinity seawater or formation water. Typically, seawater or formation brine is used for water-flooding and EOR purposes. Therefore, if we want to modify the fluid-fluid or fluid-rock properties by injecting nanoparticle enhanced water, then the stability of the nanoparticles in high salinity seawater or formation brine is extremely important. A novel method to stabilize silica nanoparticles in seawater is proposed. First, the stability of silica nanoparticles in the presence of different ions is investigated. The results show that the presence of multivalent counter-ions in the electrical double layer of nanoparticles can destabilize silica nanoparticles. To reduce

the concentration of positive multivalent ions around silica nanoparticles, a method called "H+ protected" is proposed and its effectiveness is tested by particle size, turbidity, zeta-potential, and pH measurements. Experimental results show that the H+ protected method obtained by adding hydrochloric acid (HCl) to the solution, can effectively stabilize silica nanoparticles in seawater.

By investigating the controlling parameters of nanoparticle attachment at the interface (bulk suspension properties including the concentration of nanoparticles, concentration of HCl, salinity, size and charge of nanoparticles and operating conditions i.e., temperature and pressure) and coupling them with nanoparticles' stability in the solution, the conditions under which silica nanoparticles can reduce oil-water interfacial tension are experimentally investigated. The maximum IFT reduction occurs when there is a packed monolayer of nanoparticles at the oil-water interface. For instance, increasing nanoparticles' concentration and salinity to their optimum value would lead to achieving smaller IFT values. Further increasing the concentration of nanoparticles and salinity beyond the optimum value can destabilize the nanoparticles and increase their average size in the solution, which can reduce the number of nanoparticles at the interface and thus increase the IFT value. In general, the minimum IFT occurs when the surface energy reduction due to the adsorption of nanoparticles is minimum, i.e., the chance of nanoparticles desorbing from the interface due to thermal fluctuations (especially in the elevated temperatures) is high and aggregation of nanoparticles in the bulk solution is initiated. We believe that IFT reduction is partially but not fully responsible for incremental oil recovery greater than water-flooding alone. We test our hypothesis by conducting silica nanoparticles in seawater flooding experimentally and

comparing the results with simulations that examine the effect of a) IFT reduction only and b) the effect of altering the relative permeability, wettability, and IFT reduction.

The mechanism of wettability alteration by silica nanoparticles is investigated. The impact of experimental methods in conventional contact angle measurements on the wettability alteration data is evaluated. In conventional contact angle measurements, the rock samples are either aged with (immersed in) nanoparticles-fluid before conducting the experiments or contacted with the nanoparticles-fluid before the oil droplet is attached to the rock substrate. In both cases, nanoparticles exist in the oil-rock interface before initiating the contact angle measurements (pre-existing nanoparticles). A real reservoir scenario would be to inject the nanoparticle-fluids into an already established equilibrium condition of oil-water-rock. Hence, the contact angle measurements are modified using a new displacement contact angle method to represent the injection of nanoparticle-fluids into a reservoir. The impact of pre-existing nanoparticles on the contact angle measurements is examined for simple (n-decane, NaCl brine, pure substrates) and complex (crude oil, seawater, and reservoir rock) systems at various wetting conditions of the substrates (water-wet and oil-wet). The effect of the surface and nanoparticle charge on the contact angle is evaluated by adjusting the aqueous phase salinity. We also differentiate between the disjoining pressure mechanism and diffusion of silica nanoparticles through the oil phase by testing the attachment of nanoparticles on the rock surface. The results illustrate that a substantial portion of the wettability alteration ability of nanoparticles reported in the literature may be attributed to the method of measuring the contact angles where nanoparticles can adsorb at the rock sample before contact angle measurements. Silica nanoparticles are shown to further reduce the contact angle (make the substrate more water-wet) only when we have water-wet condition initially. Under oil-wet conditions,

nanoparticles cause no notable change on the contact angle. The synergic effect of structural disjoining pressure and capillary pressure reduction might be a possible mechanism of wettability alteration in the water-wet conditions. In oil-wet conditions, the only possible mechanism is capillary pressure reduction. This chapter is presented as a paper in the International Symposium of the Society of Core Analysts.

Acknowledgments

Table of Contents

List of Tables

List of Figures

xiv

1.CHAPTER ONE

Introduction and Overview

1.1. Motivation

British Petroleum's (BP) 2035 Energy Outlook [1] estimated that global energy demand will increase 30% by 2035. The U.S. Energy Information Administration [2] predicted that worldwide petroleum and liquid fuel consumption will increase from 90 million barrels per day in 2012 to 121 million barrels per day by 2040. This demand must be met by discovering new oil fields or maximizing oil recovery from already discovered and producing oil fields. The chance of finding new large petroleum fields is negligible. Hence, maximizing oil extraction from existing reservoirs through Enhanced Oil Recovery (EOR) methods appears to be an accessible way to meet this demand.

The natural energy of a hydrocarbon reservoir is sufficient to produce only a small fraction of the initial hydrocarbons in place. Remaining oil is trapped because of the interplay between the viscous, gravity, and capillary forces in the porous media. In general, EOR refers to implementation of a recovery method that increases the recovery of oil beyond what the primary and secondary methods (natural production and pressure maintenance with gas or water, respectively) would normally be expected to yield. On average, conventional production methods produce approximately one third of the initial oil in place from a reservoir. The remaining oil is a large attractive target for EOR techniques [3].

Recently, there has been a growing interest in the application of nanoparticles in EOR processes [4-8]. Nanoparticles are defined as particles with a size, at least in one dimension, between 1 to 100 nm [9]. Due to their ultra-small size and high surface-area to volume ratio, they can penetrate pores and alter the rock-fluid and fluid-fluid properties favorably. Nanoparticle enhanced water flooding, or simply nanoparticle-EOR, may result in extra oil recovery from oil reservoirs by altering reservoirs' fluid-fluid and rock-fluid properties.

Numerous studies have evaluated the effectiveness of nanoparticle-EOR on oil recovery with some promising outcomes based on preliminary results [5-7, 10, 11]. The majority of researchers believe that the EOR potential of nanoparticles is through two important factors; oil-water interfacial tension (IFT) reduction [12-15], and wettability alteration of reservoir rock surfaces [16-19]. Despite all these efforts, there is still a long way to apply nanoparticles in real oil reservoirs as an EOR technique. Beside the feasibility of storage and transport of nanoparticles-fluids (especially for offshore reservoirs), the knowledge gap is the main limitation to the application of nanoparticles in the oil fields. The goals of this research were to characterize and assess the behaviour of nanoparticles in realistic reservoir water (aqueous one phase solution), two phases (oil and water), and three phases (oil, water, and rock) to address some of the most fundamental challenges of the nanoparticle-EOR methods.

1.2. Problem statement

Three main technical obstacles to using nanoparticles as a water flooding additive in the realistic reservoirs are:

1. **Stability of nanoparticles:** The stability of nanoparticles in high salinity, multivalent ionic solutions is the first and foremost challenge in the application of nanoparticles in practical EOR techniques. For nanoparticles to alter fluid-fluid or rock-fluid properties, they must be dispersed in seawater or formation water as the two major water resources for water flooding and EOR processes. Unlike nanoparticles in deionized water or low salinity brine solutions, nanoparticles are extremely unstable in seawater or in high salinity formation water.

2. **Effect of nanoparticles on fluid-fluid interactions**: It is still unclear whether and under which conditions nanoparticles can reduce oil-water interfacial tension (IFT).

3

The controlling parameters of nanoparticles' attachment at the oil-water interface, the influence of bulk suspension properties (the concentration of nanoparticles, concentration of stabilizer, salinity, and surface charge and size of nanoparticles in the suspension) and operating conditions (temperature and pressure) on the self-assembly of nanoparticles are still unknown or debated.

3. **Effect of nanoparticles on rock-fluid interactions:** The ability of nanoparticles to alter the wettability of reservoir rock is still being studied. Unfortunately, most studies that have evaluated the effectiveness of nanoparticles in wettability alteration by the contact angle method, have overestimated the effect of nanoparticles, due to the method of contact angle measuring, because nanoparticles can adsorb on the rock sample before contact angle measurements. The mechanism of wettability alteration by nanoparticles is still unknown; it is still unclear how nanoparticles can reach the rock surface to alter the wettability of substrate or detach the oil droplet from a surface. In practical EOR, we are dealing with three multicomponent, interconnected, complex systems for which minor changes in one phase can lead to severe alterations in the interfacial properties between phases. Nanoparticles must be dispersed in the aqueous phase, which contains various types and concentrations of ions. The interactions between the ions and nanoparticles dictate the characteristics of nanoparticles (particle size, zeta-potential, etc.) in the aqueous solution. Similarly, the oil phase may contain many surface active components like asphaltene and naphthenic acids, which can interact with nanoparticles at the oil-water and oil-rock interfaces. In reality, the rock sample is a heterogeneous, non-smooth, mixed-wet substrate composed of various minerals. The electrical charge of minerals can vary when contacted with an ionic fluid. This causes

4

alteration of the electrostatic repulsion between substrate and nanoparticles and consequently can either attract or repel the nanoparticles. Hence, the role of nanoparticles must be evaluated considering multicomponent complex fluids and real formation rock.

In this thesis, we addressed these three obstacles to facilitate the application of nanoparticles in real reservoirs.

1.3. Thesis structure

This thesis consists of six chapters as follows:

Chapter One presents the motivation of the study, states the problem and provides the structure of the thesis.

Chapter Two provides a literature review on nanoparticle-EOR technique and the fundamental surface chemistry concepts which are required to evaluate the interactions between nanoparticles, the aqueous phase, oil phase, and rock surface. We mainly focused on the studies that have investigated untreated silica nanoparticles without additional additives. Chapter two will form the basis of a review article that we will soon submit.

Chapter Three has been published in the Journal of Fuel, and describes the effective parameters in the aggregation of silica nanoparticles, proposing a novel method to stabilize silica nanoparticles in seawater (H+ protected method).

Chapter Four has been published in the Journal of Molecular Liquids and describes the behaviour of silica nanoparticles at the oil-water interface, explaining whether and under which conditions silica nanoparticles can alter fluid-fluid interactions.

Chapter Five has been published by the Society of Core Analysis (SCA), and includes a comparison of the wettability alteration capacity of silica nanoparticles in simple and complex systems, evaluation of the impact of pre-existing nanoparticles at the oil-rock interface, assessment of the mechanism of wettability alteration by nanoparticles and the effect of nanoparticles and rock surface charge on the wettability alteration capacity of nanoparticles.

Chapter six contains a summary, conclusions, and recommendations for future work.

2. CHAPTER TWO

Literature Review

2.1. Nanoparticle-EOR

EOR is used to recover post water flood or gas flood mobile and immobile residual oil from a reservoir by altering the fluid-fluid or fluid-rock properties to overcome the capillary, viscous, and gravity forces. The goal of any EOR process is to achieve a high ultimate recovery factor by reducing the mobility ratio and/or increasing the capillary number. Mobility ratio (M) is defined as the mobility of the displacing fluid over the mobility of the displaced fluid (equation 1). The mobility of a phase (λ_i) is the effective permeability of that phase (κ_i) divided by its viscosity (μ_i) and mathematically defined as equation 2:

$$M = \frac{\lambda_{displacing\ fluid}}{\lambda_{displaced\ fluid}} \tag{2-1}$$

$$\lambda_i = \frac{\kappa_i}{\mu_i} \tag{2-2}$$

The mobility ratio can be reduced by decreasing oil viscosity, increasing water viscosity, increasing the effective permeability to oil, or decreasing the effective permeability of the displacing fluid. Capillary number is defined as the ratio of the viscous forces to the capillary forces. It was reported that a three orders of magnitude increase in capillary number will result in recovery of 50% of the oil from a water-flooded reservoir and thar an increase of four orders of magnitude is required to displace 100% oil from a core [20]. EOR methods are generally divided into four broad groups [21, 22]:

- Thermal (steam/hot water injection, combustion, etc.)

- Miscible/Immiscible gas injection (CO_2, hydrocarbon gas, nitrogen, air, etc.)

- Chemical (alkali, surfactant, polymer, nanoparticles, smart water, etc.)

- Other (microbial, electrical, leaching etc.)

Nanoparticle enhanced water flooding, or simply nanoparticle-fluid EOR, is a relatively new chemical-EOR technique, which may result in extra oil recovery from oil reservoirs by altering reservoirs' fluid-fluid and rock-fluid properties. Diverse types of nanoparticles are tested to explore their potential in EOR. Some of these nanoparticles and the major outcomes of the experiments are listed in Table 2-1. As shown in the table, the positive effect of diverse types of nanoparticles on oil recovery is observed through core-flooding, micromodel experiments, IFT, and contact angle measurements. Different concentrations of NaCl solution are typically used as the aqueous phase. Silica nanoparticles (silica dioxide- SiO_2) are the most common nanoparticles tested by researchers and their positive effect on oil recovery at the laboratory scale is shown. In this research, we focused on the behaviour of silica nanoparticles in aqueous solutions (one phase), between two phases (oil and water), and in three phases (oil, water, and rock surface).

Table 2-1: Effect of nanoparticles on enhanced oil recovery

Type of nanoparticles	Major experiments	Major results	Aqueous phase	Rock Type	Reference
Silica dioxide (SiO_2)	Micromodel (WAG)	10% to 20% increase in oil recovery	3.6 wt% NaCl Brine solution		[23]
Silica dioxide (SiO_2)	Core-flooding	Up to 14% increase in oil recovery	3.0 wt% NaCl Brine	Berea Sandstone	[14]
Aluminum oxide (Al_2O_3) Titanium oxide (TiO_2) Silica dioxide (SiO_2)	IFT and Oil viscosity measurements	33% IFT reduction, 34% oil viscosity reduction for aluminum oxide 37% IFT reduction, 24% oil viscosity reduction for titanium oxide 42% IFT reduction, 8% oil viscosity reduction for silica dioxide	0.3 wt% NaCl Brine	Limestone	[24]
Silica dioxide (SiO_2)	Core-flooding	17% increase in oil recovery	DI-water	Sandstone	[8]
Polysilicon nanoparticles	Core-flooding	Up to 30% increase in oil recovery	3.0 wt% Brine	Sandstone	[25]
Silica dioxide (SiO_2)	Core-flooding	Nanoparticles increase oil recovery up to 14 % in high permeability rock, but no guarantee to	3.0 wt% Brine	Berea sandstone	[26]

Type of nanoparticles	Major experiments	Major results	Aqueous phase	Rock Type	Reference
		increase oil recovery in low permeability rocks.			
Zirconium dioxide (ZrO_2) Calcium carbonate ($CaCO_3$) Titanium dioxide (TiO_2), Silicon dioxide (SiO_2) Magnesium oxide (MgO) Aluminum oxide (Al_2O_3) Cerium oxide (CeO_2) Carbon nanotube (CNT)	Primary screening by contact angle measurements, core-flooding and spontaneous imbibition experiments for the selected nanoparticles	Based on contact angle measurements, silicon dioxide and calcium carbonate nanoparticles are selected. 8- 9 wt% increase in oil recovery observed for both silicon dioxide and calcium carbonate nanoparticles	NaCl Brine of 8-12 wt%	Carbonate	[27]
Silica dioxide (SiO_2)	IFT and contact angle measurements	20° contact angle reduction is observed in the case of 0.05 wt% nanoparticles	Seawater		[28]

The objective of nanoparticle-EOR is to mobilize and recover the immobile oil from oil reservoirs. Several mechanisms are suggested for nanoparticle-EOR including: oil-water interfacial tension reduction [29-31], wettability alteration [16-18, 32] , increasing the viscosity of the injection fluid [33], pore channel plugging [34], in-situ emulsification [35], and preventing asphaltene precipitation [36, 37]. Despite these conjectures, it is still unclear why nanoparticles mobilize oil ganglia. The experimental results reported in the literature regarding the effect of nanoparticles on fluid-fluid and rock-fluid interactions are controversial and in some cases, contradictory. The lack of knowledge about the interactions at the fluid-fluid and rock-fluid interfaces and the impact of nanoparticles in such interactions have caused imprecise analysis of laboratory results. In order to understand the reasons behind the controversial results in the nanoparticle-EOR methods, it is required to be familiar with the intermolecular forces at play in nanoparticle-EOR methods.

2.2. Basic concepts

The major intermolecular forces in nanoparticle-EOR suspensions are: van der Waals forces, electrostatic forces, steric interaction, bridging, hydrophobic interactions, and hydration-solvation interactions [38]. The balance between these forces governs the stability of the nanoparticles in bulk solution, and the adsorption of the nanoparticles at the fluid and rock interfaces.

2.2.1. van der Waals Interaction

Van der Waals forces are typically attractive forces, which arise from dipole–dipole, dipole-induced dipole, and London (instantaneous induced dipole-induced dipole) interactions [39]. The effective distance of van der Waals forces is normally limited to less than 10 nm [40]. Van der Waals interactions between two equally sized spherical particles can be calculated using the following equation [41]:

$$\frac{E_{vdw}}{k_B T} = -\frac{A_{132}}{6 k_B T} \left[\frac{2R^2}{d^2 - 4R^2} + \frac{2R^2}{d^2} + \ln(\frac{d^2 - 4R^2}{d^2}) \right] \tag{2-3}$$

where R is the particles' radius, d is the center to center distance between two nanoparticles and A_{132} is the Hamaker constant. The Hamaker constant can be obtained using the Hamaker constant of particle (surface) number 1 (A_{11}), bulk solution (A_{33}), and particle (surface) number 2 (A_{22}) using equation 2-2 [42]:

$$A_{132} = (\sqrt{A_{11}} - \sqrt{A_{33}})(\sqrt{A_{22}} - \sqrt{A_{33}}) \tag{2-4}$$

The van der Waals attraction forces (E_{vdw}) for a spherical particle (with radius R) and a surface (similar to the adsorption of nanoparticles at the oil-water interface or rock surface) can also be obtained using the following equation [43]:

$$E_{wdv} = -\frac{A_{132}}{6}[\frac{R}{d} + \frac{R}{d+2R} + ln\left(\frac{d}{d+2R}\right)] \qquad (2\text{-}5)$$

2.2.2. Electrostatic forces

Electrostatic repulsion forces are influenced by the surface charge of nanoparticles (or a surface) and the ionic strength of the surrounding medium [44]. Electrostatic force is typically active within the electrical double layer extension of a charged particle (or a surface) [45]. The idea of an Electrical Double Layer (EDL) was introduced by Helmholtz [46] and improved by Gouy-Chapman and Stern [47, 48]. When a charged particle (or surface) contacts an ionic fluid, at the first layer from the surface, a dense layer of opposite charge ions (counter-ions) is adsorbed onto its surface due to chemical interactions. This layer is called the "Stern layer". In the second ring (or layer) from the surface, the number of counter-ions still exceeds that of similar-ions. Ions interact with the surface via Coulombs forces and can move freely under the influence of electric forces or thermal motions. In this layer, the concentration of counter-ions decreases with increasing distance from the Stern layer to the outer limit where electro-neutrality is reached [47]. This layer is known as the "diffuse layer" [49]. Figure 2-1 depicts the distribution of ions surrounded a negatively charged particles (or charged surface). The electrical double layer is defined as the distance from the particle's charged surface to the outer boundary of the 'diffuse' layer, incorporating both Stern and diffuse layers. The thickness of this layer (known as the "Debye length") will change depending on the ionic strength of the solvent. Increasing ionic strength of the solution compresses the EDL and shortens the Debye length. The Debye Length (κ in nanometers) is a function of the valence (Z_i) and number density of ith ion in the solution ($\rho\infty_i$), the system's temperature (T in Kelvin), and relative permittivity of the solution (ε_r) and can be calculated using following equation [50]:

$$\kappa = \sqrt{\frac{\varepsilon_r \varepsilon_\circ K_B T}{e^2 \sum \rho \infty_i Z_i^2}} \tag{2-6}$$

where e is the elementary charge of an electron (C), $\varepsilon_\circ$ is absolute permittivity (F/C) and K_B is the Boltzmann's constant. The electrostatic repulsion between two equally sized spherical particles with diameter of a, can be calculated as [51]:

$$V_{EL} = \frac{32\pi K_B T \varepsilon_r \varepsilon_\circ \rho_\infty r \gamma^2}{k^2} e^{-\kappa^{-1}d} \qquad\qquad \kappa^{-1}a > 5 \tag{2-7}$$

$$V_{EL} \approx 2\pi \varepsilon_r \varepsilon_\circ r \psi_0{}^2 \kappa^{-1} e^{-\kappa^{-1}d} \qquad\qquad \kappa^{-1}a > \tag{2-8}$$

Equation 2-8 is known as the linear Poisson-Boltzmann approximation [50]. The γ is called the reduced surface potential and is a function of surface charge of particles (ψ_0) and the system's temperature [51]:

$$\gamma = \tanh(\frac{ze\psi_0}{4K_B T}) \tag{2-9}$$

(a)   (b)

13
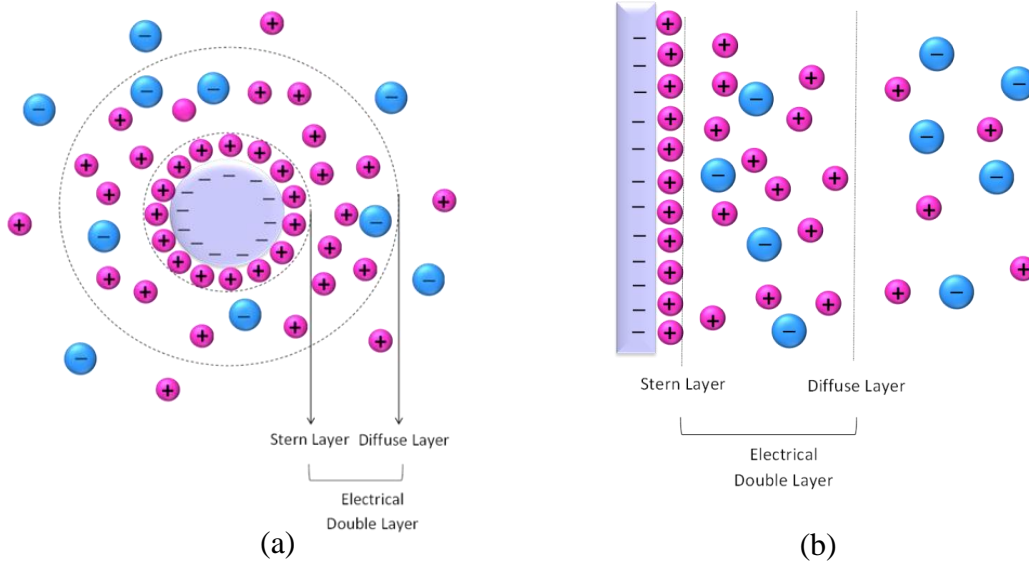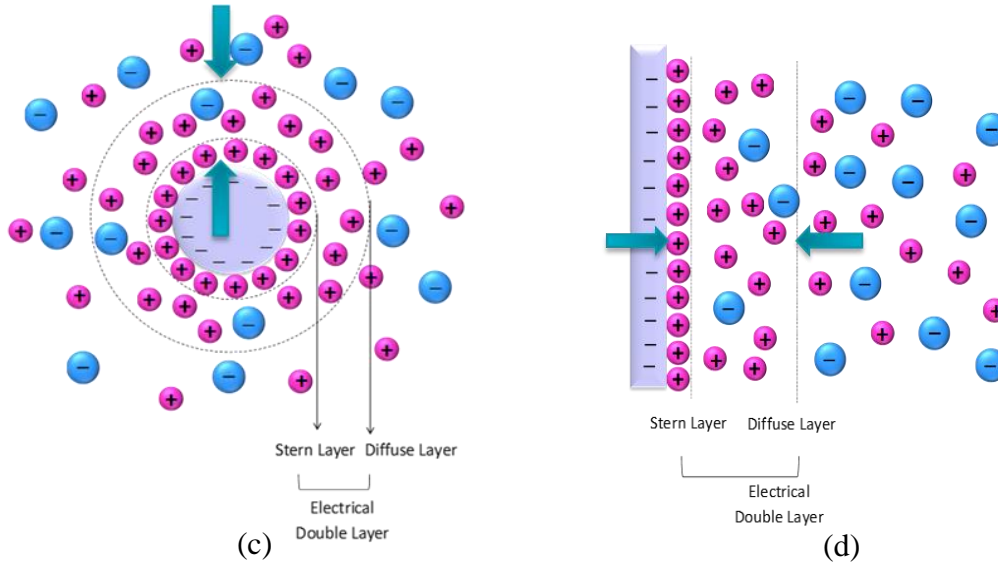
Figure 2-1: **The schematic diagram of ion distribution around a charged particle (a), a charged surface (b), and the effect of increasing salt concentration on the electrical double layer of a charged particle (c), and a charged surface (d) (after [52]).**

For the case of a spherical particle (P) with a radius of R and surface potential of ψ_p and a plate surface (S) with the surface potential of ψ_s (comparable to the adsorption of nanoparticles at the oil-water interface), the electrostatic repulsion forces (E_{EL}) can be calculated using following equation [53]:

$$E_{EL} = \pi \varepsilon_r \varepsilon_0 R \left\{ 2\psi_p \psi_s \ln\left(\frac{1 + exp(-KD)}{1 - exp(-KD)} \right) + \left(\psi_p^2 + \psi_s^2 \right) \ln[1 - exp(-2KD)] \right\} \quad (2\text{-}10)$$

where K $(= \kappa^{-1})$ is the inverse Debye length, D is the distance between the nanoparticle and the surface.

2.2.3. DLVO theory

The DLVO theory presented by Derijaguin, Landau, Overbeek, and Verwey [54, 55] was primarily used to predict the stability of a colloidal suspension in a bulk solution by comparing the net attraction (van der Waals) and repulsion (electrostatic) forces on the particles. It is currently the cornerstone of our understanding about the interactions between particles in the

solution, adsorption of components to the interface, and particle deposition to planar substrates [56]. The DLVO profile can be obtained by calculating the net potential [54, 55]:

$$Net\ \ potential = E_{EL} - E_{vdw} \tag{2-11}$$

In the DLVO theory, as depicted in Figure 2-2, the net potential is plotted versus the distance between two particles. Colloid particles must overcome the energy barrier to aggregate in the bulk solution (or adsorb at the interface or rock surface). A larger energy barrier signifies more resistance to particles' aggregation (or adsorption). Stronger energy barriers are typically found in lower ionic strength solutions. As the ion (salt) concentration increases, the electrical double layer around charged particles compresses; therefore, the electrostatic repulsive force reduces. However, the ion (salt) concentration does not affect the van der Waals attractive forces [56]. Hence, the net repulsion energy decreases without changing the attraction and, subsequently, the energy barrier decreases. In the case where there is no significant energy barrier, particles are said to be in their "primary minimum" potential, as shown in Figure 2-2. Aggregation of particles occur if particles are at primary minimum potential. The secondary minimum normally does not influence the aggregation kinetics. Particles in the secondary minimum can coalescence without changing their original size, due to a mild attractive force between particles. The aggregation of particles in the secondary minimum can be easily broken by external forces such as shear or mechanical forces [57].
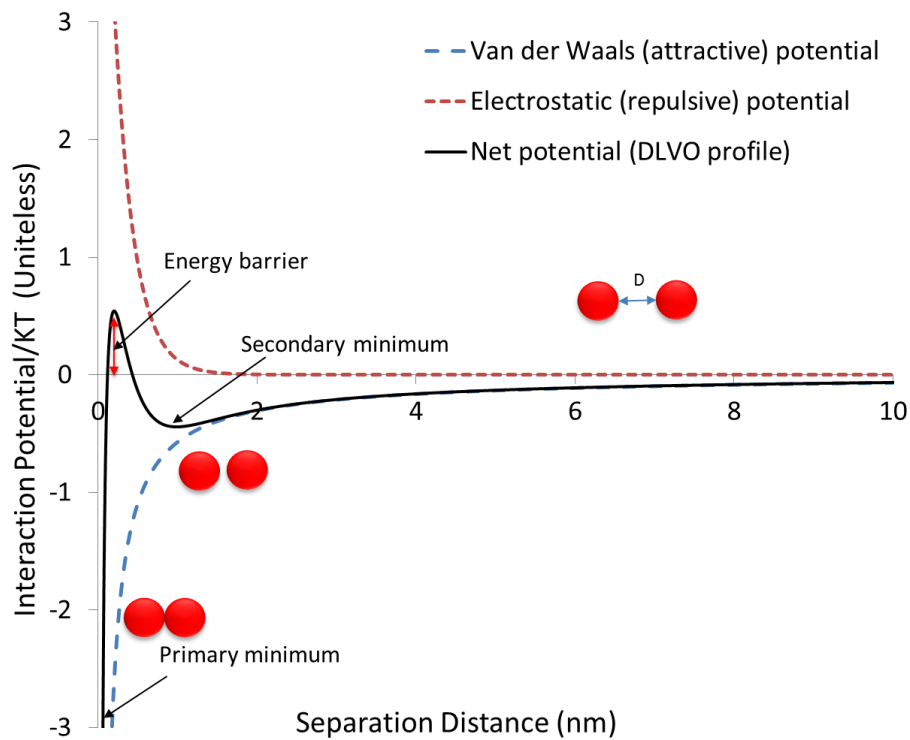
Figure 2-2: Schematic of the DLVO profile [56]

The DLVO profile is more sensitive to the presence of multivalent ions than monovalent ions. As shown in Figure 2-3, very small concentrations of multivalent ions can remove the energy barrier and causes the aggregation of particles (or adsorption of particles at the interface). Also, it is observed that in addition to ionic strength and ion type, the aggregation of particles is also influenced by the charge type (positive or negative) of ions. (We will discuss these effects in chapter three). For instance, the stability of negatively charged particles is dictated mainly by the negatively charged multivalent ions and positive ions do not have a significant effect on the aggregation of the negatively charged particles [58, 59]. As a result, the accuracy of DLVO theory in the presence of multivalent ions decreases.

16
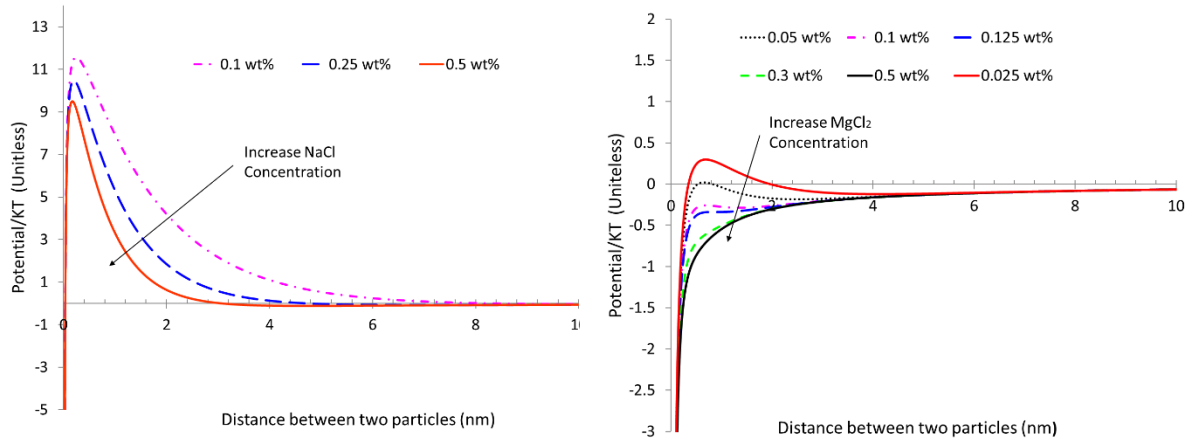
Figure 2-3: Changing the DLVO profile with altering NaCl concentration (left) and MgCl₂ concentration (right) [58]

The DLVO theory was proposed based on comparing two independent forces of van der Waals (attractive) forces and electrostatic (repulsive) forces. Researchers later developed this theory to account for the effect of other forces (non DLVO forces) such as steric forces [60, 61], hydration-solvation interaction [62, 63] and hydrophobic interactions [64, 65]. These models are classified in a general group of extended-DLVO theory.

2.2.4. Steric repulsion force and bridging

Each atom within a molecule can only occupy a limited space. When atoms come closer together, the energy of the system increases due to overlapping electron clouds [66]. An increase in the energy of the system when atoms approach each other is known as steric repulsion or steric hindrance. When two particles with an adsorbed polymer or surfactant on their surface approach to each other, as shown in Figure 2-4, the entropy per adsorbed molecule decreases, causing desorption and a simultaneous increase in the interfacial energy. Hence, additional work is required to bring the particles together and the particles repel each other [67]. Under certain circumstances, however, high molecular weight polymers can adsorb on separate particles and draw them together. This phenomenon is known as bridging flocculation

17

[68]. Bridging between particles occurs under conditions when particles are not totally coated by the polymeric or surfactant species. If particles are fully covered with polymers or surfactants, bridging can take place only if there is either detachment of some portion of the already adsorbed polymer (or surfactant) on a particle, to provide sites for attachment of polymer (or surfactant) fractions adsorbed on other particles, or polymer–polymer (surfactant-surfactant) bonding itself. It is suggested that maximum flocculation occurs when the fraction of particle surface covered by polymer molecules is close to 0.5. For steric stabilization and bridging flocculation by adsorbed polymers or surfactant, there is still no satisfactory quantitative theory [67].
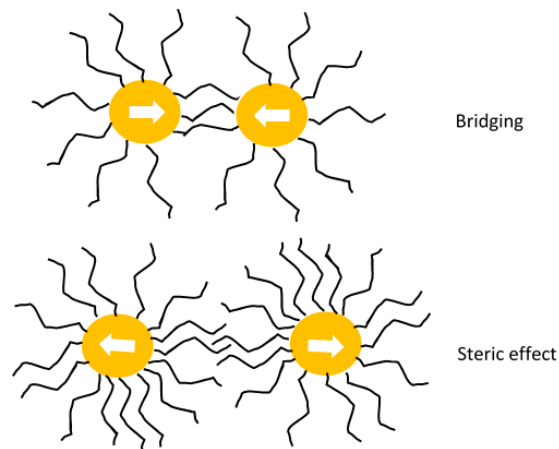
Figure 2-4: Schematic diagram of bridging and steric forces [69]

2.2.5. Hydration force

When charged surfaces are contacted with water, the surfaces induce some changes in the adjoining layers of water. The properties of this thin layer (known as the hydration layer) differ from the bulk water. Overlap of hydration layers of two approaching particles (surfaces) causes some interaction, which is called hydration force [70].

The hydration force is a strong short-range repulsive force that acts between polar surfaces separated by a thin layer of water, which decays quasi-exponentially with decay lengths of

about 1 nm [71]. Although there are some theoretical explanations about the origin of a hydration force (e.g. water-structuring models, image-charge models, excluded-volume models, and dielectric-saturation models [72]), colloidal science researchers generally believe that despite the proposed explanations, the origin of hydration repulsion remains unclear [73].

2.2.6. Hydrophobic interaction

Hydrophobic particles (surfaces) have a tendency to clump together when placed in polar solvents (typically water). This tendency is known as the hydrophobic effect. Hydrophobic surfaces can minimize their contact with water by hydrophobic interactions [74]. This force can exist naturally or be induced by the adsorbed hydrophobic species [67]. Hydrophobic forces is much stronger compared to van der Waals forces and its effectiveness distance is much longer [75]. Hydrophobic interaction (E_h) between two equally sized spherical particles with a radius of R can be calculated as:

$$E_h = -2\pi R \gamma \lambda_h \exp(-\frac{d}{\lambda_h}) \tag{2-12}$$

where γ and λ_h are empirical parameters that range between 10-50 mJ/m^2 and 1-2 nm, respectively.

2.3. Interfacial tension (IFT) reduction

Interfacial tension is a property of the interface between two immiscible fluids which arises from the net inward forces on the molecules of the fluids at the boundary of two phases [76]. The IFT is commonly expressed by mN/m or dynes/cm, which are equal. Distribution of fluids in the porous media is mainly determined by the oil-water interfacial tension. Generally, reducing IFT value can drive immobile oil, cause oil drops to flow easily through porous media and increasing oil recovery. However, the magnitude of IFT reduction required to mobilize the

19

immobile oil is controversial. Some authors believe that 2 or 3 orders of magnitude decrease in the IFT value is necessary to initiate the movement of immobile oil [77]; others stated that even less than one order of magnitude IFT reduction can be sufficient to observe a significant increase in oil recovery [78]. IFT reduction can increase the capillary number; which is defined as the ratio of viscous forces to capillary forces [79]. The mathematical model for the capillary number is given by the following equation [80]:

$$N_c = \frac{v\mu}{\sigma cos\theta} \tag{2-13}$$

where v is Darcy velocity, μ is the viscosity of displacing fluid, σ is the oil-water interfacial tension, and θ is the contact angle between the oil-water-rock interface. Based on the classic capillary desaturation curves, as shown in Figure 2-5, by increasing the capillary number beyond the critical capillary number, less residual oil can be yielded. The critical capillary number for wetting and non-wetting phases is different and a larger capillary number is required to mobilize the wetting phase [81, 82]. Most researchers propose that the critical capillary number can be achieved in the ultralow IFT values (0.1 to 0.01 mN/m) [79, 81].
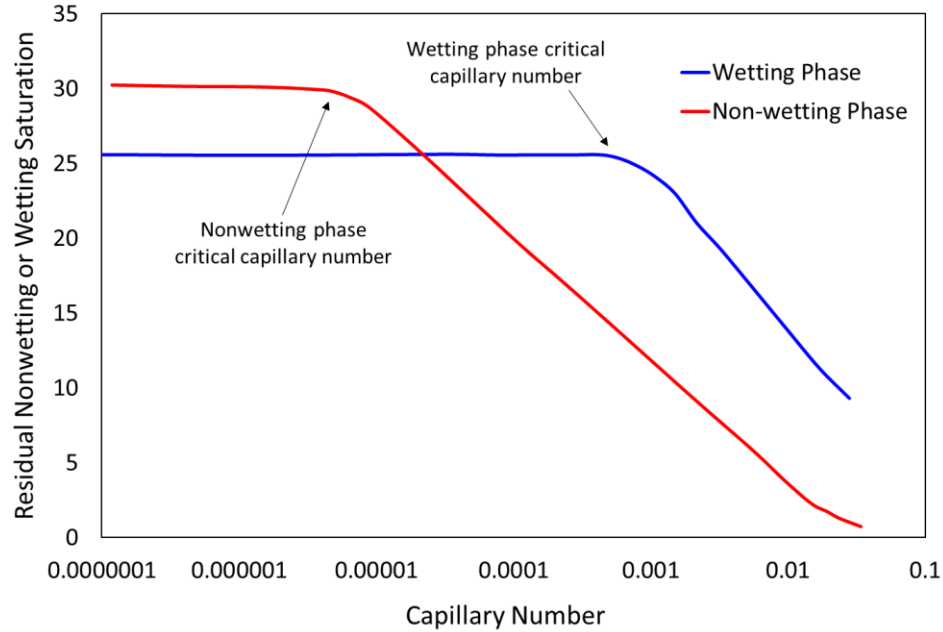
Figure 2-5: Plot of capillary number's effect on oil residual saturation [83]

IFT reduction can also affect the relative permeability [81, 84]. Although some small changes in the relative permeability curves are reported when the IFT value decreases to less than 5 mN/m [85, 86]. More remarkable changes can only be expected for ultra-low IFT (0.1 to 0.001 mN/m) [81]. Wettability alteration is another parameter which can affect the capillary number and the relative permeability during nanoparticle-EOR [87]. The wettability alteration of rock surfaces by nanoparticles will be discussed in the next section.

Surfactants are the most common materials widely used to reduce the IFT value [88]. Surface active agents or surfactants are components with at least one hydrophilic and one hydrophobic portion in their molecules. Water molecules in the aqueous phase take an equal forces in all directions. Hence, the net force is zero for these molecules. However, as shown in Figure 2-6, the molecules in the interface are experiencing unequal forces from the water molecules and oil molecules. More unbalanced force on the interface molecules leads to more oil-water interfacial tension. By increasing the similarities of the structure or intramolecular forces in

21

two phases, the IFT value decreases. Surfactants, due to their amphiphilic nature, tend to accumulate at the interface. By replacing the original oil or water molecules at the interface with surfactants, the interaction in the interface can be change from oil-water molecules to the oil-hydrophobic part of surfactant and water-hydrophilic part of the surfactant. Since the interactions between hydrophobic portion of surfactant-oil and hydrophilic portion of surfactant-water are much stronger than oil-water interactions, the tension in the interface reduces significantly [89]. The IFT value depends directly on the replacement of water molecules with surfactant molecules at the interface. The maximum IFT reduction occurs when the oil-water interface is saturated with a monolayer of surfactants.
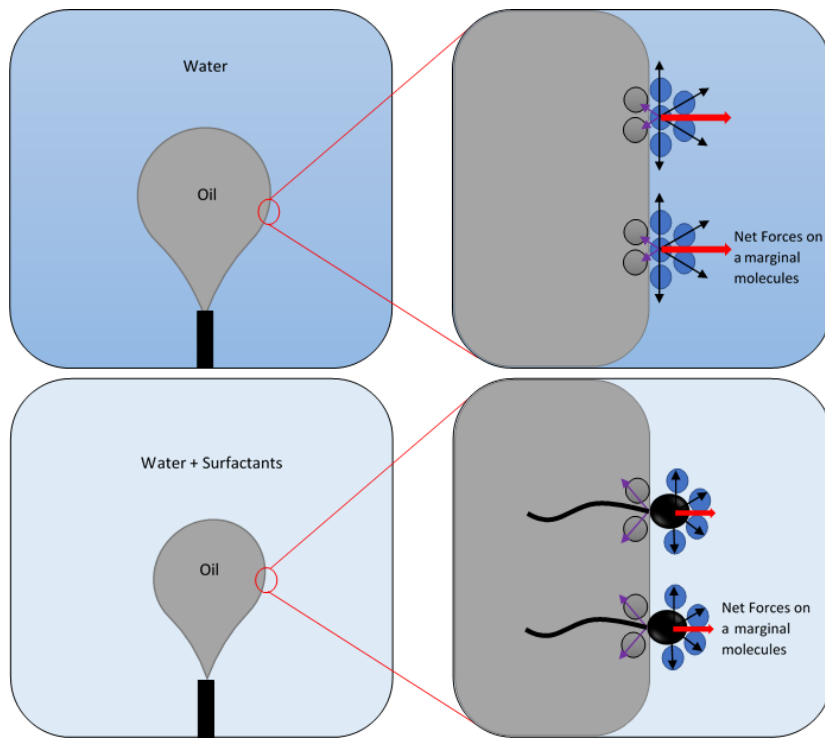
Figure 2-6: Schematic diagram of surfactant effect on the intermolecular force balance of marginal molecules at oil-water interface

The IFT reduction potential of nanoparticles is not conclusive. Some authors declared that nanoparticles can be considered as potential agents to reduce the IFT value [12-14, 90-92];

however, opposing opinions can also be found in the literature [93-95]. Using a surfactant to stabilize nanoparticles provoked this contradiction in some cases. Some researchers believe that nanoparticles alone cannot influence the IFT value significantly; however, when a surfactant is added, the synergistic effect of nanoparticles and surfactants can reduce the IFT value [93, 96-98]. However, Hendraningrat et al. [14] showed that 0.05 wt% silica nanoparticles dispersed in 3.0 wt% of NaCl brine decrease oil-brine IFT from 19.2 Nm/m to 7.2 Nm/m. Adel et al. [99] reported that silica nanoparticles and alumina nanoparticles can reduce IFT value; however, silica nanoparticles are more effective than alumina nanoparticles. Although most authors believe nanoparticles can reduce oil-water IFT, however its magnitude may not be sufficient to significantly increase oil recovery. Table 2-1 summarizes the effect of nanoparticles on oil-water interfacial tension in the literature.

Table 2-2: The effect of different nanoparticles on oil-water IFT

Type of Nanoparticles	Size of NP (nm)	Conc. (wt%)	Aqueous phase	Oil phase	Initial IFT	Final IFT	Reference
Silicon oxide (SiO$_2$)	7	0.05	3 wt% NaCl	Crude oil	19.20	16.90	[100]
Silicon oxide (SiO$_2$)	12	5	5 wt% NaCl	Crude oil	21	21	[101]
Silicon oxide (SiO2)	12	0.4	5 wt% NaCl	Light crude oil	26.5	1.95	[90]
Silicon oxide (SiO2)	12	0.4	5 wt% NaCl	Heavy Crude oil	28.3	7.3	
Silicon oxide (SiO2)	21-40	0.05	3 wt% NaCl	Crude oil	19.2	7.9	[14]
Silicon oxide (SiO$_2$)	15	1	Pure water	Hexane	51	51	[93]
Silicon oxide (SiO$_2$)	20-70	0.4	5 wt% NaCl	Crude oil	26.5	38.4	[102]
Iron oxide (Fe$_3$O$_4$)	20-35	0.3	2.5 wt% NaCl	Propane	38.5	2.25	[91]
Aluminum oxide (Al$_2$O$_3$)	40	0.3				2.75	

Type of Nanoparticles	Size of NP (nm)	Conc. (wt%)	Aqueous phase	Oil phase	Initial IFT	Final IFT	Reference
Silicon oxide (SiO$_2$)	10-30	0.3				1.45	
Aluminum oxide (Al$_2$O$_3$)	20	0.5	2 wt% NaCl+CTAB	Crude oil	8.46	1.65	[103]
Zirconium dioxide (ZrO$_2$)	40	0.5	2 wt% NaCl+CTAB	Crude oil	8.46	1.85	
Non-ferrous metal nanoparticles	90-110	0.001	Pure water+0.004 wt% Sulphanole	Crude oil	31.4	9.2	[8]

The mechanism of IFT reduction by nanoparticles is similar to that of surfactants. The presence of nanoparticles at the oil-water interface alters the force balance on the interface molecules. Increase or decrease in the IFT value depends on the strength of molecular interactions between oil-nanoparticle molecules and water-nanoparticle molecules at the interface compared to the original oil-water molecular interactions. Stronger interactions result in lower IFT values [89]. Similar to surfactants, a tightly packed monolayer of nanoparticles at the interface leads to a lower IFT value [104].

Controversial results regarding the effect of nanoparticles on the IFT value may arise from the fact that it is still unclear whether and under which conditions nanoparticles can adsorb onto the oil-water interface. For instance, it is reported that silica nanoparticles are extremely hydrophilic and have more tendency to remain in the aqueous phase instead of settling at the interface; for nanoparticles to adsorb at the interface, their surface must be modified by surfactants or polymers to reduce the hydrophilicity of silica nanoparticles and increase their tendency to adsorb onto the oil-water interface [105]. Changing the wettability of nanoparticles by surfactants depends on the relative concentrations of nanoparticles and surfactants. As shown in Figure 2-7, by increasing the concentration of surfactant in the solution, the

adsorption of surfactant as individual ions changes the wettability of the particles and provides a partially hydrophobic character to the surface; thus nanoparticles can be adsorbed onto the interface and reduce the oil-water interfacial tension. The hydrophobic property of the surface increases with surfactant concentration; however, by further increase of surfactant concentration, a surfactant bilayer will form and make the nanoparticles hydrophilic again [93]. Lan et al. [106] suggested a range for the concentration of silica nanoparticles and CTAB surfactant. Within that range, the nanoparticles and the surfactant molecules can interact with each other to reduce the paraffin oil and aqueous phase IFT more than when using CTAB alone. According to their results, the IFT decreases when CTAB concentrations are lower than 0.01 mM and the nanoparticle concentration is less than 1 wt %. They observed that by increasing nanoparticles' concentration to 2 and 5 wt %, IFT increases. However, at higher CTAB concentrations (greater than 0.01 mM) IFT increases versus nanoparticle concentration. To conclude, they reported a concentration range of less than 0.1 mM CTAB and between 0.01 and 1 wt % for silica nanoparticles, within which just enough CTAB molecules can settle at the nanoparticles' surface to modify them to be appropriately hydrophobic to adsorb on the interface and promote IFT reduction. Jafari et al. [106] proposed that silica nanoparticles without surfactants can adsorb onto the oil-water interface. However, the reduction of interfacial energy due to the adsorption of nanoparticles is not sufficient to have irreversible adsorption. Hence, nanoparticles may desorb from the interface. They concluded that an elevated temperature can increase the chance of nanoparticles desorbing from the interface due to thermally exciting the nanoparticles.

Oil phase properties such as oil composition, concentration of natural surfactants, concentration of polar components, etc. can affect IFT reduction with or without nanoparticles.

For instance, crude oil may contain natural surfactants (naphthenic acids and asphaltene); consequently the aqueous properties such as type and concentration of ions can directly affect the distribution of these surfactants in the oil or water phases [107]. The presence of salt in the aqueous solution can alter the electrostatic forces at the interface, and therefore, the natural surfactants' distribution at the interface. Naphthenic acids present in crude oil can accumulate at the interface due to a salting-out effect and lower the IFT [108]. Adsorption of charged nanoparticles onto the oil-water interface may also change the distribution of natural surfactants at the interface. Hence, based on the concentration of these surfactants in the oil phase, different IFT trends may be obtained in the same aqueous phase but for different oil phase systems. Furthermore, the oil composition can affect the strength of molecular interactions between oil-nanoparticle molecules and water-nanoparticle molecules at the interface, which dictates the ultimate IFT value.
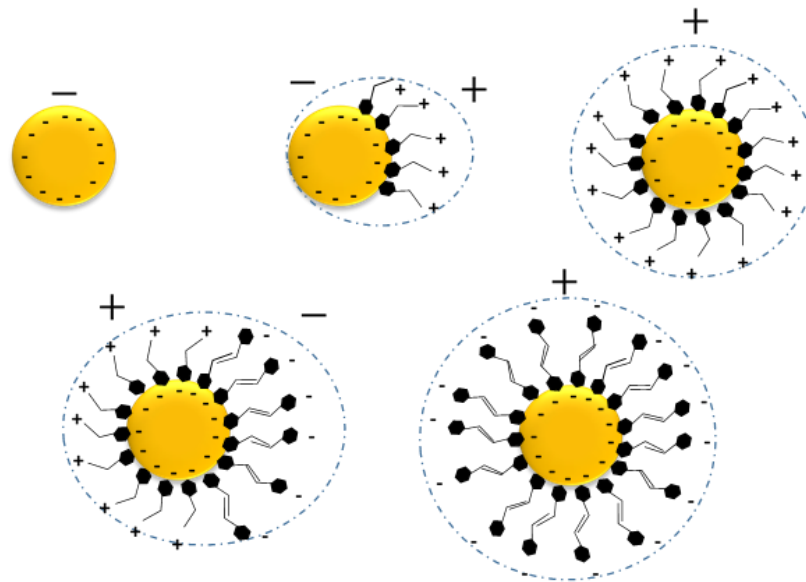
Figure 2-7: Schematic representation of nanoparticles' wettability alteration by surfactants

2.4. Wettability Alteration

Wettability is the preferential tendency of a solid (reservoir rock) to be in contact with one fluid in the presence of another fluid. In water-wet reservoirs, water preferentially wets the rock surface, as shown in Figure 2-8, where the apparent contact angle θ between the rock and water is less than 90°. In oil-wet reservoirs, the oil attaches on the rock surface and the apparent contact angle is greater than 90°. In the case of neutral or intermediate wettability, no preference is shown by the rock to either fluid [109]. Generally, for an oil-brine-rock system, the rock is considered as water-wet when the apparent contact angle between a water droplet and rock is less than 75°, intermediate wet if the contact angle is between 75-105° and oil wet if the contact angle is 105 - 180° [110, 111].

| Water-Wet | Oil-Wet | Intermediate-Wet |
| $(0° < \theta < 75°)$ | $(105° < \theta < 180°)$ | $(75° < \theta < 105°)$ |
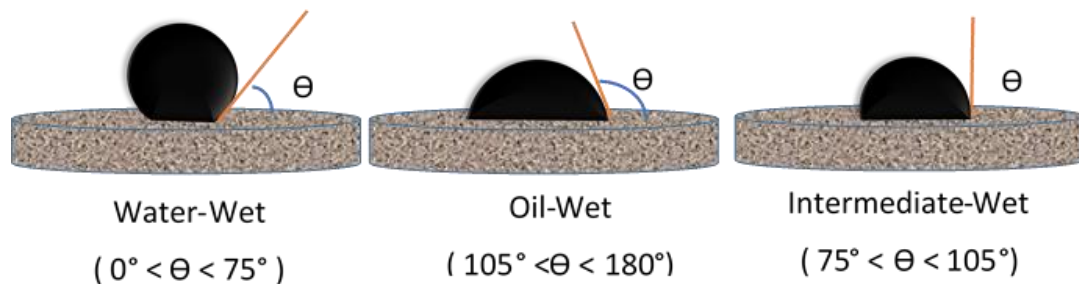
Figure 2-8: Schematic diagram of different wettability status

It is reported that nanoparticles can alter the wettability of reservoir rock from an oil-wet toward a water-wet condition [16-18, 32] which might be favorable for oil recovery. In fact, wettability alteration is proposed as the main mechanism for nanoparticle-EOR methods. Wettability can be measured on the surface of a solid substrate using the contact angle method, or within the entire core plug using the Amott Wettability test [112] or U.S. Bureau of Mines (USBM) method [113]. The wettability of a core is represented by the wettability index (WI), which can be calculated by the following equation:

$$WI = r_w - r_o \tag{2-14}$$

where r_w and r_o are the displacement-by-water ratio and the displacement-by-oil ratio, respectively, and can be calculated as:

$$r_w = \frac{\text{Spontaneous } water \; imbibition}{\text{Total Water Imbibition}} \tag{2-15}$$

$$r_o = \frac{\text{Spontaneous oil } imbibition}{\text{Total Water Imbibition}} \tag{2-16}$$

The wettability index can be a number between -1 and 1, where 1 is strongly water-wet, -1 is strongly oil-wet and 0 is neutral wettability [114]. Li et al. [115] showed that hydrophobic nanoparticles have no effect on the WI of cores; however, hydrophilic nanoparticles can increase the WI. Moghaddam et al. [27] observed that spontaneous imbibition increases in the presence of silica nanoparticles in the aqueous phase, due to the wettability alteration toward the water-wet condition.

The wettability alteration of the rock surface in the presence of nanoparticles is mainly examined using the contact angle measurement method. The effect of nanoparticles on the wettability alteration of different rock surfaces is listed in Table 2-3. Here, the focus is placed on the contact angle measurement method. As illustrated in the table, for different rock surfaces, regardless of their initial wettability, the presence of nanoparticles altered the wettability of the rock surface toward a more water-wet condition. Researchers typically use the conventional contact angle measurement method to evaluate the wettability alteration capacity of nanoparticles. In this method, the substrates are either aged with (immersed in) nanoparticle-fluids before conducting the experiments or contacted with nanoparticle-fluids before the oil droplet is introduced to the rock surface.

Table 2-3: Effect of nanoparticles on the oil-water-rock contact angle

Type	Aqueous phase	Conc. (wt%)	Oil phase	Rock Type	Aging method	Initial CA	Final CA	Reference
Silicon oxide (SiO_2)	5 wt% NaCl	2	n-decane	Calcite	Aged in nanoparticles-fluid for 3 hrs	122	30	[116]
Zirconium dioxide (ZrO_2)		0.05				152	44	
Silicon oxide (SiO_2)	5 wt% NaCl	0.4	Light Crude oil	Sandstone	Laid in nanoparticles-fluid at room temperature	135.5	66	[90]
Silicon oxide (SiO_2)	5 wt% NaCl	0.4	Heavy Crude oil			130	101	
Iron oxide (Fe_2O_3)						134	100	[91]
Aluminum oxide (Al_2O_3)	2.5 wt% brine (NaCl)	0.3 0.3 0.3	Propane	Sandstone	Aged in Nanoparticle solution for 3 hrs	131	95	
Silicon oxide (SiO_2)						132.5	82	
Silicon oxide (SiO_2)	3 wt% NaCl	0.1	Crude oil	Berea Sandstone		54	22	[14]
Aluminum oxide (Al_2O_3)	2 wt% NaCl	0.5	Crude oil	Dolomite	Submerged in nanoparticles-fluid for 48 hrs	129	124	[103]
Zirconium dioxide (ZrO_2)	2 wt% NaCl	0.5	Crude oil			135	129	
Titanium Oxide (TiO_2)	0.5 wt% NaCl	0.01	Crude oil	Sandstone		125	90	[117]
Silicon oxide (SiO_2)	3 wt% NaCl	0.05	Crude oil	Quartz		131	112	[100]

The mechanism of wettability alteration of reservoir rock in the presence of nanoparticle-fluids is not clear yet. The traditional concepts of simple liquid spreading [118], due to the complex interactions between the nanoparticles and the solid surface, do not apply to a nanoparticle-fluid [119]. Kondiparty et al. [120] experimentally evaluated the dynamic spreading of nanoparticle-fluid by directly observing the self-layering of nanoparticles from both the top and side views simultaneously using an advanced optical technique. They reached the conclusion that the three-phase contact line spontaneously decreases to reach an equilibrium

condition. Then, nanoparticles form ordered structures in the confinement of the three-phase contact region. This ordering in the wedge-film area causes an extra pressure in the film compared to the bulk solution and separaes the oil drop from the surface. This pressure is known as "structural disjoining pressure". A schematic diagram of oil drop removal by structural disjoining pressure is illustrated in Figure 2-9. Sefiane et al. [121] reported that the change in the contact angle of oil, water and rock surface can be due to a combination of "structural disjoining pressure" and "adsorption" of nanoparticles on the rock's surface.
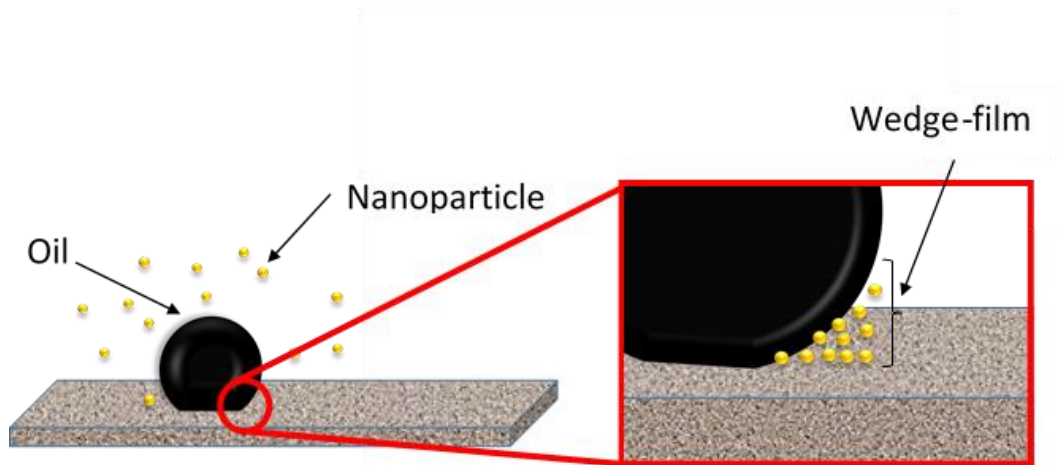
Figure 2-9: Nanoparticle assembling in wedge film causes to structural disjoining pressure (After [120])

The wettability alteration of substrates using nanoparticle-fluids is sensitive to many factors including: nanoparticle size and concentration, drop size, primary contact angle of the droplet [122], particle charge, surface wettability of nanoparticles [123], charge and roughness of the substrate, concentration of stabilizer, type and concentrations of ions in the nanoparticles-fluid, bulk pressure and temperature, etc. Wasan et al. [122] tested a canola oil drop spreading on a glass surface when surrounded by silica nanoparticles-fluid. They pointed out that by increasing the concentration of nanoparticles, the structural disjoining pressure and spreading rate of nanoparticles-fluid increases. They also noticed that the spreading rate of nanoparticle-

fluid decreased with a decrease in the drop's volume. Wang and Wu [123] examined the effect of particle charge and surface wettability of the nanoparticles on oil drop detachment from a surface using molecular dynamic simulation. Their simulation showed that full detachment of an oil droplet from a solid surface by nanoparticles is possible when the charge of particles exceeds a threshold value. They concluded that highly charged hydrophobic nanoparticles have the best performance in oil detachment. Lim et al. [124] demonstrated that an oil drop detaches faster when the temperature and hydrophilicity of the substrate increases.

3. CHAPTER THREE

Insight into the Stability of Hydrophilic Silica Nanoparticles in Seawater for Enhanced Oil Recovery Implications (Paper 1, Published)

Abstract

The stability of nanoparticles in the aqueous phase is a major challenge in the application of nanoparticles in Enhanced Oil Recovery (nanoparticle-EOR) processes. Previous studies evaluated the performance of nanoparticles for EOR purposes; either deionized water or water at very low ionic strength was used. Nanoparticles can be easily dispersed in the deionized or low salinity water, whereas they are extremely unstable in high salinity seawater or formation water. Typically, seawater or formation brine is injected for water-flooding and EOR purposes. If we want to change the fluid-fluid or fluid-rock properties by injecting nanoparticle enhanced water, then, the stability of the nanoparticles in high salinity water is extremely important. In this work, a method to stabilize silica nanoparticles in seawater is proposed. First, the aggregation of silica nanoparticles in the presence of different ions is investigated. The results show that the presence of positive multivalent ions in the electrical double layer around nanoparticles can destabilize silica nanoparticles. In order to reduce the concentration of positive multivalent ions around silica nanoparticles, a theory based on "H^+ protection" is proposed and its effectiveness is tested by particle size, turbidity, zeta-potential, and pH measurements. The effect of the concentrations of nanoparticles and HCl on the stability of silica nanoparticles in seawater is evaluated. Experimental results show that H^+ protection, which can be obtained by adding HCl to the solution, can effectively stabilize silica nanoparticles in seawater. The experiments show that the size of nanoparticles in the seawater directly depends on the concentration of nanoparticles and inversely to the HCl concentration.

KEYWORDS: Enhanced Oil Recovery, Silica Nanoparticles, Stability of nanoparticles, Electrical Double Layer, DLVO theory

3.1. Introduction

Recently, there has been a growing interest in application of nanoparticles in the Enhanced Oil Recovery (EOR) processes. Numerous experimental works has been published discussing the

effect of nanoparticles on increasing oil recovery [5-7, 10, 11]. It is reported that nanoparticles can adsorb at liquid-liquid interfaces and reduce interfacial tension [29-31]. Whether nanoparticles adsorb at the interface or they change the oil-water interfacial tension is still an ongoing debate. It is accepted that this phenomenon occurs because the adsorption lowers the total energy of the system [125]. Furthermore, nanoparticles can alter surface wettability from oil-wet to water-wet [16-18, 32] which is favorable for oil recovery.

One of the most important challenges in the application of nanoparticles for EOR methods is their stability in an aqueous solution. Nanoparticle dispersion in the aqueous phase is not a thermodynamically stable. Dispersed nanoparticles are always subject to Brownian motion with frequent collisions between them. The stability of a dispersion is thus determined by the nature of the interactions between the particles during such collisions[126]. Although the potential of silica nanoparticles in EOR processes is widely studied and their effectiveness is well-documented [7, 127, 128] the applications of hydrophilic silica nanoparticles are limited because the nanoparticles' high energetic hydrophilic surface, causes the silica nanoparticles to be easily agglomerated [129].

In most studies which evaluated performance of nanoparticles for EOR purposes with wettability, IFT measurement and core-flooding experiments, either deionized water or water at very low ionic strength (especially NaCl brine) is used [12, 13, 19, 35, 130-133]. However, nanoparticles are extremely unstable in seawater, formation water and concentrated ionic solutions of multiple types and charges of ions. Water flooding and EOR projects, especially for offshore reservoirs, use seawater. Even higher salinity formation water is present in the reservoirs as well. The stability of nanoparticles in these fluids is crucial for any successful nanoparticle-EOR processes.   In this paper, nanoparticle stability in mixed ionic solutions is

systematically investigated and a method to stabilize hydrophilic silica nanoparticles in seawater is proposed. We first examine the effect of the most common ions in seawater on the stability of silica nanoparticles. Based on the results of these experiments, a new method is proposed to stabilize silica nanoparticles in seawater. Second, the effectiveness of proposed method, using hydrochloric acid, in the stability of silica nanoparticles in seawater is tested by particle size, turbidity, zeta-potential and pH measurements. Furthermore, in each part, the results of experiments are compared with DLVO theory.

3.2. Theory of nanoparticle stability

Colloidal systems consist of one or more dispersed phases and one continuous phase. On the nano-scale, due to an increase in the surface area and possible changes in the structure and composition of the surface, surface energy, and consequently the total energy of the system, increases. Nanoparticles tend to aggregate to reduce the surface energy, thereby making a colloidal dispersion at the nano-scale non-thermodynamically stable. Particles in the colloidal systems are always subject to Brownian motion and collisions frequently occur between particles. The nature of interaction between the particles during these collisions determines their stability in the solution. Van der Waals, electrical double layer, steric interaction, bridging, hydrophobic and hydration-solvation interaction are six main types of particle–particle interaction forces that can exist in the dispersion medium [38]. The sum of the attractive (van der Waals, bridging, and hydrophobic forces) and repulsive (the electrical double layer force, steric effect, and hydration force) forces between individual particles govern the stability and aggregation of particle dispersions. In general, to prepare a stable dispersion or to kinetically slow the aggregation, repulsive forces between particles should overcome attractive forces [134].

Derijaguin, Landau, Overbeek and Verwey [54, 55] proposed the DLVO theory to explain the stability of colloids in the absence of any polymer or surfactant. This theory combined two independent van der Waals attraction and electrostatic repulsion forces, explain dispersion mechanisms of colloids in the polar solution.

Electrical double layer: Helmholtz [46] first introduced and termed the idea of the electrical double layer, which was later extended by Gouy-Chapman and Stern [47, 48].The electrical double layer is a structure that appears on the surface of a charged surface when it is exposed to a fluid. The first layer, the surface charge (either positive or negative), is comprised of ions adsorbed onto the surface due to chemical interactions. This layer, which consists of a dense layer of ions of the opposite charge (counter-ions) that form around the nanoparticle, is known as the "Stern layer". The second layer is composed of ions attracted to the surface charge via the Coulomb forces, electrically screening the first layer. This second layer is loosely associated with the surface. It is made of free ions that move in the fluid under the influence of electric attraction and thermal motion rather than being firmly anchored. It is thus called the "diffuse layer" [49]. The high concentration of counter-ions within the diffuse layer gradually decreases with increasing distance from the nanoparticle until equilibrium is reached with the ion concentration in the bulk of the solvent [47]. The distribution of ions in the electrical double layer around negatively charged nanoparticles is illustrated in Figure 3-1.
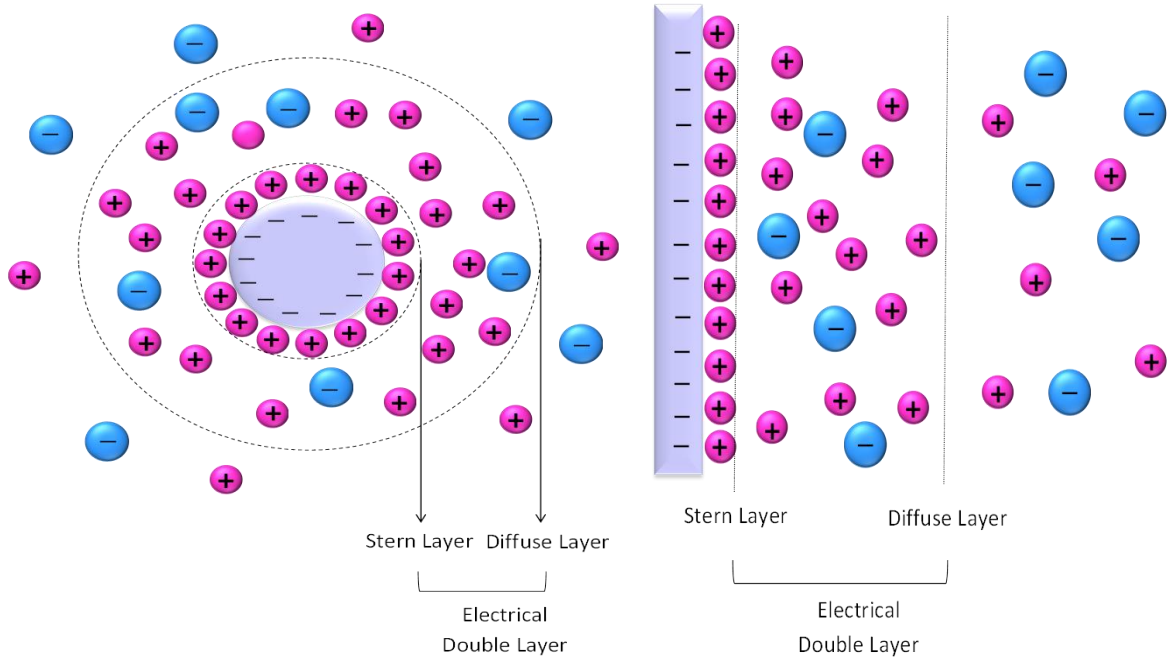
Figure 3-1: Ion distribution in electrical double layer theory (after [52]).

The thickness of the double layer that forms at the charged surface is called "Debye Length". Based on the electrolyte theories, interactions in the low ionic strength solutions decrease exponentially with distance or the Debye screening length. By increasing the ion concentration in the solution, due to effective screening of charges over short distances, this length decreases monotonically [135]. Greater nanoparticle surface charge and longer Debye length leads to increasing nanoparticle stability in the aqueous solution [136, 137]. The thickness of the double layer is a function of ionic strength. The ionic strength can be defined as [138]:

$$I = \frac{1}{2} \sum_i z_i^2 c_i$$

(3-1)

where z and c are the charge number and molar concentration of ith ion, respectively. The Debye length (κ or k^{-1}) in nanometer can be calculated as [50]:

37

$$k^{-1} = \sqrt{\frac{\varepsilon_r \varepsilon_\circ K_B T}{e^2 \sum \rho\infty_i Z_i^2}} \qquad (3\text{-}2)$$

where e is the elementary charge of an electron (C), T is the temperature (K), $\varepsilon_\circ$ is (F/C), ε_r is absolute and solution relative dielectric constant, K_B is the Boltzmann's constant, and $\rho\infty_i$ is the number density of ion i in the bulk solution. The electrostatic repulsion between two equally sized spherical particles with $ka > 5$ (where k is the reciprocal of Debye length (nm^{-1}) and a is the radius of spherical nanoparticles in nanometer) can be calculated by [51]:

$$V_{EL} = \frac{32\pi K_B T \varepsilon_r \varepsilon_\circ \rho_\infty r \gamma^2}{k^2} e^{-kd} \qquad (3\text{-}3)$$

where γ is the reduced surface potential and can be calculated as [51]:

$$\gamma = \tanh(\frac{z e E_0}{4 K_B T}) \qquad (3\text{-}4)$$

where E_0 is the potential on the surface. For a surface charge (E_0) below 30 mV or $ka < 5$, the electrostatic potential can be calculated by linear Poisson-Boltzmann approximation [50]:

$$V_{EL} \approx 2\pi \varepsilon_r \varepsilon_\circ r E_0^2 k e^{-kd} \qquad (3\text{-}5)$$

Surface charge of hydrophilic silica nanoparticle: It is well documented that when a nanoparticle is immersed in an aqueous solution, the protonation/deprotonation capacity of the particle surface is a key parameter for the charge transfer between solvent and particle. The relative basicity or acidity of the solvent and the particle indicates the direction of protonic transfer [139, 140]. Two protonation reactions (reaction R1 and R2) are suggested for silica nanoparticles (see also Figure 3-2) [141].

$$SiOH \leftrightarrows SiO^- + H^+ \quad\quad\quad\quad\quad\quad\quad\quad\quad\quad\quad\quad (R1)$$

$$SiOH_2^+ \leftrightarrows SiOH + H^+ \quad\quad\quad\quad\quad\quad\quad\quad\quad\quad\quad\quad (R2)$$
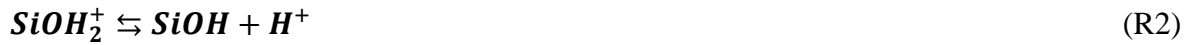
Due to the presence of a functional group containing oxygen on the surface of silica nanoparticles, the solution's pH can significantly affect the charge of silica nanoparticles. Because oxygen can be protonated or deprotonated to become charged [142]. It is impossible to directly measure the Stern potential. Instead, the zeta potential (E),   the potential at the shear plane close to the Stern plane, can be experimentally measured and is often used as a measure of the surface potential [38]. The surface charge of the hydrophilic silica nanoparticles as a function of pH is well documented in the literature [59, 143, 144]. As shown in Figure 3-3, the surface charge of silica nanoparticles is virtually unchanged for a pH greater than 6, and its point of zero charge (pzc) occurs when the pH is between 2 and 3.
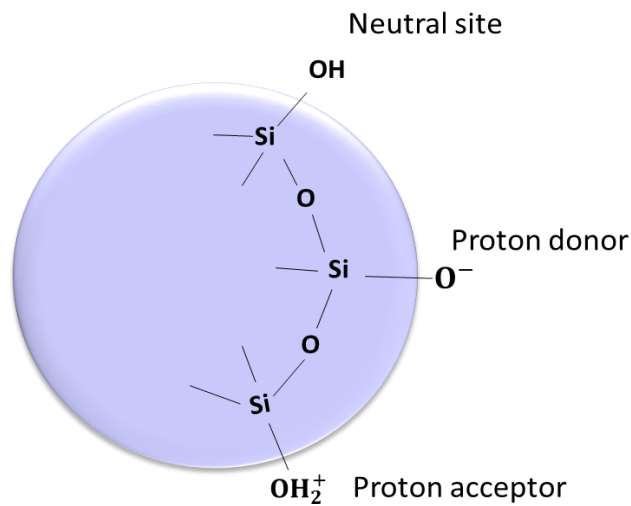
Figure 3-2: Schematic diagram of side-binding model for silica dioxide [139]
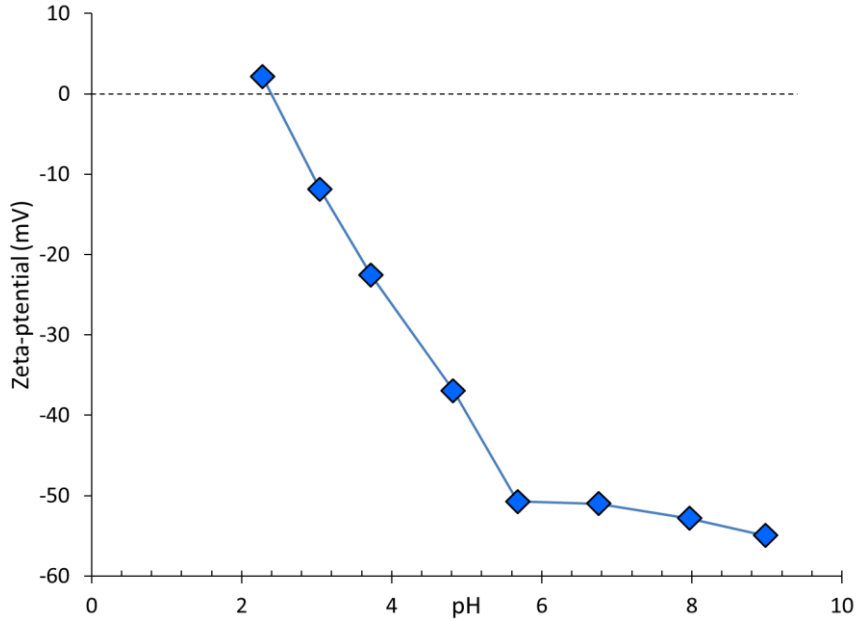
Figure 3-3: **Charge of silica nanoparticles in different pHs (after [143]).**

Van der Waals Interaction: van der Waals forces are general attraction forces that occurs between molecules and consists of dipole–dipole, dipole-induced dipole, and London (instantaneous induced dipole-induced dipole) forces [39]. For two spherical nanoparticles with radius R and center to center distance of d, the Van der Waals attraction interaction energy can be calculated as [41]:

$$\frac{E_{wdv}}{k_B T} = -\frac{A_{131}}{6k_B T}\left[\frac{2R^2}{d^2-4R^2} + \frac{2R^2}{d^2} + ln(\frac{d^2-4R^2}{d^2})\right]$$

(3-6)

where A_{131} is the Hamaker constant and accounts for the interaction between two nanoparticles of the same material (component 1) through a solvent medium (component 3). For silica nanoparticles in water, the effective Hamaker constant is reported as 36.2×10^{-22} J [145], k_B is the Boltzmann constant, and T is absolute temperature (K).

Classical DLVO theory generally fails to predict particle stability in the cases of strongly hydrophilic or hydrophobic particle suspensions [146] and aqueous phases containing

multivalent ions especially with high ionic strength [147].   It is proposed that other interaction energies (non-DLVO forces) [65, 148], in addition to van der Waals and electrostatic repulsion (DLVO forces), are the main reason for this shortcoming. In the case of hydrophilic nanoparticles in an aqueous solution with high ionic strength, hydration repulsion energy may be considerable [149, 150]. The hydration force is a strong short-range repulsive force that acts between polar surfaces separated by a thin layer of water, which decays quasi-exponentially with decay lengths of about 1 nm [71]. Although there are some theoretical explanations about the origin and mechanism of hydration force (e.g. water-structuring models, image-charge models, excluded-volume model, and dielectric-saturation models [72]), colloidal science researchers generally believe that despite the proposed explanations, the origin of hydration repulsion remains unclear [73]. The hydration force in the acidic solutions, due to the penetration of protons into the surface, is not observed [151].

Based on these studies, in the absence of any surfactant or polymer, the electrical double layer can be considered as a possible repulsion force between hydrophilic silica nanoparticles while the van der Waals forces are responsible to the attraction force for hydrophilic silica nanoparticles. Since silica nanoparticles in the seawater are extremely unstable, van der Waals attraction outweighs the electrical double layer. In this research, a new method to disperse hydrophilic silica nanoparticles in seawater with the assistance of hydrochloric acid (HCl) is proposed and its effectiveness is experimentally evaluated. It worth to mention that there are numerous works have been done using surfactants and polymers to stabilize nanoparticles in high salinity solutions [152-154]. However, using surfactants or polymers is made challenging by a number of factors, such as the adsorption of surfactant to the rock during the injection and lost their effectiveness in the hard salinity and high temperatures which raise the possible

plugging. Conventional surfactants for EOR are also sensitive to hydrolysis [117, 155]. Moreover, surfactant and polymers are relatively expensive in the compare of using HCl.

3.3. Experimental section

The general description of experiments is shown in Figure 3-4 where the experiments are divided into two general categories including part A and part B. The first part discusses the effect of most common ions in seawater on the stability behavior of silica nanoparticles. Based on the results of these experiments, in the second part, a new method is proposed to stabilize silica nanoparticles in seawater (using HCl) and its effectiveness in stabilizing silica nanoparticles in seawater is examined by visually inspecting the appearance of the dispersion, particle size, turbidity, and zeta potential measurements. It is worth to mention that the first part is done only for confirmation of previous findings (see reference [59, 156]).
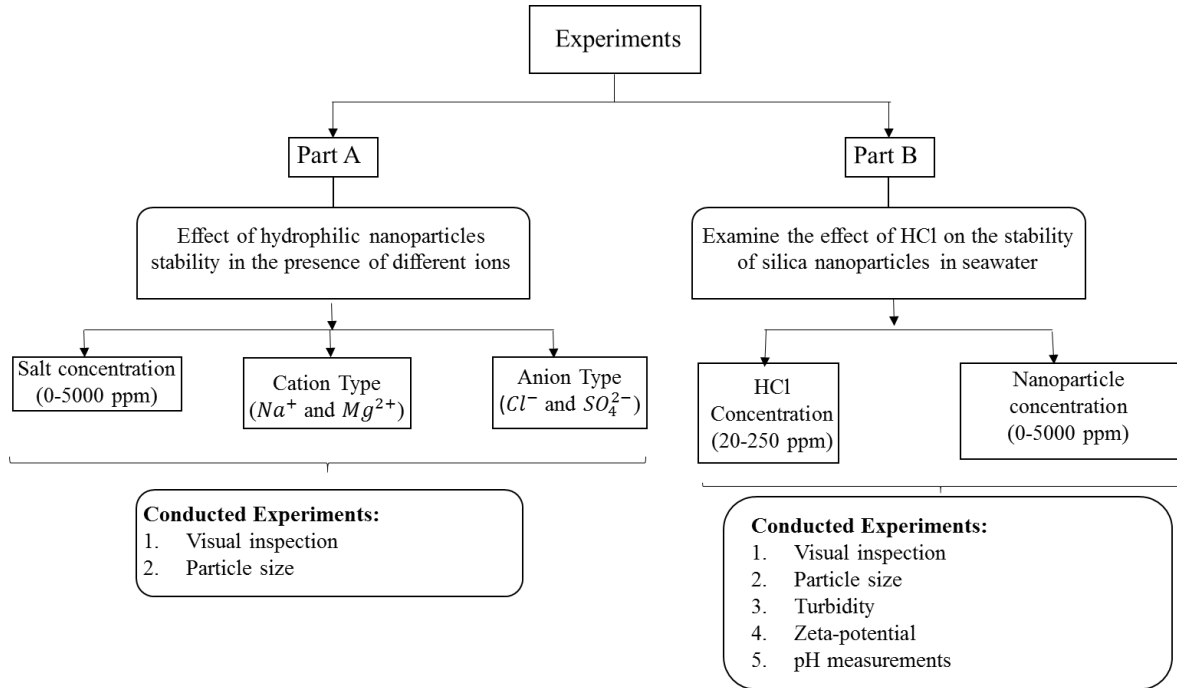
Figure 3-4: **General description of experiments**

3.3.1. Materials

Nanoparticles: The colloidal silica nanoparticle suspension (25 wt% silica nanoparticles in deionized water) with 5-35 nm diameter sizes was purchased from US Research Nanomaterial, Inc. The purity of the 25 wt% SiO_2 nanoparticles is greater than 99.99%. The solution of silica nanoparticles was used without further modifications in part A and B

Aqueous solutions: In part A, solutions of different concentrations of inorganic salts in deionized water was used as an aqueous solution. Inorganic salts including NaCl, Na_2SO_4, $MgCl_2$ and $MgSO_4$ with minimum purity of 99% was purchased from Sigma-Aldrich.

In part B, seawater was used as an aqueous solution. Seawater was collected from the Grand Banks, offshore Newfoundland which its composition is given in Table 3-1. Furthermore, different concentrations of hydrochloric acid (HCl), a 6M solution was used to form the H^+ protection layer around the nanoparticles.

Table 3-1: Seawater composition

Specification	Concentration (ppm)
Sodium (Na^+)	1,078
Magnesium (Mg^{2+})	1,284
Calcium (Ca^{2+})	412
Potassium (K^+)	399
Chloride (Cl^-)	19,353
Sulfate (SO_4^{-2})	2,712
Bicarbonate (HCO_3^-)	126
Other ions	114
Total Salinity	**35,181**

3.3.2. Methods

Stability of hydrophilic silica nanoparticles in the presence of different ions: In this part, the stability of silica nanoparticles in the presence of different ions is evaluated. These experiments are designed to investigate the effect of type, and concentration of most common ions in seawater (Na^+, Mg^{2+}, Cl^- and SO_4^{-2}) on the stability of silica nanoparticles. Hence, salt solutions with diff erent concentrations of inorganic salts were prepared. Then, 0.05wt% silica nanoparticles are added to the prepared solution and ultra-sonicated for 15 minutes. To study the effect of salt concentration on the stability of silica nanoparticles, the salt concentration was changed from 0 to 0.5 wt%. This range of salt concentration appears to be sufficient for Mg^{2+} and SO_4^{-2} ions because their concentrations in seawater are less than 0.5 wt%. However, for Cl^- and Na^+ ions, due to their higher concentrations in seawater, the stability of silica nanoparticles in the presence of Cl^- and Na^+ ions is examined up to the critical salt concentration of NaCl. Critical salt concentration is the maximum concentration of a salt in a nanoparticle solution in which the solution is still stable.

The influence of cations on the stability of silica nanoparticles was explored by selecting the salt solutions with the same anions but different cations. For instance, in order to evaluate the effect of Na^+ and Mg^{2+} ions on the stability of silica nanoparticles, the stability of nanoparticles in the solutions of NaCl and $MgCl_2$, or Na_2SO_4 and $MgSO_4$ was compared. In these cases, the effect of anions on the stability of nanoparticles in the both solutions is similar and the differences are due to cations. Similarly, to examine the effect of anions, the salts with the same cation but different anions were selected (NaCl- Na_2SO_4 and $MgCl_2$- $MgSO_4$).

In all experiments, the procedure described in supplementary material is used to evaluate the stability of silica nanoparticles. According to this procedure, in the first step, the samples are

visually inspected. The duration of this step depends on the required stability period for the practical application. In this study, the duration of the first step for all experiments was 48 hours. The purpose of this step is to inspect and record the cloudiness of solutions and possible sediments in the solutions. At the end of this step, the solutions without obvious precipitation or severe cloudiness were selected for particle size measurement and solutions with precipitation or severe cloudy solutions were considered unstable. It should be noted that the analysis of appearance characteristics can be only used for screening of the obvious unstable solutions with possible stable ones and the final decision about the stability or instability of solutions cannot be made in this stage.   In order to judge the stability or instability of solutions, first, based on the purpose of experiments and its practical applications, the term of "stability" should be defined clearly. Then, the particle size measurements should be conducted to see how the solutions meet the defined criteria.

The "stability of nanoparticles" needs to be defined clearly for enhanced oil recovery purposes. To use nanoparticles in the EOR processes safely, the size of nanoparticles in the solution should be far less than pore throats diameter to avoid possible plugging in the pore throats (log-jamming). In the conventional oil reservoirs, the size of pore throats (diameters) is generally greater than 2 μm [157]. For instance, for the coarse sandstone reservoirs this size is mostly ranging between 4 to 7 μm [157, 158] and for carbonate reservoirs range of 3 to 10 μm is reported in the literatures [159, 160]. In addition of pore throat size and particle size, log jamming is also affected by particle hydrophobicity, particle retention, fluid ion strength, and formation conditions [161]. Hence, it is difficult to find a unique size for nanoparticles to prevent log jamming.   Based on the definition of nanoparticles, the particle that their size (at least in one dimension) is between 1 to 100 nm [9], we choose 100 nm, assuming that if the

size of nanoparticles in solution is less than 100 nm, the samples are still "stable" and can be applied for EOR processes. However, if the size of nanoparticles is greater than 100 nm or the particle size measurement instrument did not pass the quality check, the solution is considered unstable. Normally, in the case of high polydispersity or bad optical quality (severe cloudy samples) the instrument does not pass the quality criteria.

In this research, the size of the nanoparticles is measured with a Malvern Zetasizer Nano Series ZS instrument which calculates the size of the particles by measuring the Brownian motion of the particles in a sample using Dynamic Light Scattering (DLS).

Effect of hydrochloric acid on the stability of silica nanoparticles:

Several experiments were designed to assay the impact of hydrochloric acid on the stability of silica nanoparticles in seawater. The detail of experiments is provided in the supplementary section. The appearance characteristics of nanoparticle solution for the listed concentrations of HCl and silica nanoparticles were analyzed. Then, particle size, turbidity, zeta-potential and pH of solutions were measured. In order to avoid any contamination during measurements, the solutions after preparation were split into five samples. One sample was used for visual inspection and four of the samples were separated for the following experiments.

Particle size measurements: After completing the visual inspection, the visually stable solutions were selected for particle size measurement. It should be noted that DLS-based instruments like the Malvern zetasizer, measure the hydrodynamic size of the nanoparticles. This size is directly related to the diffusive speed of the particles in the solution. The diffusive speed can be affected by altering the Debye length. Hence, the hydrodynamic diameter not only depends on the size of the particle "core", but is also governed by the surface structure,

46

the type of ions, and the ionic strength of the solution. At low ionic strengths, the thickness of the electrical double layer or Debye length increases and consequently, the diffusion speed reduces, and a larger apparent dynamic diameter is obtained.

The size of nanoparticles in each sample was measured in three separate runs at ambient temperature and pressure. For each run, the intensity-weighted mean diameter was recorded and the average of the three runs is reported. The intensity-weighted average is very sensitive to the presence of aggregates and contaminants.

pH measurement: One of the four sets of samples was selected to measure the pH. The pH of the samples was measured with a Denver instrument up-5 pH-meter. In order to avoid any contamination, the pH probe was carefully cleaned with deionized water and calibrated using standard or "buffer" solutions before each measurement. For each nanoparticle solution, three separate pH measurements were conducted for repeatability and the average value is reported.

Turbidity measurement: To detect very small changes in the solution clarity, the turbidity of the samples was measured using a Turbidimeter 2100Q StablCal Standards instrument. The turbidity-meter measures the cloudiness or haziness of the fluid sample and normally is reported in Nephelometric Turbidity Units (NTU). The instrument was calibrated by using the StablCal® turbidity standards and the calibration was checked regularly during measurements. The turbidity of each nanoparticle solution was measured four times for repeatability and the average value was taken.

Zeta-potential measurement: The zeta-potential of the samples was measured with a Malvern Zetasizer nano series ZS. Before each zeta-potential measurement, the zeta cell was rinsed carefully with alcohol and deionized water. In order to ensure the accuracy of the measured

data, we ensured the instrument's quality check passes for each nanoparticle solution and the measurements were repeated three times.

DLVO calculation: The results of the experiments were compared with the well-known DLVO theory. To calculate the DLVO theory, equations 3-1 to 3-5 were used to calculate the electrostatic repulsion (E_{EL}) and equation 3-6 were used to calculate the Van der Waals attraction forces (E_{vdw}). The total potential was calculated by using the following equation:

$$Total\ potential = E_{EL} - E_{vdw} \qquad\qquad (3\text{-}7)$$

3.4. Results and discussion

3.4.1. Effect of different ions

The sizes of silica nanoparticles in the solutions containing different salt concentrations were investigated and the results were compared with DLVO theory. As depicted in the supplementary section, for the nanoparticle solutions containing up to 0.5 wt% of NaCl and Na_2SO_4 salts, no remarkable change in the size of the nanoparticles was observed and the silica nanoparticles were stable in both solutions. The NaCl and Na_2SO_4 have the same cation (Na^+) but different anions (Cl^- and SO_4^{2-} , respectively). Since silica nanoparticles are negatively charged in a wide pH range, anions are repelled with the nanoparticles while the cations are attracted. Hence, it is safe to assume that the concentration of anions in the electrical double layer of silica nanoparticles is far less than that of cations. Therefore, the stability of silica nanoparticles is mostly governed by the type and concentration of cations. Since the type of cation in both cases was the same (Na^+), the stability of silica nanoparticles was only dependent on the concentration of the cation. The concentration of Na^+ in Na_2SO_4 is twice that of NaCl (for the same salt concentrations), however, tested concentrations are far less than the critical

salt concentrations of Na^+ and because of that, the size of nanoparticles is virtually the same for both cases. It is worth to mention that critical Na^+ concentration was obtained as high as 6 wt%.

The stability of silica nanoparticles in the presence of Na_2SO_4 and NaCl is modeled with DLVO theory and the results are illustrated in Figure 3-5. DLVO calculations show that there is a relatively large "repulsive energy barrier" or "energy barrier" for the aggregation of nanoparticles in both salts solutions. In other words, the electrostatic repulsion in both cases of the calculated concentrations is stronger than the attractive van der Waals force in a wide range of distances between particles. Hence, when nanoparticles approach each other, the energy barrier prevents them from sticking and aggregating.

The value of repulsive energy barrier for the NaCl solution in all concentrations is higher than Na_2SO_4. The repulsive energy barrier of NaCl is about 5x higher than Na_2SO_4 in 0.1 wt% and it increases to around 9x in 0.5 wt%. There are two main reasons for this trend. First, in the same concentration of both salts, the concentration of Na^+ in the Na_2SO_4 is twice that of NaCl. Second, the charge of SO_4^{2-} is also twice that of Cl^-. These differences cause a shorter Debye length for nanoparticles in the Na_2SO_4 and consequently less electrostatic repulsion and less of an energy barrier. On the other hand, there is a secondary minimum in the Na_2SO_4 solution especially for the solution of 0.5 wt%, which it is not observed in the same concentration of NaCl. The secondary minimum shows a weak aggregation structure which can be broken with modest shear stress. In general, DLVO theory predicts the stable solution for both cases which have a great harmony with experiments.
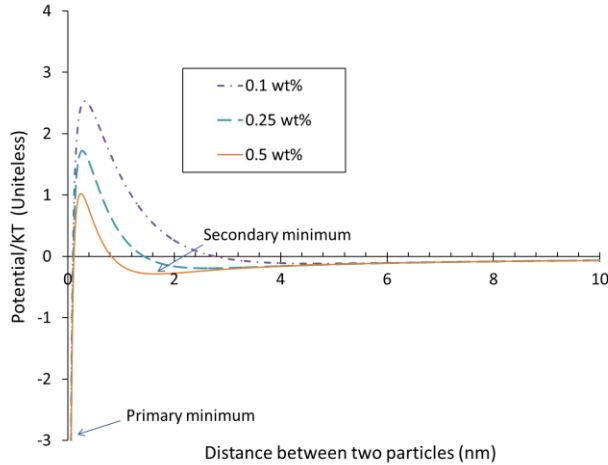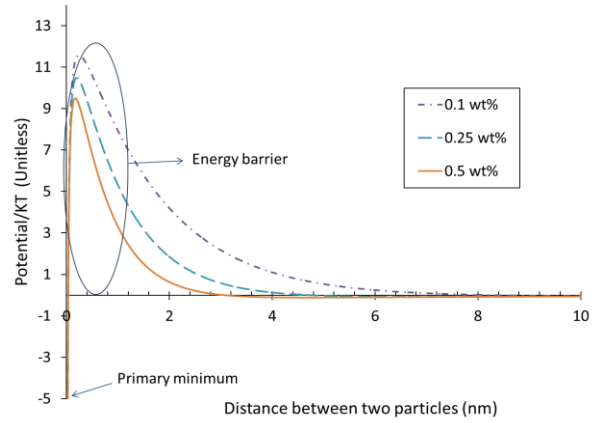
Figure 3-5: DLVO calculation for silica nanoparticles in the presence of (a) Na$_2$SO$_4$ and (b) NaCl

The size of silica nanoparticles in the presence of different concentrations of NaCl-MgCl$_2$ and Na$_2$SO$_4$-MgSO$_4$ is illustrated in Figure 3-6a and Figure 3-6b, respectively. It was observed that for concentrations higher than 0.1 wt% of MgCl$_2$ and MgSO$_4$, the size of the nanoparticles grew rapidly and the silica nanoparticles were not stable. However, they were stable in the solution of NaCl and Na$_2$SO$_4$ salts in the tested concentrations. Again, this stability behavior of silica nanoparticles should be sought in the cations of the salts. The results show that Mg^{2+} as a divalent ion can destabilize nanoparticles more effectively than Na$^+$ as a monovalent one. These results are consistent with the literature [59, 156]. In general, it appears that divalent ions are screening the charge of silica nanoparticles more effectively than monovalent ions where divalent (and multivalent) ions in the electrical double layer of nanoparticles can destabilize the nanoparticles in the solution.

50

The stability of silica nanoparticles in the presence of different concentrations of $MgSO_4$ and $MgCl_2$ is modeled by DLVO theory and the results are shown in Figure 3-7. For $MgCl_2$ salt in 0.025 wt%, a repulsive energy barrier is predicted which it goes zero in 0.5 wt%. Therefore, the critical salt concentration is predicted to be 0.05 wt%. This means that the silica nanoparticles in solutions that contain less than 0.05 wt% $MgCl_2$ are stable. However, they are unstable in solutions of higher concentrations. For $MgSO_4$ salt, the DLVO theory predicts an unstable solution for all modeled concentrations. In general, DLVO theory has a great consistency with experimental data in the high salt concentrations. However, while the DLVO theory was predicted to be an unstable solution for all concentrations of $MgSO_4$, experimental results show that for less than 0.1 wt% of $MgSO_4$, nanoparticles are stable.

(a)   (b)
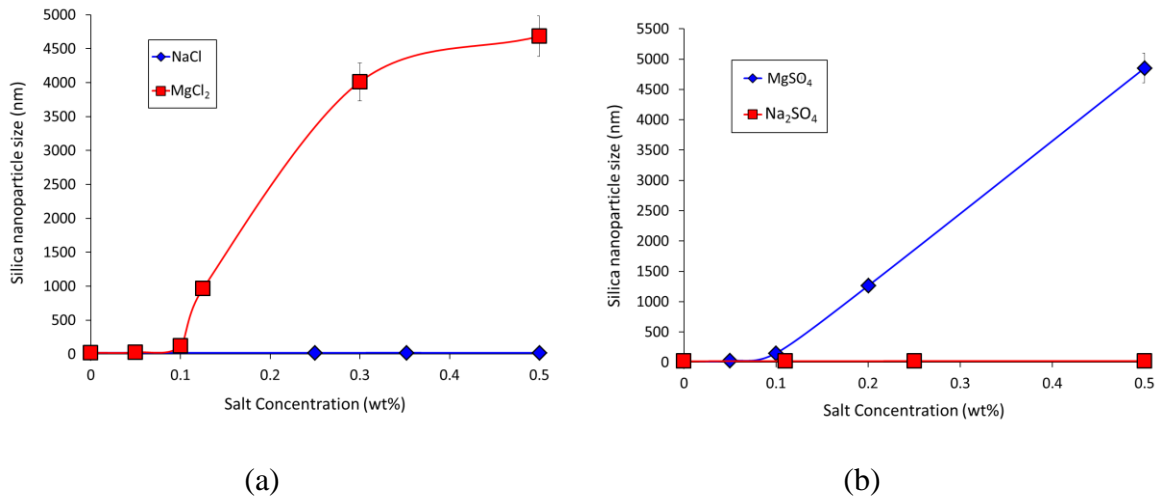
Figure 3-6: **Silica nanoparticle size in the presence of (a) NaCl and $MgCl_2$ ions, and (b) Na_2SO_4 and $MgSO_4$ ions**

(a)

(b)
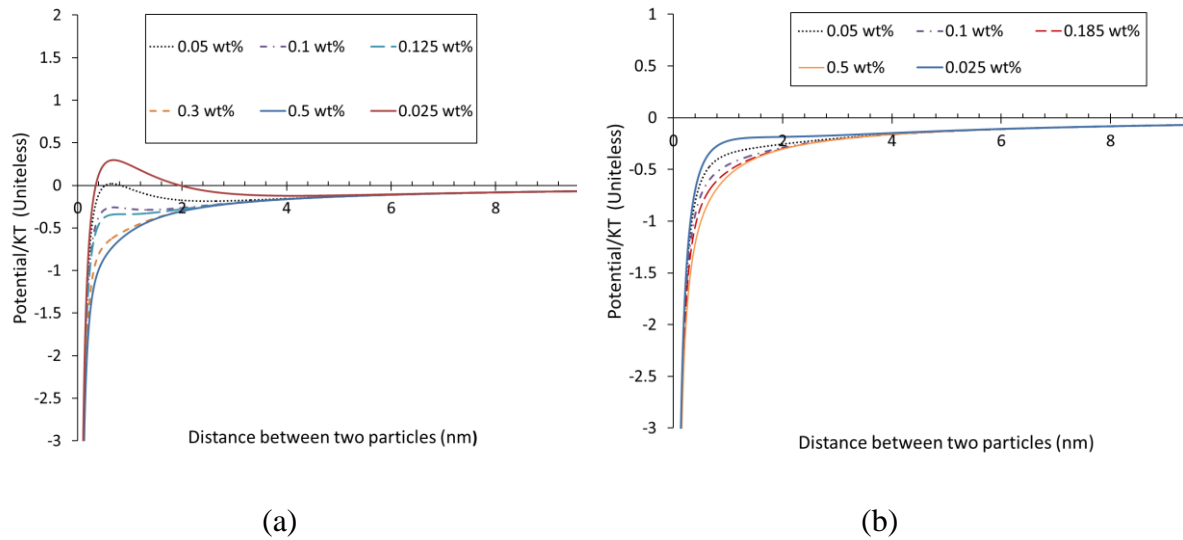
Figure 3-7: **DLVO calculation for silica nanoparticles in the presence of (a) MgCl$_2$ and (b) MgSO$_4$.**

3.4.2. Stability of silica nanoparticles in seawater and H+ protected theory

As Keller et al. [162] studied, metal oxide nanoparticles are not stable in seawater. To confirm the instability of silica nanoparticles in seawater, two solutions of 0.15 wt% of hydrophilic silica nanoparticles in seawater were prepared. One solution was ultra-sonicated for 15 minutes and another one was mixed by a magnetic stirrer for one hour. After 48 hours, their picture was taken and the results are illustrated in Figure 3-8. It was observed that silica nanoparticles aggregate rapidly when they are introduced in seawater and they sediment in a short time (less than 1 hour).

Silica nanoparticles
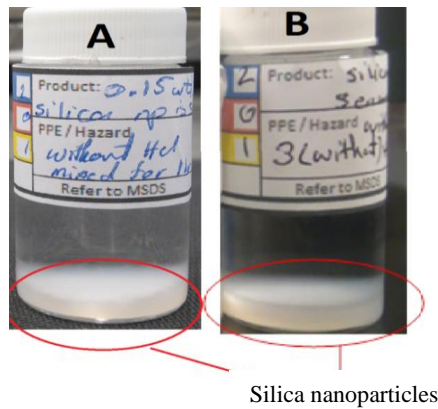
Figure 3-8: **Silica nanoparticles in seawater without HCl after mixing with magnetic stirrer (A) and ultra-sonication (B).**

The stability of silica nanoparticles in seawater was also modeled with DLVO theory. As shown in Figure 3-9, DLVO theory predicts a small energy barrier to aggregation of silica nanoparticles in seawater. However, there is also a relatively large secondary minimum which nanoparticle can trap in that. If we consider that the nanoparticles are trapped in the secondary minimum, then their aggregation most probably is reversible and they should disperse again with a magnetic stirrer or by using ultra-sonication. However, as mentioned, the experimental results show that the proposed methods are not effective in stabilizing nanoparticles and breaking the aggregations.
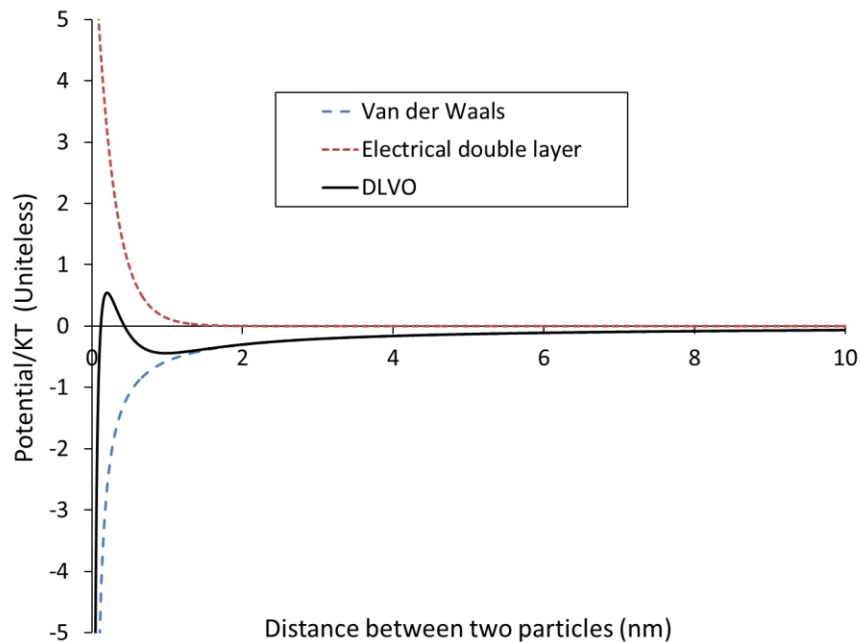
Figure 3-9: DLVO calculation of silica nanoparticles in seawater.

We propose a new method to stabilize silica nanoparticles in seawater and call it "**H⁺ protection**". As discussed in the part A of this research, the stability of silica nanoparticles is mostly governed by the presence of multivalent ions in the electrical double layer of nanoparticles. It was observed that even small concentrations of multivalent ions can destabilize silica nanoparticles. Hence, to stabilize silica nanoparticles in a solution, the presence of multivalent ions in the electrical double layer of nanoparticles should be limited. Tombácz, and Szekeres reported that H^+ has a very high affinity to neutralize negatively charged surfaces [163]. Hence, H^+ and multivalent ions in seawater (mostly Ca^{2+} and Mg^{2+}) compete to be present in the electrical double layer of silica nanoparticles. More recently, it is reported that HCl can influence the surface chemistry iron oxide nanoparticles [164].

We now demonstrate that H^+ ions can stabilize silica nanoparticles in seawater. The positively charged cations including H^+, Na^+, Ca^{2+}, and Mg^{2+}, H^+ ions are attracted and want to concentrate in the electrical double layer of silica nanoparticles. We believe that with the

sufficient H$^+$ ions in solution, the H$^+$ ions can form a protective layer around silica nanoparticles to reduce the concentration of multivalent ions in the electrical double layer of silica nanoparticles. This is represented in Figure 3-10.   First, we examine solution preparation of the H$^+$ protection and its effect on the stability of silica nanoparticles in seawater, after which we examine the effect of concentration of the silica nanoparticles and HCl used to H$^+$ protect and stabilize the silica nanoparticles in seawater.
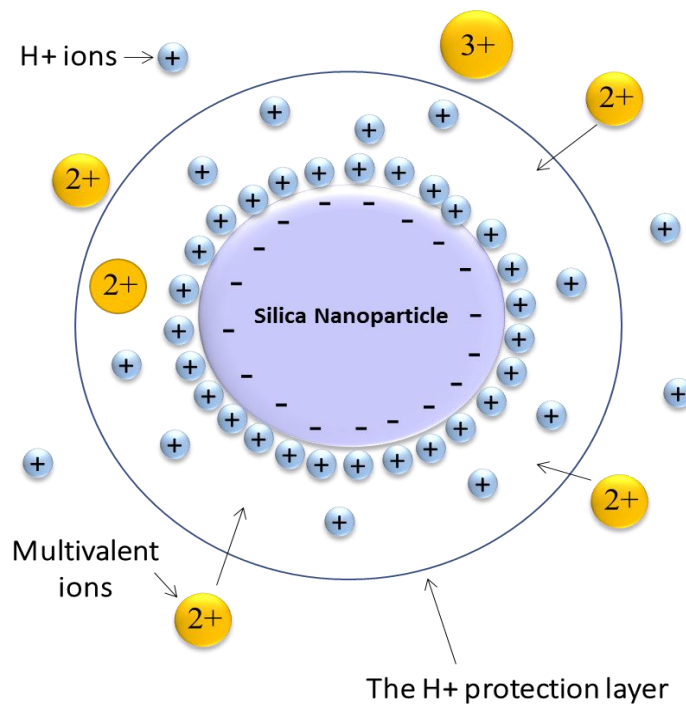
Figure 3-10: H$^+$ protection layer around silica nanoparticles

Preparation procedure: To determine whether or not the preparation procedure influences the stability of silica nanoparticles in seawater, solutions are prepared based on two different procedures. As shown in Figure 3-11, in the first procedure, hydrochloric acid (less than 10 µL) is initially diluted with a small amount of seawater (about 1000 µL) to form an acidic solution.   Then, silica nanoparticles were added into the solution. In the last step, the prepared nanoparticle dispersion was further diluted with the desired amount of seawater to achieve the

desired concentration. In the second procedure, the silica nanoparticles were added to the seawater and then, hydrochloric acid was added to the solution. All solutions, after preparation, are mixed with a magnetic stirrer for 15 minutes. Two samples with described procedures were prepared. Table 3-2 provides detailed information about the prepared samples. The results show that the size of the silica nanoparticles in the sample A after 48 hours was still around 20 nm showing that the silica nanoparticles in this solution are stable. However, the average size of silica nanoparticles in the sample B after 48 hours was 436.5 ± 4 nm showing that the nanoparticles are aggregating.

In the sample A, by initially diluting the HCl with a small volume of seawater, an extremely acidic solution was created. By adding the nanoparticles to this solution, there were sufficient free H^+ ions in the solution to accumulate in the electrical double layer of nanoparticles. Hence, the H^+ protection layer formed quickly and with a further addition of seawater, the protection layer was still stable. Preparation method B is when the nanoparticles were directly added to the seawater (neutral pH) and then the HCl was added. The multivalent ions were first to occupy the nanoparticle electrical double layer and when the HCl was added, the free H^+ ions could not invade the electric double layer to form an H^+ protection layer. Hence, multivalent ions that accumulated in the electrical double layer could destabilize the silica nanoparticles. Adding the H^+ ion to this solution could not remove the attracted multivalent ions from the electrical double layer of silica nanoparticles and the nanoparticles aggregated in preparation method B.
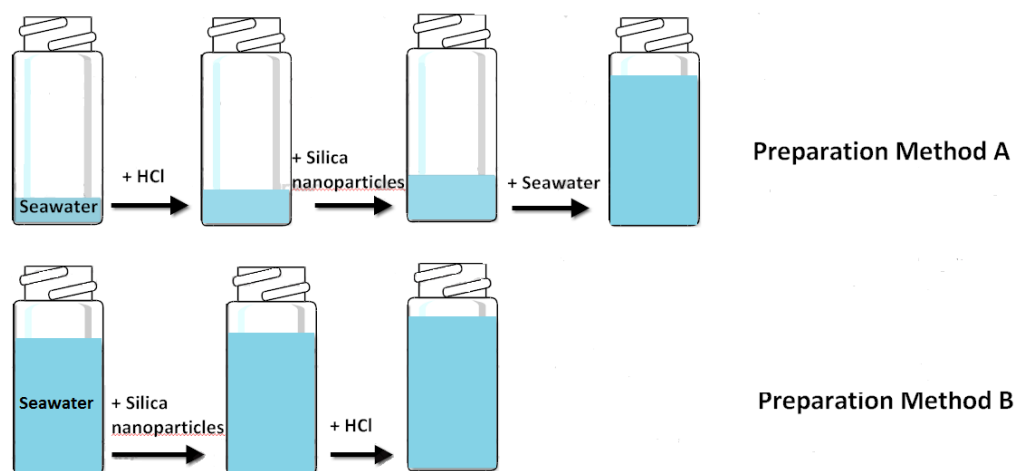
Figure 3-11: Two different preparation procedures (A & B) to prepare H$^+$ nanoparticle seawater solutions

Table 3-2: The composition of two prepared samples and their stability

Preparation Method	Nanoparticle concentration (wt%)	Seawater Volume (ml)	HCL(aq) 6M Volume (ml)	HCl Concentration (wt%)	Measured pH	Visual Stability?	Particle size after 48 hours (nm)
A	0.15	100	0.01	0.0022	6.70 ± 0.05	Stable	20.02 ± 0.8
B	0.15	100	0.01	0.0022	6.58 ± 0.05	Unstable	436.5 ± 4.0

pH of solution is another evidence for the formation of the H$^+$ protection layer. The pH of preparation method A is higher than preparation method B. This implies that in sample A, some of the free H$^+$ ions were attracted in the electrical double layer around nanoparticles and there was less free H$^+$ for the pH meter to detect.

3.4.3. Effect of HCl on the stability of silica nanoparticles in seawater

The effect of HCl on the stability of silica nanoparticles in the solutions that contain different concentrations of nanoparticles and HCl was investigated. All samples were prepared according to sample preparation method A and the stability of nanoparticles was tested based

on the procedure described in the supplementary section. The samples were visually inspected after 48 hours. Figure 3-12 to Figure 3-15 show the visual status of different concentrations of silica nanoparticles in the solutions of 0.025, 0.0076, 0.003 and 0.002 wt% HCl after 48 hours, respectively. As shown in the figures, at low concentrations of silica nanoparticles, the solutions are clear and there are no sediments or cloudiness. However, with increasing concentrations of nanoparticles, the solutions become cloudy. The change in clarity also depends on the concentration of HCl. Decreasing the concentration of HCl shows that the samples become cloudy in lower concentrations of silica nanoparticles. For instance, in Figure 3-12, for samples containing 0.025 wt% HCl, a little cloudiness is observed for samples with nanoparticle concentrations of 0.4, 0.45 and 0.5wt%. However, in Figure 3-13, for samples with 0.0076 wt% HCl, the obvious cloudy condition begins at sample 7 (sample with 0.3 wt% silica nanoparticles) and increases in Samples 8 to 11.

Figure 3-12: The visual status of silica nanoparticles with different concentrations (the concentrations are written on the top of each sample) in the solution of seawater with 0.025 wt% HCl after 48 hours.
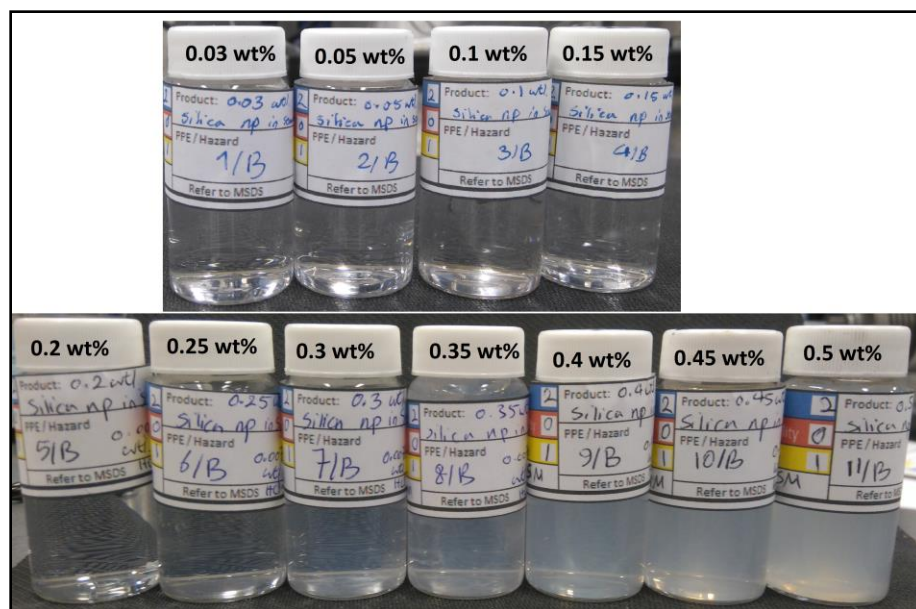
Figure 3-13: The visual status of silica nanoparticles with different concentrations (the concentrations are written on the top of each sample) in the solution of seawater with 0.0076 wt% HCl after 48 hours.
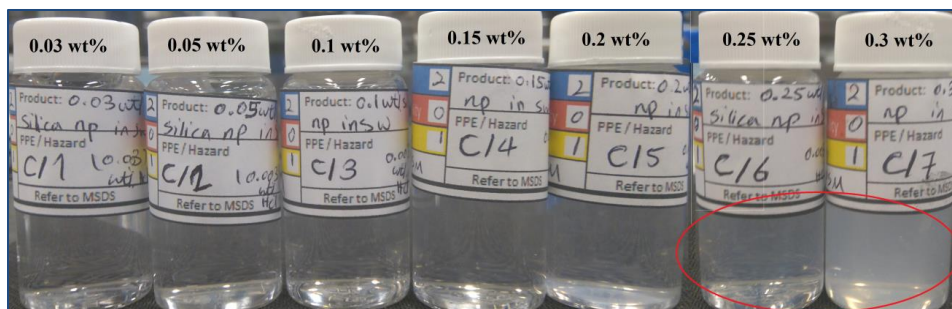
Figure 3-14: The visual status of silica nanoparticles with different concentrations (the concentrations are written on the top of each sample) in the solution of seawater with 0.003 wt% HCl after 48 hours.
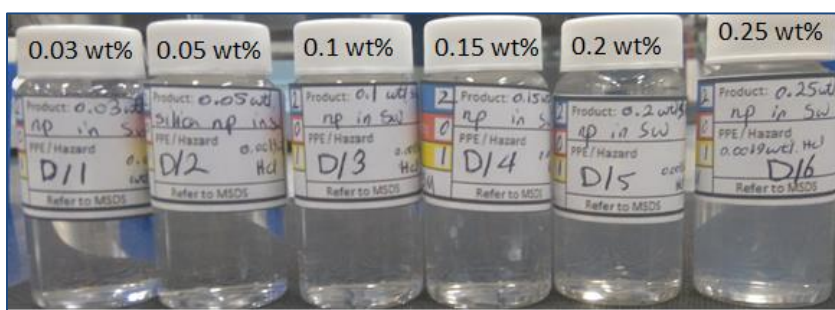
Figure 3-15: The visual status of silica nanoparticles with different concentrations (the concentrations are written on the top of each sample) in the solution of seawater with 0.002 wt%.

Turbidity is a better measure of cloudiness than visual inspection. The turbidity of the prepared samples was measured and the results are reported in Figure 3-16. As expected, the turbidity of samples is directly related to the concentration of nanoparticles and reversely to the HCl concentration. For the samples containing 0.025 wt% HCl, the turbidity does not change significantly by increasing the concentration of silica nanoparticles. Furthermore, it is observed that for samples containing 0.0076, 0.003 and 0.002 wt% HCl, the cloudiness is starting from samples 6, 6 and 5, respectively. The turbidity of these samples is pointed in Figure 16. For the samples containing 0.003 and 0.002 wt% HCl, the observations are confirmed with the turbidity measurements. However, in the sample with 0.0076 wt%, the cloudiness is starting from sample number 6 which is not distinguishable with visual observations. Hence, in order to reduce the possible human errors, replacing the visual observations with the turbidity

measurements can be considered as an option. It is worth to mention that the accuracy of measured turbidity is ± 0.05 NTU.
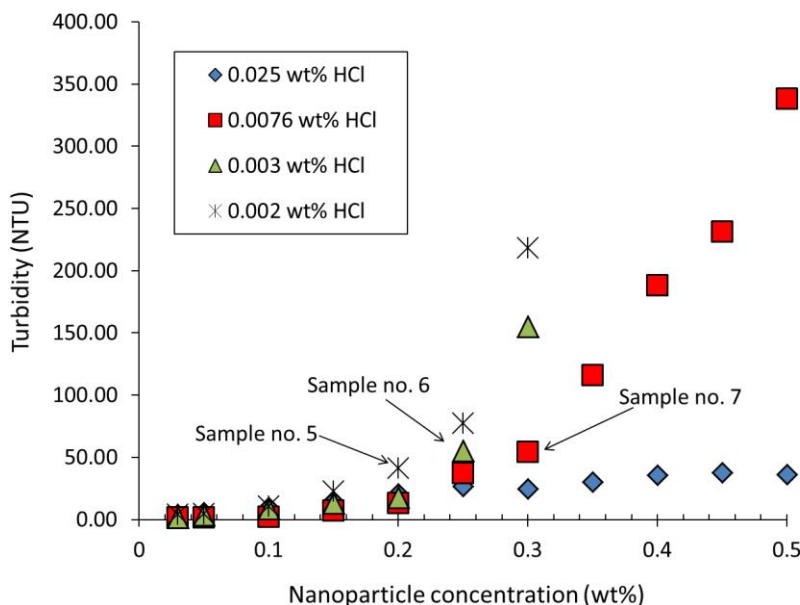
Figure 3-16: The turbidity of samples as a function of the concentration of nanoparticles and HCl

In the second step of the stability analysis, the average size of nanoparticles is measured. The change in the average size of nanoparticles by altering the concentration of nanoparticles in the solutions of four distinct HCl concentrations including 0.025, 0.0076, 0.003 and 0.002 wt% HCl is shown in Figure 3-17. The error in the measurement of particle size is ±0.8 nm. As illustrated in the figure, for all four HCl concentrations, with increasing the concentration of silica nanoparticles from 0.03 wt%, the average size of nanoparticles exponentially increases. However, the rate of increasing is different for the samples with different HCl concentrations. For instance, in the solution of 0.025 wt% HCl, increasing in the size of nanoparticles is very gentle, however, for 0.003 and 0.002 wt% of HCl, the relatively sharp increasing in the size of nanoparticles is observed. Generally, with decreasing the HCl concentrations, the rate of increasing in the size of silica nanoparticles, increases. The exponentially increasing in the size

61

of nanoparticles is ending at the "break point concentration" where with further increasing of the concentration of nanoparticles, the size of nanoparticles is jumping to very high values. The "break point concentration" for the solutions of 0.0076, 0.003 and 0.002 wt% HCl are obtained as 0.45, 0.25 and 0.25 wt% of silica nanoparticles, respectively. These points are illustrated with arrows in Figure 3-17. For the solutions containing 0.025 wt% HCl, the "break point concentration" is higher than 0.5 wt% of silica nanoparticles. The stability analysis experiments are ended at the "break point concentrations". After this concentration, the samples not only are not stable, but also the nanoparticles may sediment during operation.
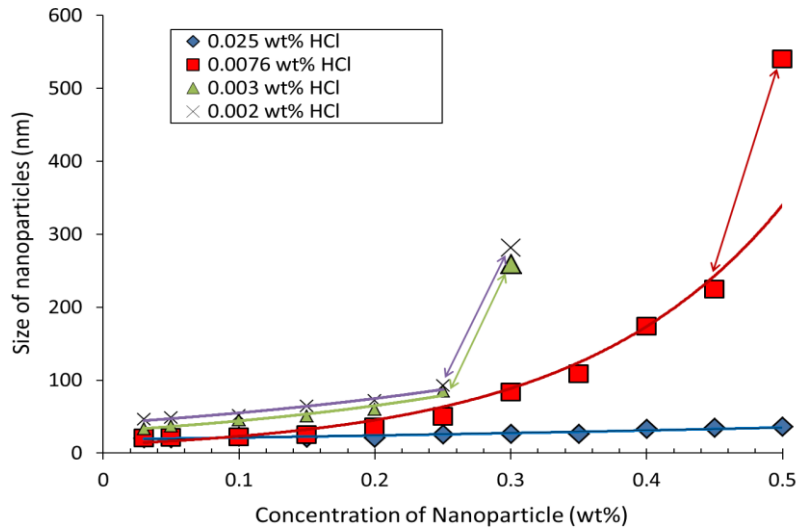
Figure 3-17: The size of silica nanoparticles in the solutions with different HCl and silica nanoparticles- The arrows are showing the "break point concentrations"

Based on the stability definition, as shown in Figure 3-18, all samples with 0.025 wt% HCl, samples 1 to 7 for 0.0076 wt% HCl and samples 1 to 6 for solutions with 0.003 and 0.002 wt% HCl are considered as a stable sample. It is worth to mention that maximum oil recovery can be obtained using solutions in which the concentration of nanoparticles varies between 0.05 to 0.1 wt% [14, 32, 165]. These concentrations are obtained using core displacement experiments.
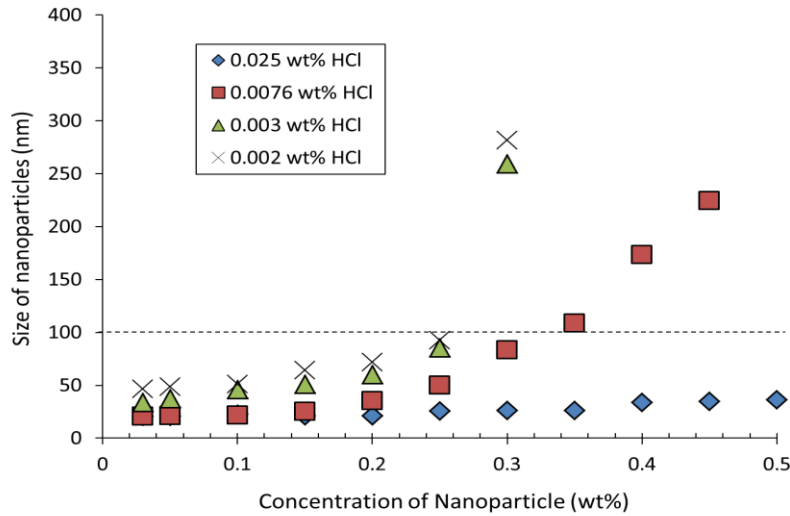
Figure 3-18: The samples with less than 100 nm size

In the solutions with constant HCl concentration, at low concentrations of silica nanoparticles, there are sufficient free H^+ ions in the solution to accumulate in the electrical double layer of each nanoparticle. Hence, the H^+ ions form an effective protection layer and prevent nanoparticles to aggregate. However, by increasing the concentration of silica nanoparticles, constant number of H^+ ions should be divided into more numbers of silica nanoparticles. Hence, the concentration of H^+ ions in the electrical double layer of silica nanoparticles, with increasing the concentration of nanoparticles, decreases. In this case, the multivalent ions had an opportunity to present in the electrical double layer of nanoparticles. Therefore, the H^+ ions could not completely prevent the nanoparticles from aggregation and the size of nanoparticles (aggregation of nanoparticles) increases. This can be observed in the change of pH in the solution. In fact, the pH-meter is measuring the number (concentration) of free H^+ ions in the solution.   As illustrated in Figure 3-19, for four samples of HCl, without silica nanoparticles, the pH is less when silica nanoparticles are introduced into the solution. With increasing the concentration of silica nanoparticles, the pH increases. The rate of increasing in the pH is sharp for low concentrations and the rate decreases with increasing the concentration of silica

63

nanoparticles till reach plateau at high concentrations of silica nanoparticles. This trend shows that with introducing the silica nanoparticles in a solution, the free H^+ ions are accumulating around silica nanoparticles and the concentration of free H^+ ions in the solution decreases. With further increasing the concentration of silica nanoparticles, the concentration of H^+ ions in the solution is not enough to form a complete H^+ protection layer around all nanoparticles. In this point, nanoparticles have adsorbed almost all added H^+ ions and the pH of solution moves toward the neutral pH and do not change anymore.
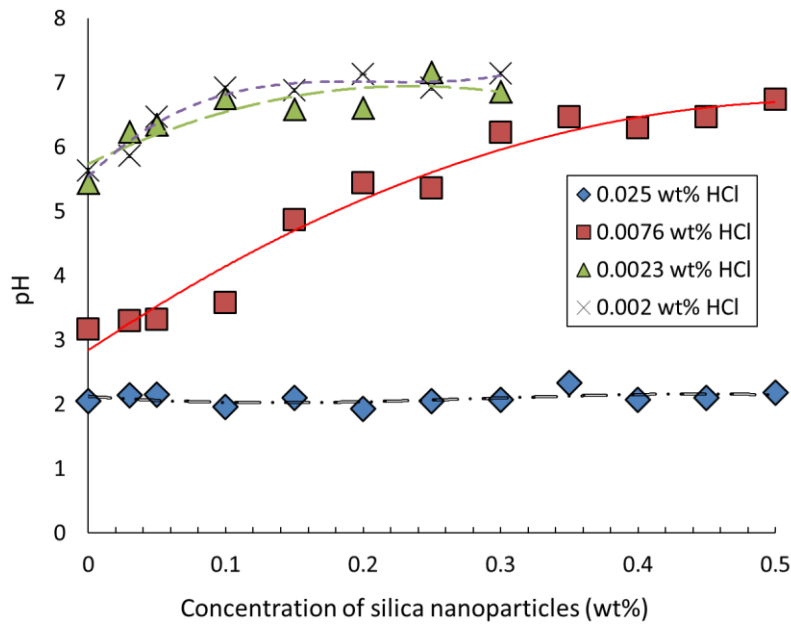
Figure 3-19: Change in the pH of samples with altering the concentration of silica nanoparticles in different concentrations of HCl

Zeta-potential measurement is another useful method to understand the mechanism of dispersing silica nanoparticles in seawater in the presence of HCl. As shown in Figure 3-20a, with increasing the concentration of HCl in the solutions, the zeta-potential of silica nanoparticles from negative values is moving toward zero, and then to positive values. On the other hand, except for the samples with 0.025 wt% HCl, the zeta-potential of samples has a decreasing trend. Regardless of HCl or silica nanoparticle concentration, the absolute value of

64

the zeta-potential in the most samples is less than 10 mV and for some samples is even less than 4 mV. At this ranges of zeta-potentials, due to the weaker electrostatic repulsion force, it is expected that the nanoparticles aggregate rapidly. However, as discussed before, the nanoparticles are stable in these ranges after 48 hours. It appears that some H^+ ions are screening the charge of silica nanoparticles with firmly sticking on the surface of silica nanoparticles between the surface of nanoparticles and the shear plane which are also the part of H^+ protection layer. Furthermore, as shown in Figure 3-20b, the zeta-potential of silica nanoparticles is not completely the function of pH. For instance, for the pH range 6-7, the zeta-potential of silica nanoparticles can be any value between -11 mV to -4 mV. It appears that in the presence of sufficient free H^+ ions in the solution, nanoparticles are adsorbing H^+ ions and the zeta-potential of nanoparticles goes to near zero or positive values. However, when the concentration of H^+ ions in the solution is not enough to screen all charge of nanoparticles, only a portion of the charge of nanoparticles is neutralized with the H^+ ions and the final zeta-potential of nanoparticles remain negative. It is worth to mention that the zeta-potential of silica nanoparticles in DI-water and at neutral pH was -22±0.5 mV.
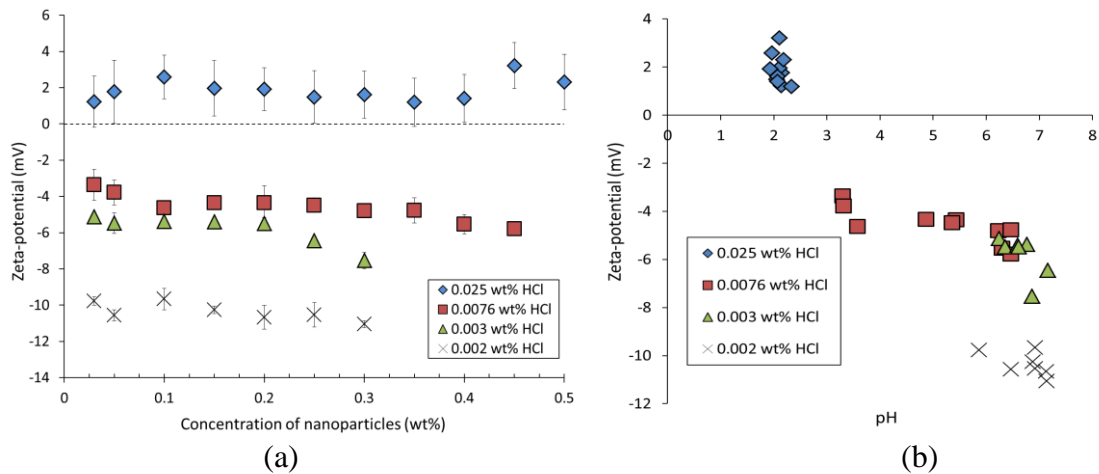
Figure 3-20: (a) Zeta-potential of silica nanoparticles in the samples with different HCl and nanoparticle concentrations, and (b) Zeta-potential of nanoparticles as a function of pH

3.5. Conclusion

In this paper, a method to stabilize silica nanoparticles in seawater is proposed. Silica nanoparticles are extremely unstable in seawater and they aggregate as soon as they are introduced in seawater. Ultra-sonicating or mixing the solution is not effective in stabilizing nanoparticles and breaking the aggregations. Based on the stability of silica nanoparticles in the presence of various ions in the aqueous solution, using hydrochloric acid to stabilize silica nanoparticles in seawater is proposed and its effectiveness is tested. It was observed that hydrochloric acid can effectively stabilize silica nanoparticles in the seawater.

The "H^+ Protection" is the possible mechanism for stabilizing of silica nanoparticles in seawater by using HCl. H^+ ions limit the presence of multivalent ions in the electrical double layer of nanoparticles and prevent them from aggregation. We observed that the average size of nanoparticles in seawater is increasing by raising the concentration of nanoparticles and decreasing the HCl concentration.

4. CHAPTER FOUR

Understanding the behavior of silica nanoparticles at oil-water interface for Enhanced Oil Recovery Implications (Paper 2, Published)

Abstract

A large number of core-flooding and micromodel experiments have examined the potential of nanoparticles to increase oil recovery. The mechanism of enhanced oil recovery using nanoparticles (nanoparticle-EOR) is still unclear. Nanoparticles may aid enhanced oil recovery because they may alter rock wettability and possibly reduce oil-water interfacial tension (IFT). The effect of nanoparticles on the oil-water IFT is controversial, as some have found that nanoparticles reduce IFT and others have illustrated that they have no significant effect. Nanoparticles' attachment at the oil-water interface, which causes IFT reduction is complex and bulk fluids properties (water and oil) directly affect their self-assembly. Fully understanding the driving forces causing self-assembly of nanoparticles at the oil-water interface and its controlling parameters are crucial for determining the effect of nanoparticles on IFT.

In this research, by investigating the controlling parameters of nanoparticle attachment at interface (bulk suspension properties including the concentration of nanoparticles, concentration of HCl, salinity, size and charge of nanoparticles, and operating conditions i.e. temperature and pressure), and coupling them with nanoparticles' stability in the solution, the conditions under which silica nanoparticles can reduce oil-water interfacial tension are experimentally investigated. The results reveal that by appropriately designing the operating conditions, H^+-protected silica nanoparticles can reduce oil-water interfacial tension. The maximum reduction of the oil-water IFT was obtained for 0.20 wt% of silica nanoparticles in a solution containing 0.025 wt% HCl and 0.15 wt% nanoparticles in 0.0076 wt% HCl, where IFT reduced from 23.56 ± 0.36 mN/m to 12.81 ± 0.77 mN/m and from 22.61 ± 0.41 mN/m to 14.01 ± 0.87 mN/m, respectively. However, the minimum IFT reduction occurs when the

surface energy reduction due to the adsorption of nanoparticles is minimal, i.e. the chance of nanoparticles to desorb from the interface due to thermal fluctuations is high, and nanoparticles' aggregation on the bulk surface is initiating.

Keywords: Enhanced Oil Recovery, Silica Nanoparticles, Interfacial Tension, Self-assembly, Adsorption Kinetics

4.1. Introduction

According to BP's 2035 Energy Outlook [1], the global energy demand will increase by 30% by 2035. At least for the foreseeable future, fossil fuels such as oil and gas will continue to play a significant role in the energy supply. Beside other techniques such as accelerating the use of renewable energies and discovering new oil fields, maximizing oil recovery from discovered and producing oil fields through Enhanced Oil Recovery (EOR) will help to meet this demand. EOR, in general, is the recovery of oil beyond primary and secondary methods (natural production and pressure maintenance with gas or water, respectively). On average, conventional production methods produce approximately one-third of the initial oil in place. The remaining oil is a large attractive target for EOR techniques.

Recently, the potential of using nanoparticles as an EOR method has been explored and some promising results have been obtained in primary evaluations [4-8, 166-168]. Nanoparticles with their ultra-small size and high surface-area to volume ratio have the ability to penetrate pores and alter the rock-fluid and fluid-fluid properties favorably. It is reported that nanoparticles may affect the oil-water interfacial tension [12-15] and rock wettability [16-19]; the effect of nanoparticles on the oil-water interfacial tension is not conclusive. Some researchers have shown that nanoparticles can reduce the oil-water interfacial tension [12-14,

69

90-92, 169], but opposing results can also be found in the literature [93-95]. In some cases, this contradiction arises from using surfactants as the stabilizer of nanoparticles in the solvent. It is well-documented that surfactants can stabilize nanoparticles in a high salinity aqueous solution by providing steric repulsion forces [170, 171]. Some researchers believe that nanoparticles alone cannot change the oil-water interfacial tension and the IFT reduction is due to the synergistic effect of surfactant and nanoparticles [96-98]. Ravera *et al.* [93] showed that silica nanoparticles alone are completely hydrophilic; hence they have no effect on the oil-water interfacial tension. However, by increasing the concentration of surfactant in the solution, the adsorption of the surfactant as individual ions alters the wettability of particles and provides a partially hydrophobic character to the surface, thus nanoparticles can be adsorbed at the interface and reduce the oil-water interfacial tension. The hydrophobic property of the surface increases by surfactant concentration; however, if the concentration of used surfactant is increased further, a surfactant bilayer will form which would make the nanoparticles hydrophilic again. These controversial results can also be found in experiments using nanoparticles without any surfactant. Table 4-1 summarizes the effect of pure nanoparticles (without additional additives) on oil-water interfacial tension. Hendraningrat *et al.* [14] showed that 0.05 wt.% of silica nanoparticles in 3.0 wt% NaCl brine can reduce the crude oil-brine IFT from 19.2 Nm/m to 7.2 Nm/m. However, Ravera *et al.* [94] illustrated that silica nanoparticles alone (without any surfactant) in 0.06 wt% NaCl had no effect on the oil-water interfacial tension. Since the reduction of the oil-water interfacial tension can reduce the capillary pressure and helps to recover the trapped oil, it is necessary to resolve this uncertainty. To this end, the mechanism of oil-water IFT reduction by nanoparticles and the conditions

70

under which the nanoparticles can reduce oil-water interfacial tension should be addressed in detail.

Table 4-1: The effect of different nanoparticles on oil-water IFT

Type of Nanoparticles	Size of NP (nm)	Conc. (wt%)	Aqueous phase	Oil phase	Initial IFT	Final IFT	Reference
Silicon oxide (SiO₂)	7	0.05	3 wt% NaCl	Crude oil	19.20	16.90	[100]
Silicon oxide (SiO₂)	12	0.4	5 wt% NaCl	Light crude oil	26.5	1.95	[90]
Silicon oxide (SiO₂)	12	0.4	5 wt% NaCl	Heavy Crude oil	28.3	7.3	
Silicon oxide (SiO₂)	12	5	5 wt% NaCl	Crude oil	21	21	[101]
Silicon oxide (SiO₂)	15	1	0.06 wt% NaCl	Hexane	51	51	[94]
Silicon oxide (SiO₂)	15	1	Pure water	Hexane	51	51	[93]
Silicon oxide (SiO₂)	21-40	0.05	3 wt% NaCl	Crude oil	19.2	7.9	[14]
Silicon oxide (SiO₂)	20-70	0.4	5 wt% NaCl	Crude oil	26.5	38.4	[102]
Non-ferrous metal nanoparticles	90-110	0.001	Pure water	Crude oil	31.4	9.2	[8]
Iron oxide (Fe₃O₄)	20-35	0.3				2.25	
Sluminum oxide (Al₂O₃)	40	0.3	2.5 wt% NaCl	Propane	38.5	2.75	[91]
Silicon oxide (SiO₂)	10-30	0.3				1.45	

Nanoparticles must first adsorb on the oil-water interface if they are to affect the interfacial tension. The first challenge is to determine whether, and under what conditions, nanoparticles can adsorb onto fluid-fluid interface. Nanoparticles can adsorb on the interface by forming a Langmuir monolayer (also called "spreading monolayer" [172]), or Gibbs monolayers (or "adsorption monolayer" [173]). In the Langmuir monolayer, a particle film with the assistance of a spreading solvent directly deposited onto the interface [174]; however, in the Gibbs

monolayer, the nanoparticles spontaneously adsorb onto the interface from the bulk suspension [175]. Specific circumstances are required to form Gibbs monolayers. Adsorption needs to be energetically favorable [174], in other words, particles move from the bulk solution to the lowest-energy position at the interface [174]. Hence, for strong trapping of nanoparticles at the interface, a significant decrease in the free energy of the interface is required [173]. Surface (interfacial) energy reduction (ΔE) due to the adsorption of a single spherical particle can be obtained by the following equation [176]:

$$\Delta E = -\gamma_0 \pi r^2 (1 - |cos\theta|)^2 \tag{4-1}$$

where r is the radius of the spherical particle, γ_0 is the pristine interfacial tension and θ is the contact angle of the nanoparticle at the interface. In order to have an irreversible adsorption, ΔE needs to significantly exceed thermal fluctuation of particles ($K_B T$). Adsorption of micrometer-sized particles at the oil-water interface is extremely stable due to very high attachment energy ($10^7 K_B T$, where K_B is the Boltzmann constant and T is temperature) [177]. However, for nanoparticles, the attachment energy is on the order of thermal fluctuations ($K_B T$), which makes them very unstable at the oil-water interface [178]. Therefore, adsorption of nanoparticles at the oil-water interface at reservoir conditions (high temperature) can also be limited by thermal fluctuation of nanoparticles at high temperature.

Measuring the particle contact angle at the interface is very challenging [179]. It makes equation 4-1 difficult to use in the practical calculations. Hence, a new alternative equation is proposed to calculate the surface energy reduction [180]:

$$\Delta E = \frac{\gamma_0 - \gamma_\infty}{\emptyset_\infty} \pi r^2 \tag{4-2}$$

where γ_∞ is the interfacial tension and $\emptyset_\infty$ is the fractional coverage of the interface at steady state condition. Bizmark *et al.* [148] developed a new model to calculate the adsorption energy (ΔE) exclusively by using dynamic interfacial tension measurements. At early time, the nanoparticle adsorption to the interface can be calculated by:

$$early\ time{:}\ t \to 0 \qquad\qquad \gamma = \gamma_0 - \tag{4-3}$$

$$2N_A|\Delta E|C_0\sqrt{\frac{Dt}{\pi}}$$

where N_A and C_0 are Avogadro's number and molar bulk concentration, respectively. D can be calculated using the Stokes-Einstein equation:

$$D = \frac{K_B T}{6\pi\mu r} \tag{4-4}$$

where K_B is the Boltzmann constant, T is temperature and μ is the viscosity of the solvent.

Further adsorption of particles at the interface may be shielded by other nanoparticles that are already adsorbed at the interface [174]. Spontaneous adsorption occurs when enough space is created at the interface for new particles to adsorb in the adsorption time scale [181].

The adsorption mechanism of charged nanoparticles from a polar solvent onto the interface can be even more complicated. If the particles in the aqueous phase and oil-water interface carry the same charge, particles will be repelled by the interface [98]. This phenomenon is common when the particles are introduced from the aqueous phase. Overlap in the electrical double layer around particles and the interface creates a strong repulsion that prevents particles from adsorbing at the interface [182]. Moreover, the interactions between adsorbed charged particles at the interface can hamper further adsorption [173]. This phenomenon illustrates

itself in the later times of dynamic IFT measurements which the following equation is proposed to model that [173].

$$late\ time:\ t \rightarrow \infty \qquad\qquad \gamma = \gamma_\infty + \qquad\qquad (4\text{-}5)$$

$$\frac{K_1 |\Delta E|}{(\pi r^2)^2 N_A C_0} \sqrt{\frac{1}{Dt}}$$

where K_1 is a dimensionless adsorption parameter which can be calculated by the following equation:

$$K_1 = \sqrt{\frac{\pi r^2 N_A C_0 D \emptyset_\infty^3}{K_a\ 4.64}} \qquad\qquad (4\text{-}6)$$

where K_a is the adsorption constant. The ultimate coverage of hydrophilic silica nanoparticles at oil-water is controlled by van der Waals and electrostatic forces. The theoretical ultimate coverage can be obtained using equation 4-7 [183]. A hexagonal area is used to calculate the theoretical ultimate coverage because, in the case of repulsive net inter-particle forces, the adsorbed nanoparticles would be expected to rearrange themselves in a hexagonal pattern [184].

$$\emptyset_\infty = \frac{occupied\ area}{total\ hexagonal\ area} = \frac{3\pi d^2}{[6\sqrt{3}(d+h)^2]} \qquad\qquad (4\text{-}7)$$

We recently proposed a novel method to stabilize silica nanoparticles in seawater using H^+-protected method [58]. We used hydrochloric acid (HCl) to form an H^+ layer within the electrical double layer of silica nanoparticles to prevent the accumulation of multivalent ions in the diffuse layer of nanoparticles and thus stabilize them. In this research, the self-assembly of H^+-protected silica nanoparticles at the oil-water interface is studied. The nanoparticles are dispersed in an aqueous phase (NaCl and seawater) and the influence of some controlling

parameters such as bulk solution properties (concentration of nanoparticles, concentration of HCl, size and charge of nanoparticles), and operating parameters (temperature and pressure) on the self-assembly of nanoparticles and interface energy reduction is investigated. The behavior of H^+-protected silica nanoparticles dispersed in seawater is compared with silica nanoparticles dispersed in the NaCl solutions. Based on these evaluations, the condition under which H^+-protected nanoparticles can reduce oil-water IFT is proposed. Finally, the possibility of IFT reduction as a main nanoparticle-EOR mechanism is evaluated by simulating core-flooding experiments. The main goal of this study is to investigate the role of IFT reduction (due to the presence of nanoparticles) on oil recovery. We believe that IFT reduction is partially but not fully responsible for incremental oil recovery greater than waterflooding alone. We test our hypothesis by conducting silica nanoparticles in seawater flooding experimentally and comparing the results with simulations that examine the effect of a) IFT reduction only and b) the effect of altering the relative permeability, wettability, and IFT reduction.

4.2. Experimental Section

4.2.1. Materials

Nanoparticles: Amorphous hydrophilic silicon dioxide nanoparticles (SiO_2) (25 wt.% in deionized [DI] water) with the average diameter of 19.0 ± 0.8 nm and purity of greater than 99.9% were purchased from US Research Nanomaterial, Inc.

Aqueous solutions: Two distinct aqueous solutions were used in this research: a) different concentrations of NaCl solutions (1, 5, and 6 wt%) and b) seawater which was collected from the Grand Banks, offshore Newfoundland (NL). Silica nanoparticles are not stable in seawater

and they quickly aggregate. Hence, the method described in [58], "H$^+$ protected" method was used to disperse silica nanoparticles in seawater. Based on this method, hydrochloric acid prevents the multivalent ions in seawater to accumulate in the electrical double layer of silica nanoparticles by forming an H$^+$-protected layer and thus stabilizes them in seawater. We used 0.025 and 0.0076 wt% of 6M HCl (ACS Reagent, 37%, Sigma-Aldrich) to stabilize silica nanoparticles in seawater. The general properties of seawater is provided in Table 4-2.

Table 4-2: General properties of seawater

Properties	Unit	Value
Density at 22°C	g.cm^{-3}	1.02
Compressibility factor of seawater[46]	psi^{-1}	4.2×10^{-8}
Thermal expansion of seawater [46]	°C^{-1}	2.78×10^{-6}

The NaCl solution, due to its simplicity, gives us the opportunity to evaluate the effect of salinity and adsorption kinetics with a great accuracy. However, injection of silica nanoparticles dispersed in NaCl solution for nanoparticle-EOR is not practical. Seawater is widely used for water-flooding and water-based EOR methods in offshore; the dispersion of nanoparticles in seawater allows us to study the effect of silica nanoparticles on oil-water interfacial tension at practical conditions. Furthermore, discussion about the mechanism and the conditions of IFT reduction by silica nanoparticles when the nanoparticles are dispersed in seawater helps us to design more effective nanoparticle-EOR projects.

Oil phase: Newfoundland offshore crude oil was used as the oil phase in all experiments. General properties of the crude oil are listed in Table 4-3.

Table 4-3: General properties of the crude oil

Properties	Unit	Value

Gravity of dead Oil	°API	35
Density at 22°C	$g.cm^{-3}$	0.875
Oil compressibility factor	psi^{-1}	10×10^{-6}
Thermal expansion	$°C^{-1}$	0.0007

4.2.2. Methods

The experiments conducted are shown schematically in Figure 4-1 where we investigated the behavior of silica nanoparticles at the oil-water interface using two distinct aqueous phases of: a) NaCl solution and b) seawater. Nanoparticles are dispersed in seawater using H^+- protected method. The purpose of the experiments is to study the self-assembly of nanoparticles at the interface and its controlling parameters in the conventional brine solutions with different ionic strength and compare these parameters with the H^+-protected silica nanoparticles dispersed in seawater. We used dynamic interfacial tension method to study the self-assembly of the nanoparticles. Dynamic interfacial tension measurement is widely used to analyze the behavior of nanoparticles and evaluate the adsorption of nanoparticles onto the interface [43, 148, 185, 186]. Since adsorption of nanoparticles on the interface and nanoparticles' stability in the dispersed medium takes place concurrently [65], it is necessary to couple these two properties to have a clearer picture of the behavior of nanoparticles at the interface. Hence, we also conducted particle size and zeta-potential measurements for NaCl and seawater experiments.

The critical salt concentration of NaCl (the maximum concentration of a salt in which the nanoparticles are still stable in the solution) was reported to be 6 wt% at ambient conditions [58]. Therefore, the NaCl concentration in this study varied up to 6 wt%. The concentrations of HCl and silica nanoparticles were selected based on our previous study [58], where we found that we could stabilize up to 0.3 wt% nanoparticles in seawater using 0.0076 and 0.025 wt%

HCl. The pressure and temperature ranges are chosen to represent North Atlantic offshore oil reservoir conditions (temperatures up to 90 °C and reservoir pressures up to 5000 psi).
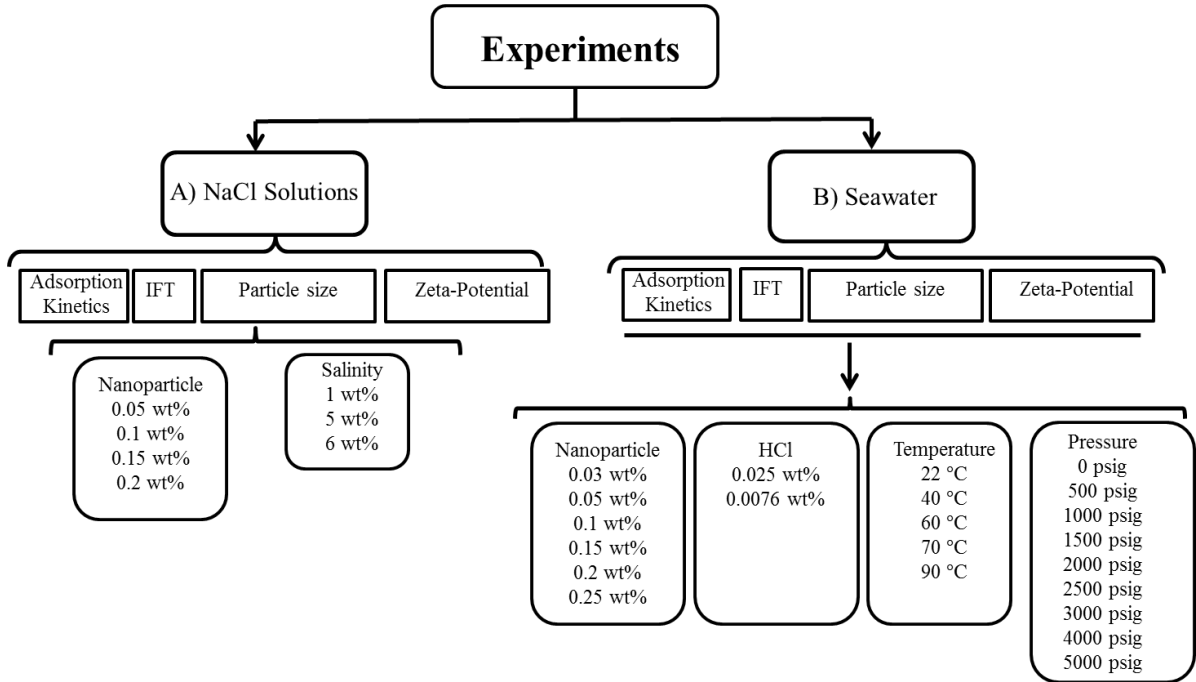
Figure 4-1: Schematic diagram of conducted experiments

IFT measurements: The pendant drop method (Vinci IFT700 instrument) was used to measure the oil-water interfacial tension. The oil phase was injected from a needle at the bottom of the cell and the image of the drop was taken at a frequency of one image per second. The schematic diagram of the oil-water interfacial tension measurement is illustrated in Figure 4-2. As shown in the figure, the droplet is held by a needle in the aqueous solution at the experimental conditions. The oil-water interfacial tension is determined from the image of the droplet, where the shape of the droplet was fitted to a shape predicted by the Young-Laplace equation and the oil-water interface is calculated by the Vinci software. The density of the crude oil and the aqueous phase was measured experimentally at ambient conditions. The density at experimental conditions was calculated based on the ambient density,

compressibility and thermal expansion of the oil and aqueous phase. To check the repeatability of the measurements, the oil-water IFT was measured three times and the average value is reported.
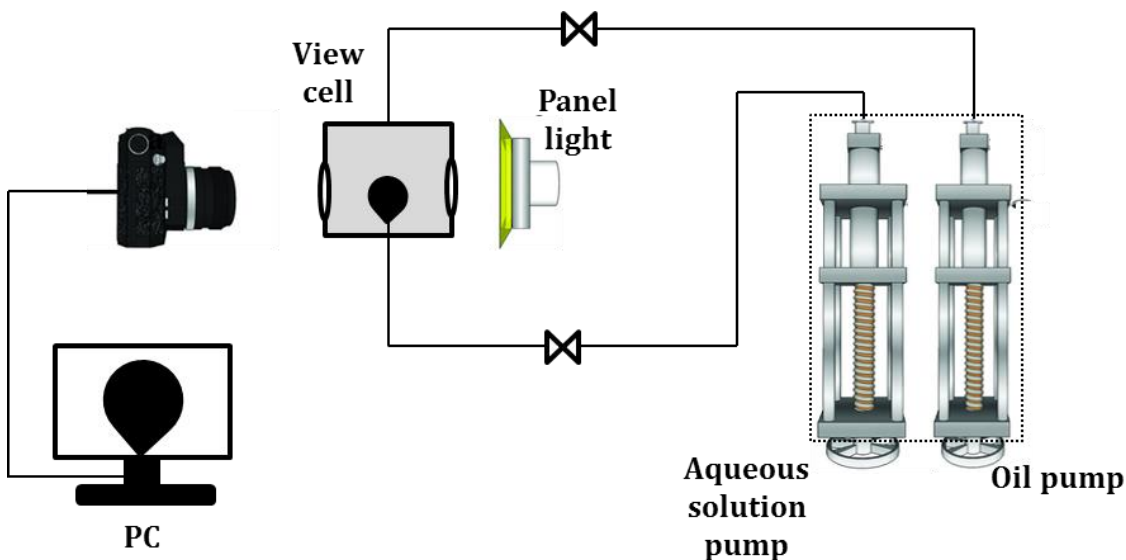
Figure 4-2: Schematic diagram of the IFT measuring instrument

Particle size and zeta-potential measurements: The size and zeta-potential of nanoparticles in different solutions were measured using Malvern Zetasizer Nano Series ZS instrument. This device measures the hydrodynamic size of nanoparticles using Dynamic Light Scattering (DLS) [47]. Disposable cells were used to measure the size of nanoparticles and to check the repeatability of the measured values, the size of nanoparticles for each sample is measured in three separate runs and the average reported.

It is not practical to directly measure the surface potential within the Stern layer. Hence, the zeta potential, as the best approximation for the surface potential, can be experimentally measured and is often used as a measure of the surface potential [38]. Prior to measuring the zeta-potential, the cell (clear disposable zeta cells DTS1060) was cleaned with ethanol and

deionized water. Then, the cell was rinsed with the prepared nanoparticle solution and filled. To prevent bubble formation in the cell, the nanoparticle solution was injected very slowly. The cell was then placed into the zetasizer and the zeta-potential of nanoparticles was measured in three replications with 150 runs for each replicate and the average is reported.

To measure the charge of the oil-water interface, the method described in [187] is used to form oil-in-water emulsions. This method is proposed to overcome the difficulties such as rapid creaming and coalescence of the emulsion droplets encountered in the preparation of oil-in-water emulsions in the absence of surfactants. In this method, to produce finely dispersed emulsions, the oil and water are mixed at the evaluated temperature of 60°C for 1 hour. Then, the solution is cooled down to the ambient condition. They [54] proposed that at elevated temperatures, the solubility of oil in water increases. Hence, some oil may dissolve in the aqueous phase and upon cooling, the excess dissolved oil may separate in fine emulsion droplets. They concluded that this method decreases the aggregation kinetics of oil-in-water emulsions (stabilizes the emulsions for a few tens of minutes) and provides sufficient time to conduct the zeta-potential measurements. Based on this method, we added one volume percentage of oil into the aqueous phase and mixed the solution for 1 hour at 60 °C using a magnetic mixer at approximately 1000 rpm. Then, the solution was filtered using a micro-size filter to achieve micro-size oil-in-water emulsions. The charge of oil-water interface was measured using Malvern Zetasizer Nano Series ZS instrument. To make sure about the repeatability of the measured zeta-potential, three distinct solutions were prepared using the described method and the zeta-potential was measured three times for each solution. The average value and standard deviation for each solution are reported.

.

4.3. Simulation Section

DLVO calculations: The interaction between oil-water interface and hydrophilic H^+-protected silica nanoparticles is described using Derijaguin, Landau, Verwey and Overbeek (DLVO) [54, 134] theory. This theory explains the interaction between a spherical colloid particle (H^+-protected silica nanoparticle) and a charged surface (oil-water interface) by combining two independent van der Waals attraction and electrostatic repulsion forces. It is plausible that in the case of adsorbing hydrophilic silica nanoparticles to the interface, due to the absence of polymer or surfactant in the solution, the steric repulsion or bridging forces are unlikely to exist. Furthermore, hydrophobic interaction normally occurs between two hydrophobic surfaces in the polar solvent. Hence, for hydrophilic silica nanoparticles in water, it is unlikely to have a hydrophobic interaction. Therefore, it appears that DLVO theory is adequate to describe the interaction between H^+- protected silica nanoparticles and oil-water interface.

The electrostatic repulsion (E_{EL}) between a spherical particle (P) and a plate surface (S) can be obtained using following equation [53]:

$$E_{EL} = \pi \varepsilon_r \varepsilon_0 a \{ 2\psi_p \psi_s \, ln \left(\frac{1 + exp(-\kappa D)}{1 - exp(-\kappa D)} \right) + \left(\psi_p^2 + \psi_s^2 \right) ln[1 - exp(-2\kappa D)] \}$$

(4-8)

where ε_r is the relative dielectric constant of water (equals to 78.5), ε_0 is the dielectric permittivity of vacuum (equals to 8.854×10^{-12} CV^{-1}m^{-1}), κ is the inverse Debye length, D is the distance between the nanoparticle and the surface, a is the radius of nanoparticle, ψ_p and ψ_s are the surface potential of the nanoparticle and the surface, respectively. The Debye length (κ^{-1}) in nanometer can be calculated as [50]:

$$\kappa^{-1} = \sqrt{\frac{\varepsilon_r \varepsilon_\circ K_B T}{e^2 \sum \rho \infty_i Z_i^2}} \tag{4-9}$$

where e represents the elementary charge of an electron (C), T is the absolute temperature (K), K_B is the Boltzmann's constant, and $\rho\infty_i$ is the number density of ion i in the bulk solution. The Van der Waals attraction forces (E_{vdw}) for a spherical nanoparticle and a surface can be calculated as [43]:

$$E_{wdv} = -\frac{A_{132}}{6}[\frac{a}{D} + \frac{a}{D+2a} + ln\left(\frac{D}{D+2a}\right)] \tag{4-10}$$

The silica nanoparticle-water-oil Hamaker constant (A_{132}) can be obtained using the Hamaker constant of silica nanoparticles (A_{11}=6.5 $\times$ 10^{-20} J) , water (A_{33}=4 $\times$ 10^{-20} J) and oil (we assumed decane) (A_{22} =5 $\times$ 10^{-20} J) [42]:

$$A_{132} = (\sqrt{A_{11}} - \sqrt{A_{33}})(\sqrt{A_{22}} - \sqrt{A_{33}}) \tag{4-11}$$

The total potential can be calculated using the following equation:

$$Total\ potential = E_{EL} - E_{vdw} \tag{4-12}$$

Core-flooding simulation: The effect of IFT reduction on oil recovery is evaluated by simulating core-flood experiments. CMG reservoir simulation software was used to mimic the core-flooding experiments and the effect of IFT reduction on oil recovery from a sample core is simulated.

4.4. Results and discussion

Before examining the effective parameters on the IFT values, the time required to stabilize the IFT value was tested. Two distinct solutions were prepared: 1) 0.15 wt% silica nanoparticles were dispersed in the 1 wt% NaCl solution, and 2) 0.15 wt% silica nanoparticles were dispersed

in seawater containing 0.0076 wt% HCl. For each solution, two sets of experiments were conducted. For the first set, the IFT measurements were continued to about 10^3 seconds and in the second set, the IFT measurements continued to 5×10^3 seconds. As shown in Figure 4-3, the main changes in the dynamic IFT values are recorded in the first 10^3 seconds and no significant changes are observed for the times greater than 10^3 second. Hence, the later measurements in this study are conducted for approximately 10^3 seconds.
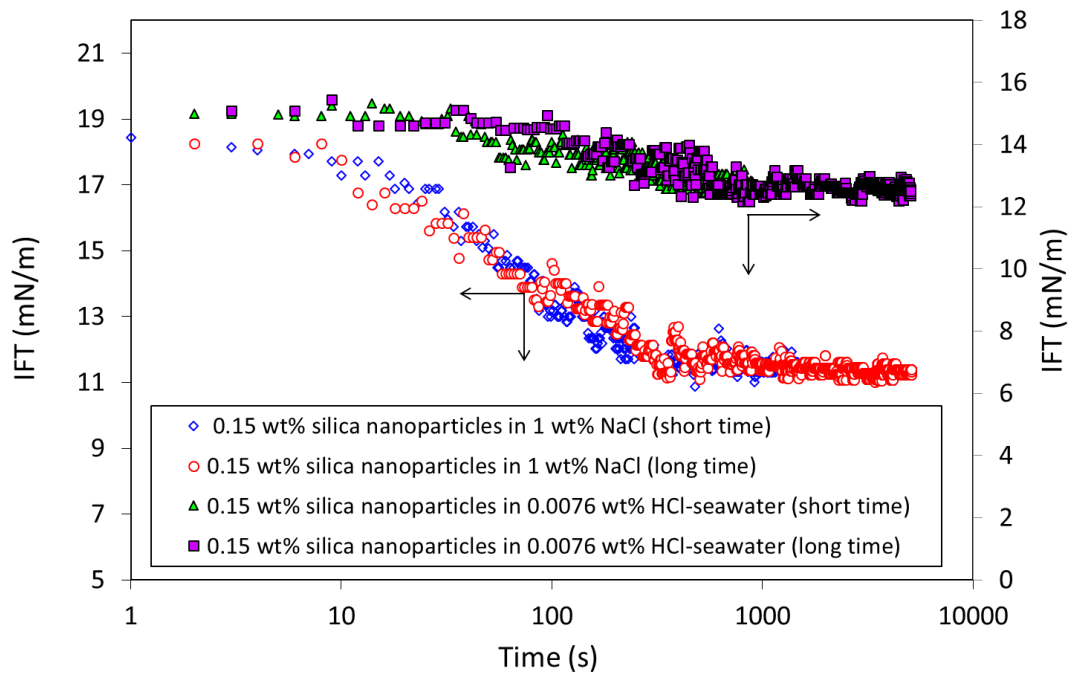
Figure 4-3: Long vs short time IFT measurement for 0.15 wt% silica nanoparticles in 1wt% NaCl solution and 0.0076 wt% HCl-seawater solutions

4.4.1. Kinetic adsorption of silica nanoparticles from NaCl brine

The adsorption of nanoparticles onto the oil-water interface is causing a change in the interfacial tension. In this section, the kinetic adsorption of silica nanoparticles onto the oil-water interface was investigated using dynamic interfacial tension measurements. The kinetic adsorption of silica nanoparticles to oil-water interface from an aqueous solution containing 1 wt% NaCl and different concentrations of silica nanoparticles (0, 0.05, 0.1, 0.15 and 0.2 wt%)

83

is illustrated in Figure 4-4a. At very low nanoparticle concentrations (0.03 wt%) significant changes in the IFT value is not recorded. The data overlaps with "no nanoparticle data", so we do not show the 0.03 wt% data in Figure 4-4a. As shown in this figure, in the aqueous solution without silica nanoparticles, the oil-water interfacial tension is quite constant over the measured time, with an average IFT equal to 22.24 ± 0.44. However, in the presence of silica nanoparticles in the aqueous phase, completely different trends are observed. Immediately after introducing the oil droplet to the nanoparticle-NaCl solution, the oil-water IFT reduces sharply (phase A, early time data < 60 s). At intermediate times (phase B, 60 s < intermediate time period < 500 s), the slope of oil-water interfacial tension reduction decreases. Finally, at late time periods (phase C, late time data > 500s), the oil-water interfacial tension reaches its minimum value and it remains constant.

(a)   (b)
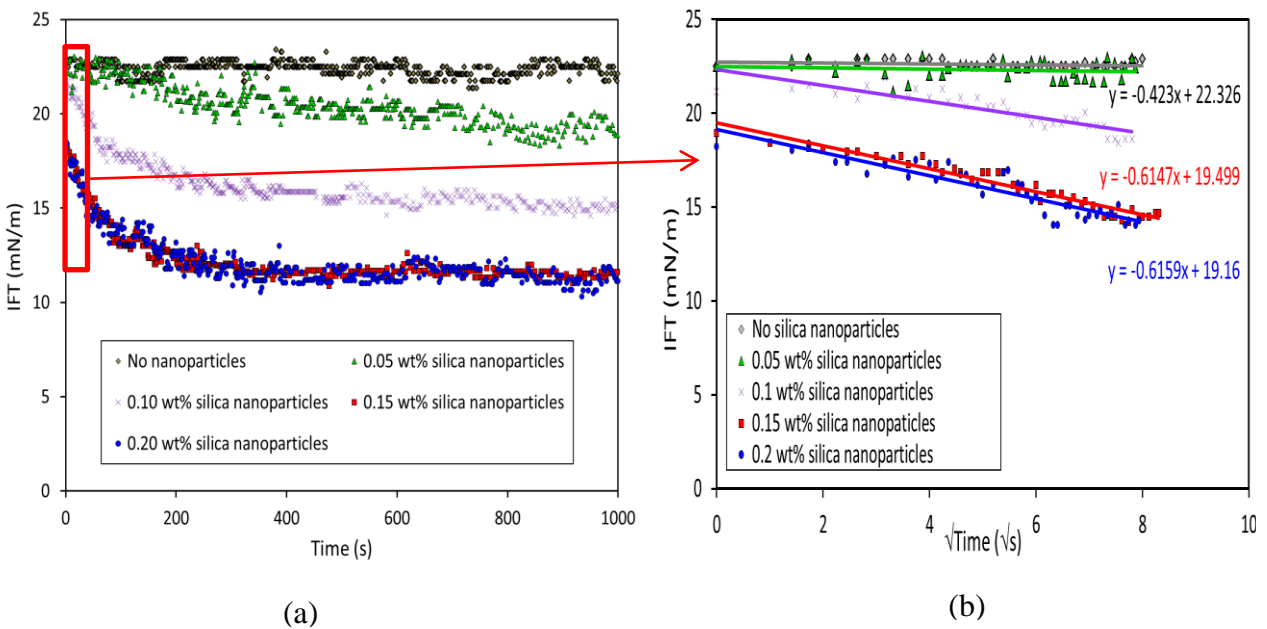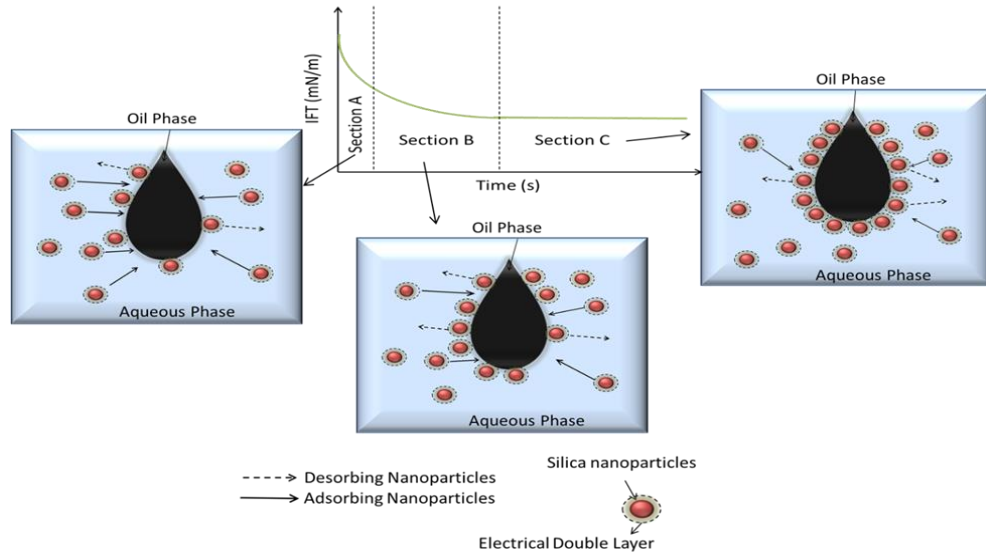
(c)

Figure 4-4: a) Change of the kinetic adsorption of nanoparticle at oil-water interface with various concentration of nanoparticle at 1 wt% NaCl and ambient temperature and pressure, b) Early time dynamic interfacial tension data against √t early time, c) Three distinct regions for nanoparticle adsorption

The reduction of interfacial energy due to the adsorption of nanoparticles (ΔE) is calculated by plotting early time dynamic interfacial tension data against √t (Figure 4-4b) and employing equation 4-3 [148]. The dynamic interfacial tension measured before 60s is suggested as early time data [65]. Table 4-4, summarizes the reduction of interfacial energy due to adsorption of silica nanoparticles from NaCl solution with different nanoparticle concentrations. The diffusion coefficient (D) is estimated based on Stokes-Einstein equation (equation 4-5). As shown in Table 4-4, ΔE for nanoparticles is far less than colloid particles (10^7 KBT). Hence, the adsorption of nanoparticles at the interface can be reversible and some nanoparticles may desorb from interface. The balance between adsorption and desorption rate of silica nanoparticles at interface governs the general trend of dynamic oil-water interfacial tension. The adsorption/desorption rate reaches an equilibrium at the late time and the final value of oil-water interfacial tension depends on the number of nanoparticles trapped at the interface at any moment. When there are more nanoparticles at the interface, a lower oil-water IFT can be

85

expected. At the early times (Figure 4-4c, phase A), there is no strong barriers to adsorption of nanoparticles at the interface, subsequently, nanoparticles are rapidly adsorbed and IFT sharply reduced. In other words, the adsorption rate of nanoparticles at the oil-water interface is much higher than the desorption rate. At intermediate times (Figure 4-4c, phase B), the presence of previously adsorbed nanoparticles on the oil-water interface hampers further adsorption and reduces the adsorption rate. However, the adsorption rate is still higher than the desorption rate. Hence, the IFT reduction rate is not as pronounced. Finally, at late times, nanoparticle adsorption reaches a dynamic equilibrium in phase C and the maximum reduction in oil-water interfacial tension is reached.

Table 4-4: Reduction of interface energy due to adsorption of silica nanoparticles from 1 wt% NaCl solution

Conce. of nanoparticles (wt%)	$C \times 10^6$ (mole m^{-3})	$D_{S-E} \times 10^{11}$ (m^2 s^{-1})	$\frac{d\gamma}{d\sqrt{t}} \times 10^4$ (N m^{-1}s$^{-0.5}$)	$\lvert\Delta E\rvert$ [$K_B T$]	Final IFT (mNm^{-1})
0.10	147.38	2.151	-4.234 ± 0.67	223.47	15.26 ± 0.33
0.15	221.07	2.151	-6.147 ± 0.58	216.49	11.47 ± 0.23
0.20	290.40	2.141	-6.159 ± 0.47	165.53	11.32 ± 0.39

At low nanoparticle concentrations (less than 0.05 wt%), the number of nanoparticles around the interface is relatively low. Therefore, the adsorption/desorption rate reaches an equilibrium with a sparse monolayer around the interface. In other words, the number of nanoparticles at the interface at any moment is not sufficient to form a compact monolayer at the interface. The small changes in the oil-water IFT occur solely due to the single adsorption or very sparse monolayer of nanoparticles at the interface. As illustrated in Figure 4-5, the adsorption rate is directly related to the nanoparticles' concentration; by increasing the concentration of

nanoparticles, more compact monolayer around the oil droplet can be formed and thus less IFT

value can be achieved. The maximum IFT reduction occurs when all accessible sites on the

interface are filled with nanoparticles.
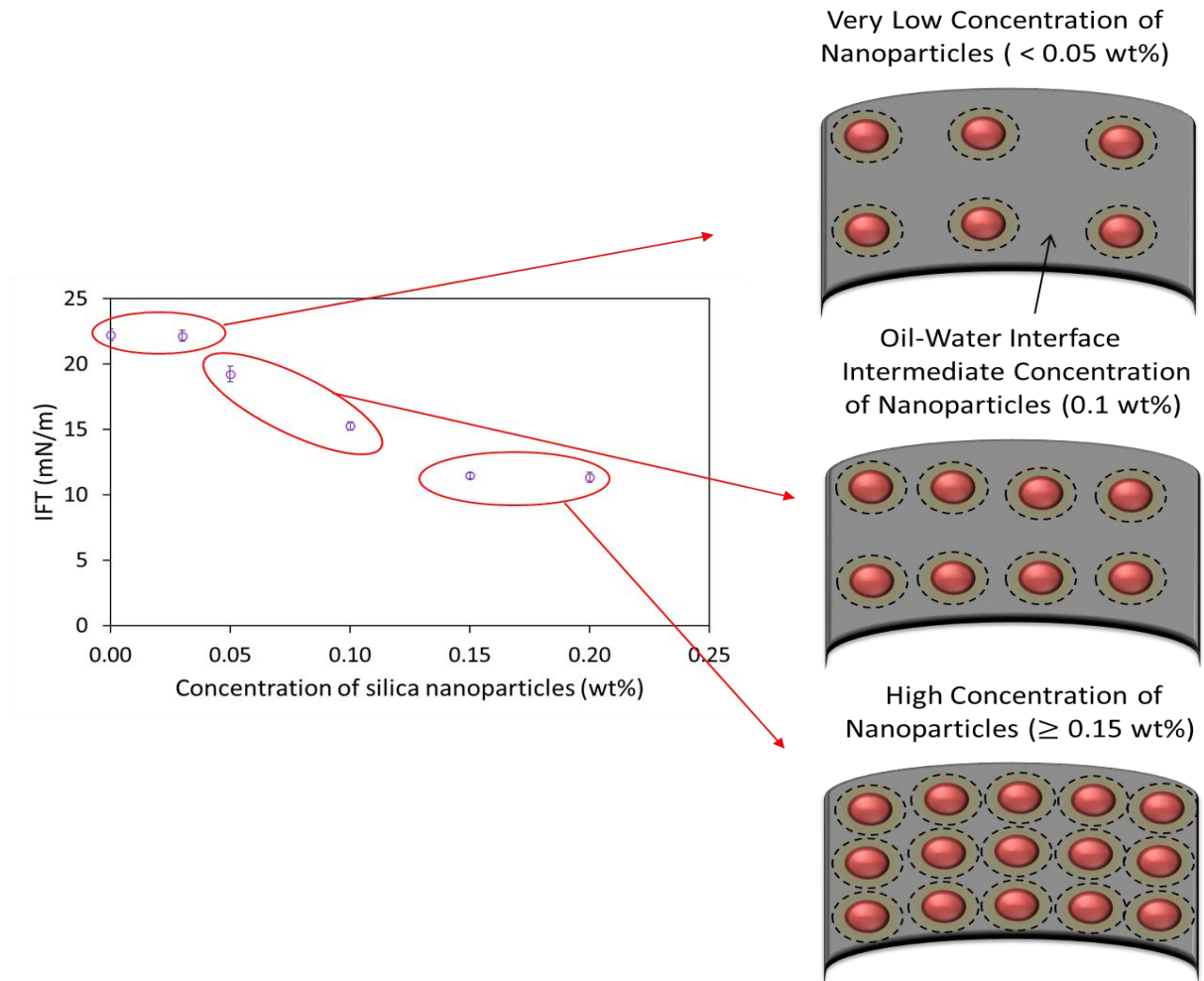
Figure 4-5: Schematic number of nanoparticles in different adsorption/desorption equilibrium

In order to examine the effect of salinity on the kinetic adsorption of silica nanoparticles onto

the interface, the concentration of silica nanoparticles are set at 0.15 wt% and the salt

concentration varied (1, 5 and 6 wt%). As shown in Figure 4-6, the general trend of dynamic

oil-water interfacial tension is similar for all salinities. However, some small differences can

be also observed. First, at phase A, the oil-water interfacial tension reduces more sharply by

increasing the salt concentrations. By raising NaCl concentration in the solution, as shown in

Figure 4-7, the zeta-potential of nanoparticles decreases. Furthermore, the electrical double layer around the nanoparticles and the oil-water interface compresses. Consequently, the electrostatic barriers for the adsorption of nanoparticles decrease with NaCl concentration and the adsorption rate (especially in phase A, refers to the zoomed section of Figure 4-6) increases. Second, by increasing the salinity, the final value of oil-water interfacial tension in phase C reduces (Figure 4-7). The equilibrium IFT value for 0.15 wt% silica nanoparticles in 1, 5 and 6 wt% NaCl solutions are obtained 11.48 ± 0.43, 9.65 ± 0.37 and 8.77 ± 0.61, respectively. By compressing the electrostatic double layer around nanoparticles and reducing the zeta-potential of the nanoparticles, the repulsion between adsorbed nanoparticles at the interface decreases and more space at the interface is created for new nanoparticles. Hence, the nanoparticles form a more compacted monolayer at the interface which leads to less oil-water interfacial tension value. The maximum compression of the electrical double layer occurs at the critical salt concentration because further increasing the salt concentrations can lead to nanoparticle aggregation. The critical salt concentration for NaCl is reported as 6 wt% [58]. Hence, the maximum IFT reduction is expected to achieve in the 6 wt% NaCl solution. Measuring the IFT value for higher NaCl concentrations (higher than 6 wt%) is not feasible due to the turbidity of the solution. By increasing the salt concentration from 1 wt% to 5 and 6 wt%, the size of nanoparticles slightly increases from 21.52 ± 0.21 to 23.21 ± 0.27 and 24.64 ± 0.18, respectively. The space created due to the reduction of electrostatic repulsion forces appears to be larger than space occupied due to increase in the size of nanoparticles.
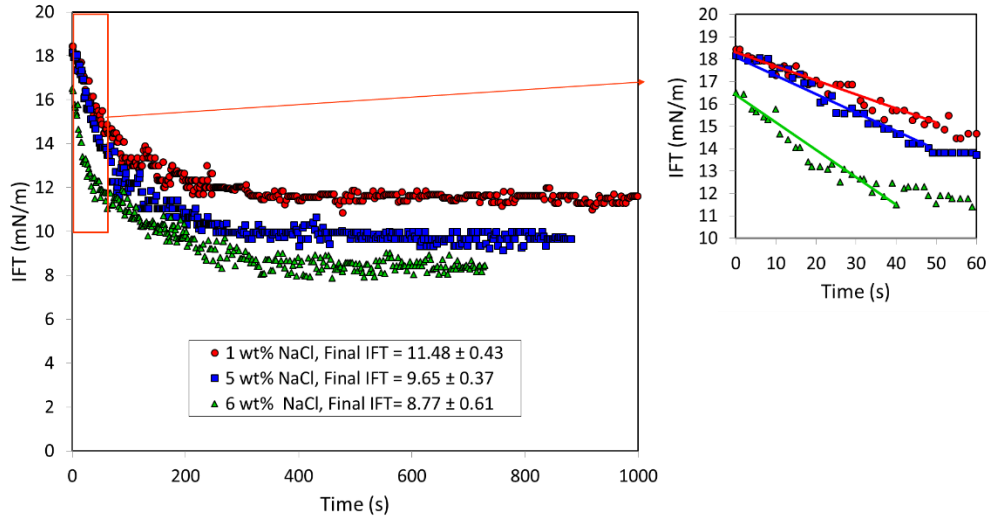
Figure 4-6: Effect of ionic strength on oil-water interfacial value at 0.15 wt% silica nanoparticles
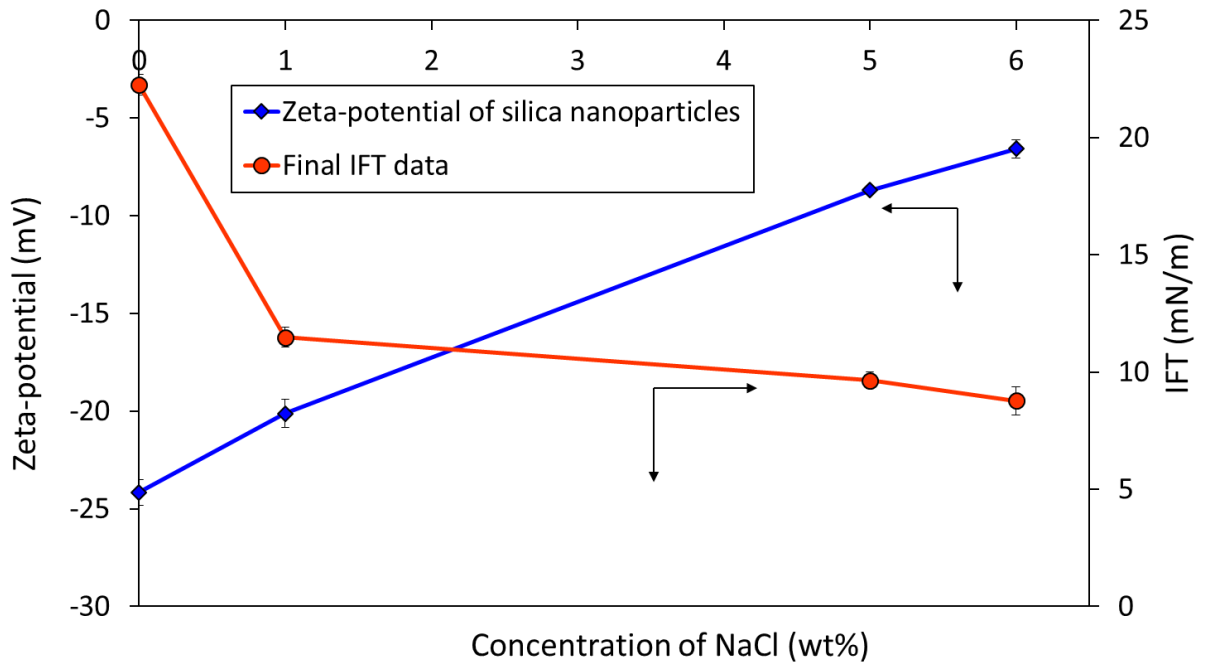
Figure 4-7: Zeta-potential and final IFT value for 0.15 wt% silica nanoparticles in different concentrations of NaCl solution

4.4.2. Kinetic adsorption of silica nanoparticles from seawater

In the next step, different concentrations of silica nanoparticles (0.03, 0.05, 0.10, 0.15, 0.20, 0.25 wt%) are dispersed in seawater and the kinetic adsorption of the silica nanoparticles from

seawater onto the oil-water interface is investigated. Hydrochloric acid is used to form the "H$^+$ protection layer" around nanoparticles to stabilize nanoparticles in seawater [58]. Two different HCl concentrations of 0.025 wt% and 0.0076 wt% are used in the experiments and the kinetic adsorption of nanoparticles are reported in Figure 4-8a and Figure 4-8b, respectively. In the absence of nanoparticles in the solution, the oil-water interfacial tension is constant over the time; however, even at low concentrations of silica nanoparticles (0.03 wt%) in seawater, the IFT changes significantly. This trend was not observed in the NaCl brine. The three mentioned phases for kinetic adsorption of nanoparticles from NaCl brine onto the interface with small differences can also be observed in seawater. However, in phase A (early times data), immediately after contacting seawater-nanoparticle solution with the oil drop, the oil-water interfacial tension reduced suddenly. Hence, the time for phase A is far shorter for the seawater-nanoparticle solution compared to the NaCl-nanoparticle solution. The change in the oil-water interfacial tension at t = 0 s for different concentrations of nanoparticles in 1 wt% NaCl solution, 0.0076 wt% and 0.025 wt% HCl in seawater are illustrated in Figure 4-9. As shown in Figure 4-9, the drop in the IFT value of 1 wt% NaCl solution at t = 0 s is far less than solutions containing different concentrations of HCl in seawater. These differences are also greater for 0.05 wt% silica nanoparticles where for 1 wt% NaCl solution we only observed 0.32 ± 0.14 (mN/m) reduction in IFT at t = 0 s, while this difference is 3.01 ± 0.36 and 5.66 ± 0.42 for 0.0076 wt% and 0.025 wt% HCl in seawater solutions, respectively. The trend of the dynamic reduction of IFT in phases B and C are similar for NaCl and seawater nanoparticles solutions.
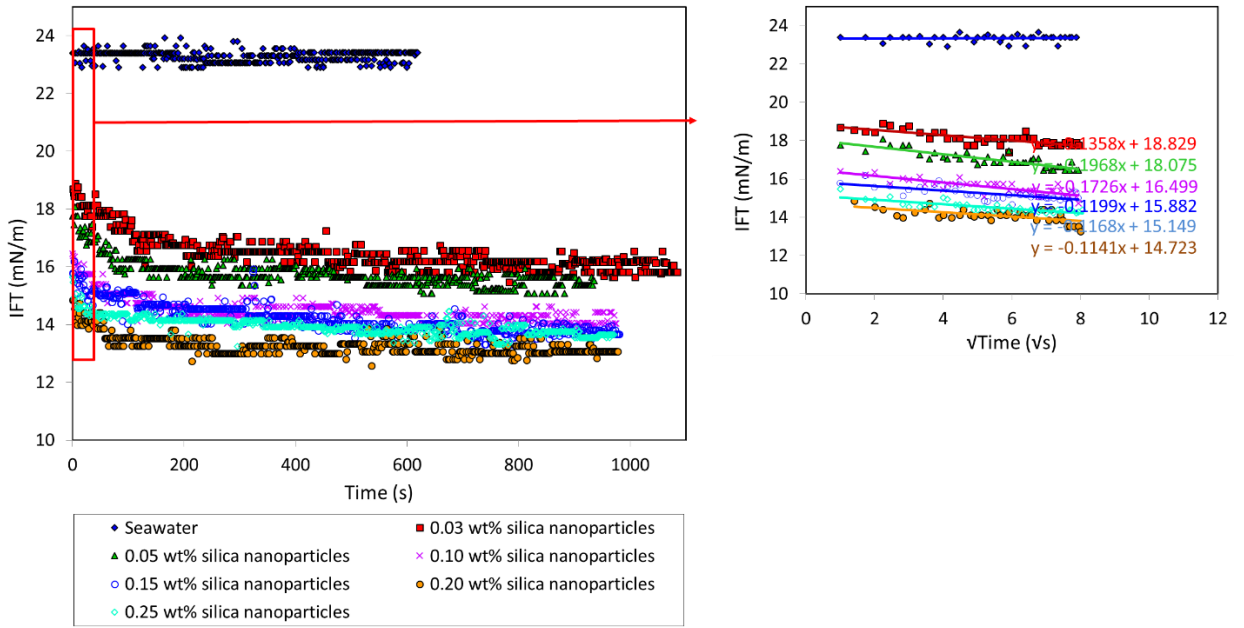
(a)
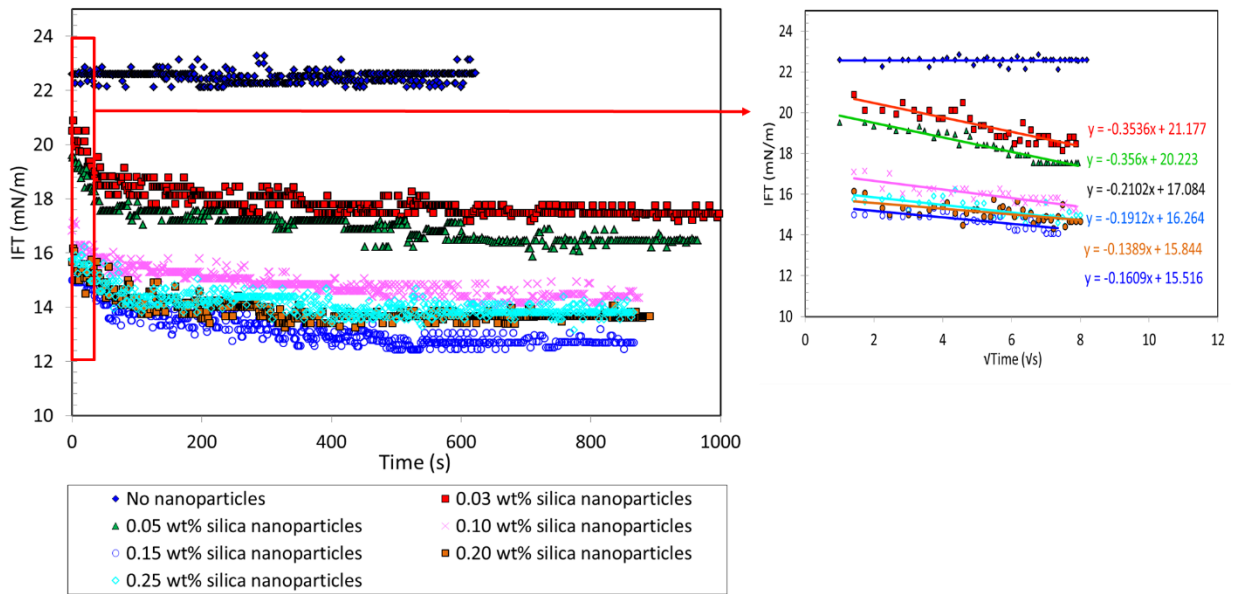
(b)

Figure 4-8: Kinetic adsorption of silica nanoparticles from seawater containing a) 0.025 wt% and b) 0.0076wt% HCl onto oil-water interface
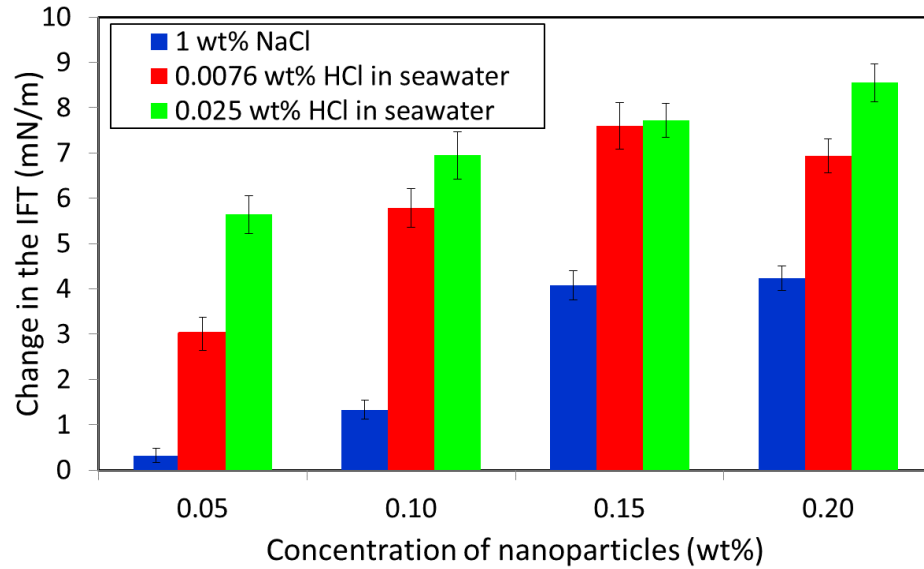
Figure 4-9: Change in the IFT value at t=0 s for different concentrations of nanoparticles in 1 wt% NaCl, 0.0076 wt% HCl in seawater and 0.025 wt% HCl in seawater

When silica nanoparticles are dispersed in seawater using "H^+ protection layer", the H^+ ions accumulate at the electrical double layer of the nanoparticles and they shield the charge of silica nanoparticles and causing the zeta-potential to change from negatively charged zeta-potential to less negatively, neutral, or positive charge depending on the concentrations of HCl. As shown in Figure 4-10, the zeta-potential of silica nanoparticles in the NaCl solution and seawater is very different. The zeta-potential of silica nanoparticles in seawater is fluctuating around +1 and -4 mV for 0.025 and 0.0076 wt% of HCl, respectively, while it is around -21 mV for NaCl solutions. This difference leads to less repulsion force between nanoparticle-interface and nanoparticle-nanoparticle. Hence, immediately after contacting nanoparticles with oil drop, the nanoparticles are rapidly adsorbed to the interface and the oil-water interfacial tension reduces suddenly. It is worth to mention that the zeta potential reduction in the H+ protected method does not destabilize silica nanoparticles in seawater and the nanoparticles were stable in all tested solutions as we previously confirmed [58].
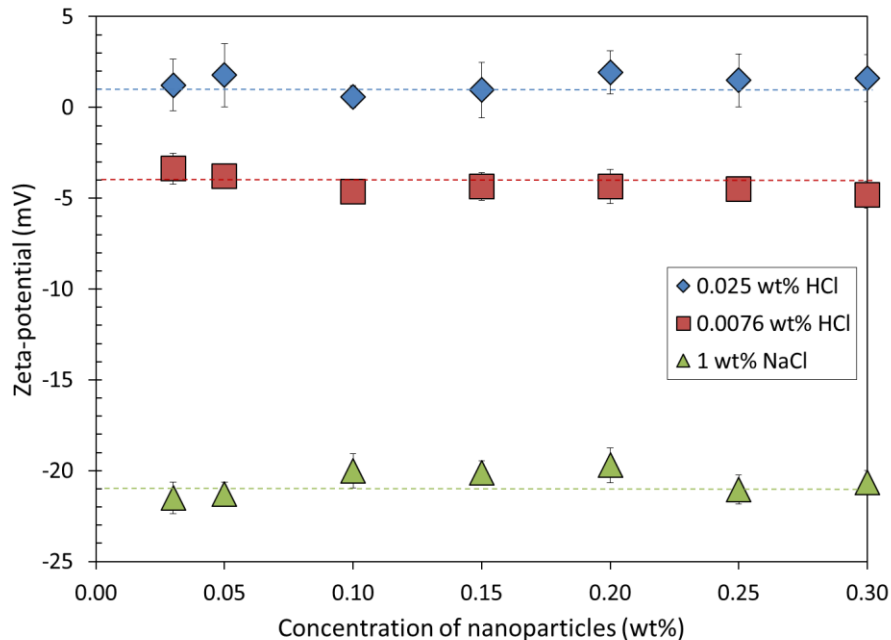
Figure 4-10: Zeta-potential of samples in different concentrations of nanoparticles

In order to distinguish the effect of HCl and divalent ions (Mg^{2+} and Ca^{2+}) on the zeta-potential of silica nanoparticles, three solutions with the same concentration of silica nanoparticles (0.15 wt%) is prepared. In the first sample, we dispersed silica nanoparticles in 1 wt% NaCl solution. In the second one, the nanoparticles are dispersed in 1 wt% NaCl + 0.025 wt% HCl. By comparing the zeta-potential of these two solutions, the influence of HCl on the zeta-potential of silica nanoparticles is revealed. As shown in Table 4-5, the presence of 0.025 wt% HCl causes the zeta-potential to change from -20.12 ± 0.66 to 1.08 ± 0.53. To understand the effect of divalent ions, another solution (synthetic solution) with 1 wt% NaCl, 0.13 wt% $MgSO_4$ and 0.04 wt% $CaCl_2$ is prepared and 0.025 wt% HCl and 0.15 wt% silica nanoparticles is added into the solution. By comparing the third solution with the second one in Table 4-5, we observed that the presence of divalent ions can reduce the absolute value of zeta-potential. However, its effect on the zeta-potential in the compare of HCl effect is not significant.

Table 4-5: Zeta-potential silica nanoparticles in three different solutions

93

Sample No.	Solution	Zeta-potential (mV)	pH
1	0.15 wt% silica nanoparticles in 1 wt% NaCl, no HCl	-20.12 ± 0.66	7.38 ± 0.05
2	0.15 wt% silica nanoparticles in 1 wt% NaCl + 0.025 wt% HCl	1.08 ± 0.53	2.16 ± 0.07
3	0.15 wt% silica nanoparticles in synthetic solution + 0.025 wt% HCl	0.27 ± 0.12	2.24 ± 0.04

4.4.3. Reasons for nanoparticles' adsorption at the interface

Changing the oil-water interfacial tension value due to the presence of H+-protected silica nanoparticles reveals that nanoparticles are self-assembled onto the oil-water interface. However, it is still unclear why nanoparticles are adsorbing on the oil-water interface. To address this question, the energy reduction of the interface due to adsorption of H+-protected silica nanoparticles is calculated. For nanoparticles to adsorb spontaneously onto the interface, the energy of the interface should be reduced by the nanoparticles' adsorption.

The interfacial energy changes due to adsorption of nanoparticles $|\Delta E|$ from seawater solution containing 0.025 wt% and 0.0076 wt% HCl is provided in Table 4-6 and Table 4-7, respectively. As shown in these tables, adsorption of H^+-protected silica nanoparticles at the oil-water interface reduces the interfacial energy. The minimum energy reduction occurs at 0.20 wt% nanoparticles for 0.025 wt% HCl solution and 0.15 wt% nanoparticles for 0.0076 wt% HCl. On the other hand, minimum IFT value is also obtained at the same nanoparticle concentrations (see Figure 4-13). Hence, minimum IFT is achieved when the chance of nanoparticles to desorb from the interface is relatively high. Therefore, operating conditions especially temperature can have a significant effect on the performance of nanoparticles. By thermally exciting the nanoparticles the adsorption/desorption balance is lost and nanoparticles

can easily escape from the interface. We will discuss the effect of temperature and pressure in the upcoming sections. As shown in the tables, the minimum IFT value in both HCl concentrations is obtained in the maximum molar concentration of nanoparticles. Hence, the molar concentration of nanoparticles seems to be a better criterion to evaluate the performance of nanoparticles than weight percent concentration because, in addition to the number of nanoparticles, it also considers the size of nanoparticles in the solution.

Table 4-6: Reduction of interface energy due to adsorption of silica nanoparticles from seawater-0.025 wt% HCl solutions

Conc. Of nanoparticles (wt%)	*C×10⁶ (mole m⁻³)*	*$D_{S-E}×10^{11}$ (m² s⁻¹)*	*$\frac{d\gamma}{d\sqrt{t}}×10^4$ (N m⁻¹s⁻⁰·⁵)*	*Particle Diameter (nm)*	*|ΔE| [K_BT]*	*Final IFT (mNm⁻¹)*
0.03	40.83	2.095	-1.358	20.57 ± 0.28	262.39	15.19 ± 0.93
0.05	66.30	2.077	-1.968	20.82 ± 0.27	235.19	14.85 ± 0.93
0.10	115.20	1.981	-1.726	21.82 ± 0.76	121.54	13.78 ± 0.71
0.15	187.35	2.035	-1.199	21.24 ± 0.25	51.22	13.16 ± 0.69
0.20	*249.097*	*2.034*	*-1.168*	*21.26 ± 0.39*	*37.54*	*12.81 ± 0.77*
0.25	160.779	1.632	-1.141	26.54 ± 0.33	63.44	13.13 ± 0.91

Table 4-7: Reduction of interface energy due to adsorption of silica nanoparticles from seawater-0.0076 wt% HCl solutions

Conc. Of nanoparticles (wt%)	*C×10⁶ (mole m⁻³)*	*$D_{S-E}×10^{11}$ (m² s⁻¹)*	*$\frac{d\gamma}{d\sqrt{t}}×10^4$ (N m⁻¹s⁻⁰·⁵)*	*Particle Diameter (nm)*	*|ΔE| [K_BT]*	*Final IFT (mNm⁻¹)*
0.03	40.83	2.095	-3.554	20.64 ± 0.10	683.22	17.48 ± 0.63
0.05	58.89	1.996	-3.560	21.35 ± 0.32	488.62	16.48 ± 0.91
0.10	113.32	1.970	-2.1202	21.94 ± 0.38	150.88	14.83 ±0.64
0.15	*147.16*	*1.878*	*-1.609*	*23.06 ± 0.19*	*91.10*	*14.01 ± 0.87*
0.20	53.05	1.215	-1.389	35.59 ± 0.13	271.29	14.3 ± 0.73
0.25	23.85	0.864	-1.921	50.06 ± 0.48	989.67	15.16 ± 0.82

To calculate the force balance between H^+-protected silica nanoparticles and the oil-water interface, the DLVO theory is applied. In order to calculate the electrostatic and van der Waals equations, the charge of nanoparticles and oil-water interface is required. The oil-water interfacial charge for different aqueous solutions and offshore NL crude oil is summarized in Table 4-8. As shown in the table, in the presence of 0.15 wt% silica nanoparticles and HCl, the charge of the oil-water interface reduces from -14.1 ± 0.53 to -2.80± 0.55 and -3.51± 0.57 for 0.025 and 0.0076 wt% HCl solutions, respectively. This reduction in the charge of the oil-water interface reduces the electrostatic repulsion between oil-water interface and nanoparticles and leads to adsorption of nanoparticles to the interface. The balance between van der Waals attraction forces and electrostatic repulsion governs the adsorption of nanoparticles at the interface. This balance can be calculated using DLVO theory. As shown in Figure 4-11a, in the case of 0.15 wt% silica nanoparticles dispersed in seawater containing 0.025 and 0.0076 wt% HCl, van der Waals attraction forces are stronger than electrical repulsion force. Hence, H^+-protected silica nanoparticles adsorb to the interface and reduce the IFT value. The DLVO profile for nanoparticles-nanoparticles in seawater containing 0.025 and 0.0076 wt% HCl and different NaCl concentrations (1, 5, and 6 wt%) is illustrated in Figure 4-11b (corresponding equations for DLVO calculations are taken from [58]). The results show an energy barrier against aggregation of nanoparticles in all solutions. Hence, DLVO calculations predict the stable suspensions for all samples. The stability of the samples is also experimentally confirmed through particle size measurements and visually [58].

Table 4-8: Charge of the interface of different aqueous solutions and Hibernia crude oil

Aqueous solution	Interfacial Charge
Seawater	-14.1 ± 0.53
0.0076 wt% HCl in seawater	-12.2 ± 0.73
0.0076 wt% HCl in seawater + 0.15 wt% silica nanoparticles	-3.51 ± 0.57
0.025 wt% HCl in seawater	-9.53 ± 0.68
0.025 wt% HCl in seawater + 0.15 wt% silica nanoparticles	-2.80 ± 0.55

(a)   (b)
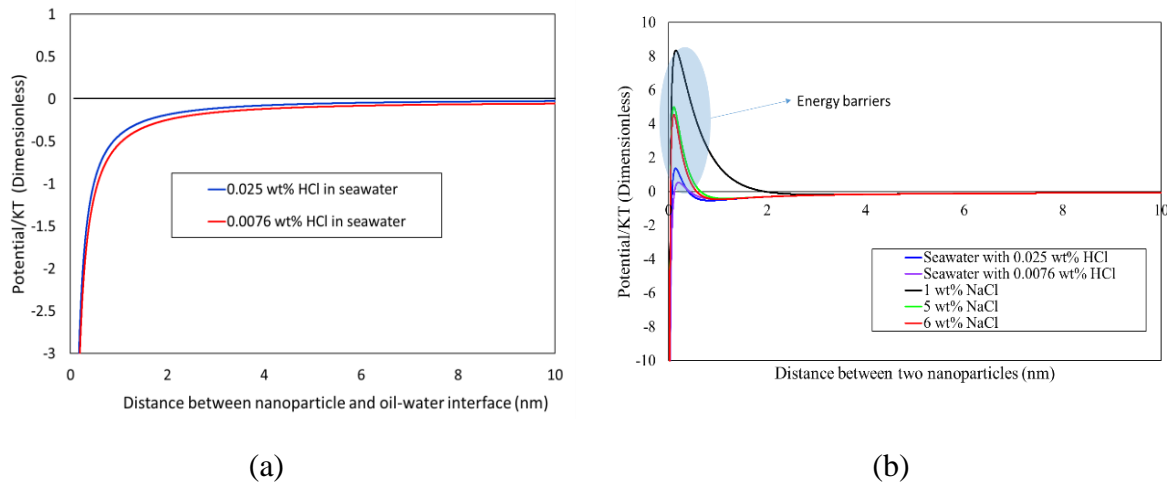
Figure 4-11: DLVO calculation for a) silica nanoparticles and oil water interface (silica nanoparticles is 0.15 wt% for two solutions) and b) nanoparticle-nanoparticle in the different solutions DLVO

The IFT reduction in the presence of nanoparticles indirectly illustrates the adsorption of nanoparticles onto the oil-water interface. From an energy balance point of view, as shown in Table 4-6 and Table 4-7, the interface energy reduces due to the adsorption of nanoparticles i.e. the adsorption of nanoparticles at the interface is energetically favorable. From a force balance perspective, as shown in Figure 4-11a, the DLVO profile for the adsorption of a spherical silica nanoparticle to the oil-water interface indicates that the van der Waals attraction force is much larger than electrostatic repulsion forces. Hence the force balance indicates

adsorption of silica nanoparticles at the interface. It is still unclear as to what happens at the molecular level to drive the nanoparticles to the oil-water interface. It might be explained by the induced charge re-distribution within the electrical double layer of nanoparticles in the presence of a charged oil-water interface. When a nanoparticle moves closer to the interface, charged ions may redistribute in the electrical double layer of the nanoparticles; consequently, as shown in Figure 4-12, induced positive and negative sections may form around the nanoparticles. These induced charges may initiate the adsorption of nanoparticles to the interface. More research is required to confirm this mechanism.
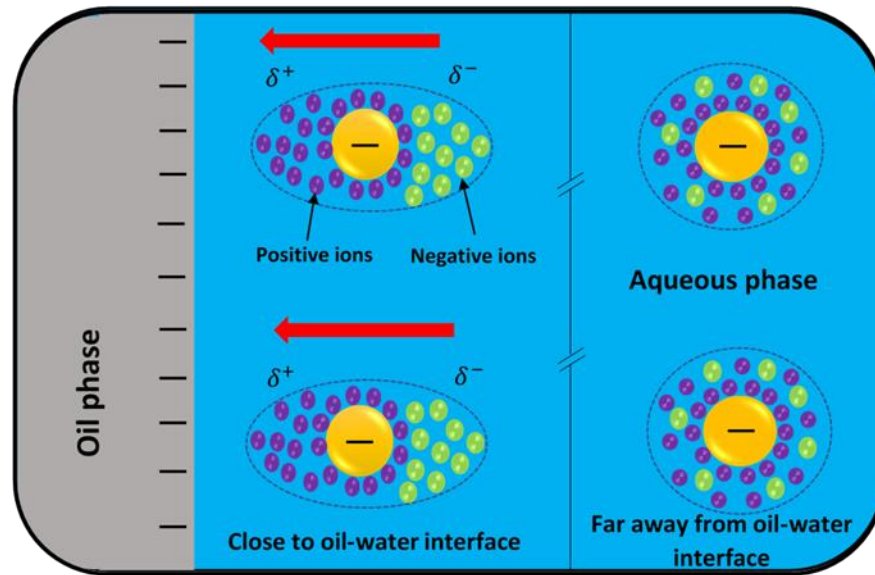
Figure 4-12: Schematic possible mechanism of silica nanoparticle adsorption at the oil-water interface

4.4.4. Effect of silica nanoparticles on oil-water IFT at different conditions

Different concentrations of silica nanoparticles (0.03 wt% to 0.05, 0.10, 0.15, 0.20 and 0.25 wt%) in seawater solutions with two HCl concentrations (0.0076 and 0.025 wt%) were made and the equilibrated IFT values recorded and shown in Figure 4-13. The interfacial tension value between seawater and the crude oil is 22.24 ± 0.44 mN/m at ambient conditions. As shown in this figure, adding 0.0076 and 0.025 wt% HCl into the system increases the oil-water

interfacial tension to 22.61 ± 0.41 and 23.56 ± 0.36 (mN/m), respectively. By introducing silica nanoparticles and increasing the concentration of nanoparticles, the oil-water IFT first decreases and then increases. The maximum reduction in oil-water IFT is obtained at 0.15 wt% nanoparticles stabilized using 0.0076 wt% HCl, where IFT value reduces from 22.61 ± 0.41 mN/m to 14.01 ± 0.87 mN/m. The maximum reduction in oil-water IFT value is obtained at 0.20 wt% silica nanoparticles stabilized using 0.025 wt% HCl, where the IFT value reduces from 23.56 ± 0.36 mN/m to 12.81 ± 0.77 mN/m. As shown in Figure 4-13, the IFT reduction trend observed for both HCl concentrations was similar. The oil-water interfacial tension decreases due to the increased concentration of nanoparticles. A high concentration of nanoparticles means that more nanoparticles can attach at the interface. On the other hand, as shown in Figure 4-13, the size of nanoparticles also increasing when the concentration of nanoparticles increases in the solution. The size increasing trend starts gently for low concentrations of silica nanoparticles and it continues sharply for concentrations higher than 0.20 wt% for 0.025 wt% HCl solutions and 0.15 wt% for solution containing 0.0076 wt% HCl, i.e. the nanoparticles are going to aggregate in the bulk solution. Hence, at nanoparticle concentrations higher than these concentrations, the number of nanoparticles is limiting at the interface due to the size of nanoparticles. Generally, the balance between the size of nanoparticles and the concentration of nanoparticles governs the maximum IFT reduction.
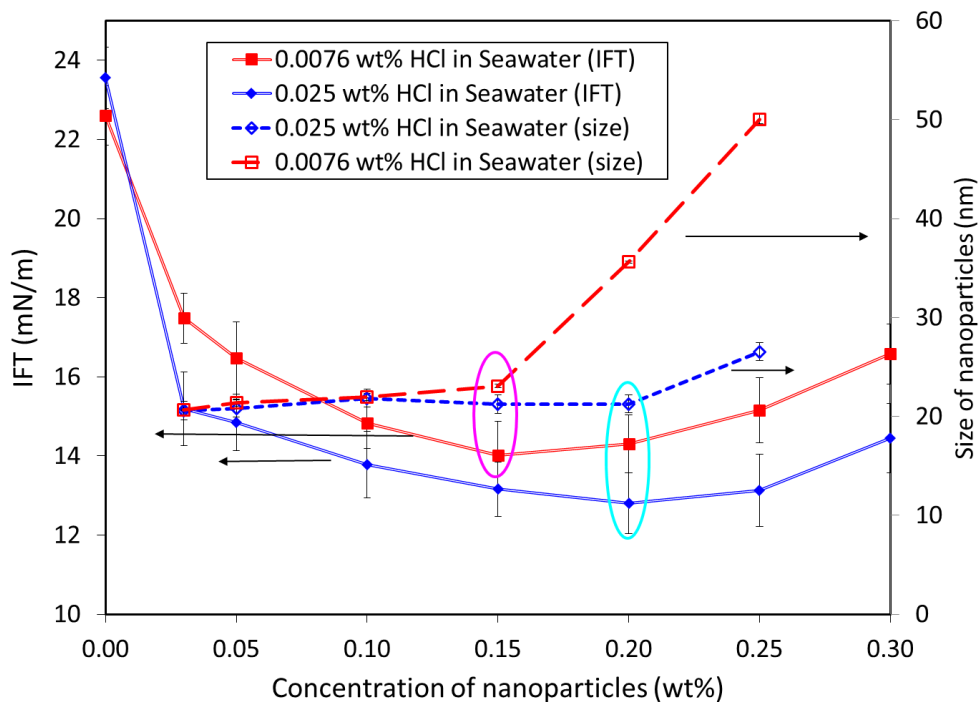
Figure 4-13: Oil-water interfacial tension and hydrodynamic size of silica nanoparticles in seawater in different concentrations of nanoparticles

Effect of temperature and pressure: The effect of temperature and pressure on the oil-water interfacial tension in the presence of various concentrations of silica nanoparticles (0.03, 0.05, 0.10, 0.15, 0.20, 0.25 and 0.30 wt%) in two distinct seawater-HCl (0.025 and 0.0076 wt%) solutions is investigated. The equilibrated IFT for the mentioned nanoparticle concentrations is measured at 22°C to 40, 60, 70 and 90°C and illustrated in Figure 4-14. As shown in this figure, at 22, 40 and 60°C, the oil-water interfacial tension by increasing the concentrations of nanoparticles decreases to reach its minimum value and then increases. However, for 70 and 90°C, adding 0.03 wt% of silica nanoparticles in the aqueous solution, causes IFT increasing. Then, by a further increase in the concentration of silica nanoparticles, IFT value first decreases and then increases again. It should be noted that the IFT value at 70 and 90°C in the presence of nanoparticles is always higher than the case of without nanoparticles. Hence, in the evaluated temperatures, the presence of silica nanoparticles in the aqueous phase worsened the

100

IFT value compared to the no nanoparticles case. During adsorption of the nanoparticles at the interface, some natural surfactants in crude oil (naphthenic acids and asphaltene) may attach on the surface of nanoparticles. Since, at elevated temperature, the adsorption/desorption rate of nanoparticles is very high, the nanoparticles may deplete the interface from natural surfactants and cause an increase in interfacial tension.
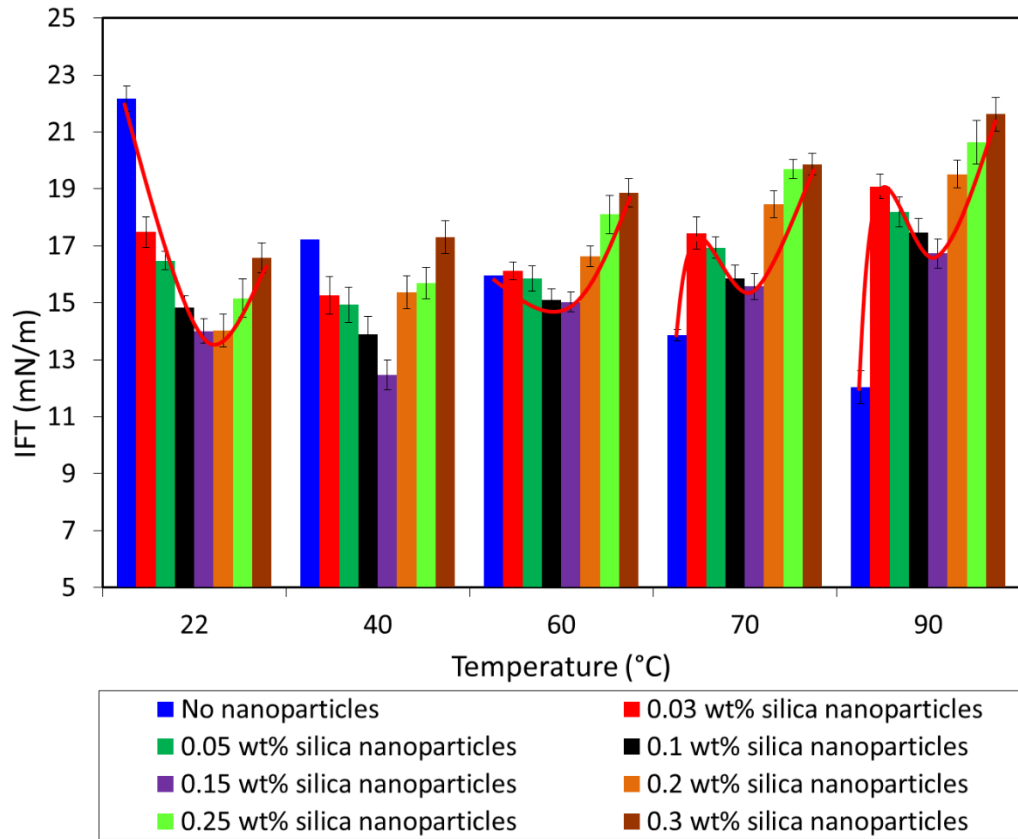
(a) Seawater containing 0.0076 wt% HCl
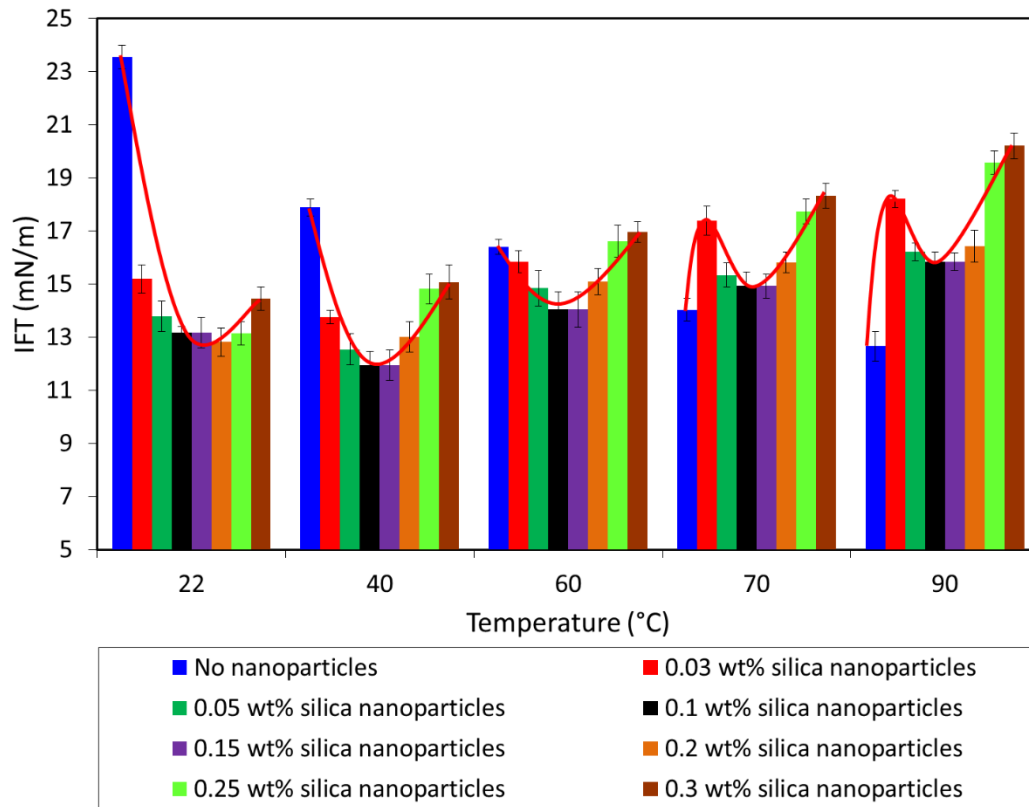
(b) Seawater containing 0.025 wt% HCl

Figure 4-14: Effect of pressure on oil-water interfacial tension a) 0.0076 wt% HCl and b) 0.025 wt% HCl

As shown in Figure 4-15, based on the nanoparticle's concentration in the aqueous solution, three different trends are observed for oil-water interfacial tension as a function of temperature. In the absence of silica nanoparticles, as predicted, oil-water interfacial tension reduces with increasing temperature (Trend A). In the presence of low concentrations of nanoparticles (0.03 wt% to 0.15 wt% silica nanoparticles), by increasing the temperature from ambient condition to 40°C, the oil-water interfacial tension decreases and then increase with further increasing the temperature (Trend B). Finally, for 0.2 wt% to 0.3 wt% silica nanoparticles, the oil-water interfacial tension increases with increasing temperature (Trend B). The trends were similar for both solution containing 0.025 wt% and 0.0076 wt% HCl. The IFT is inversely proportional to temperature and nanoparticle concentration at the interface. That is why, the IFT decreases

when the temperature is raised from 22°C to 40°C. However, as previously discussed, the attachment energy for nanoparticles is in the order of thermal fluctuations. Hence, with increasing temperature, due to thermal fluctuations of nanoparticles, the nanoparticles desorb from the interface. Subsequently, the concentration of nanoparticles at the interface decreases and IFT increases. Another unfavorable consequence of increasing temperature is the aggregation of nanoparticles in the dispersed solution. By increasing the temperature, the chance of collision between nanoparticles and their aggregation increases. This appears to be more severe for solutions containing high concentrations of silica nanoparticles and may explain the direct correlation of IFT and temperature for high concentrations of silica nanoparticles.
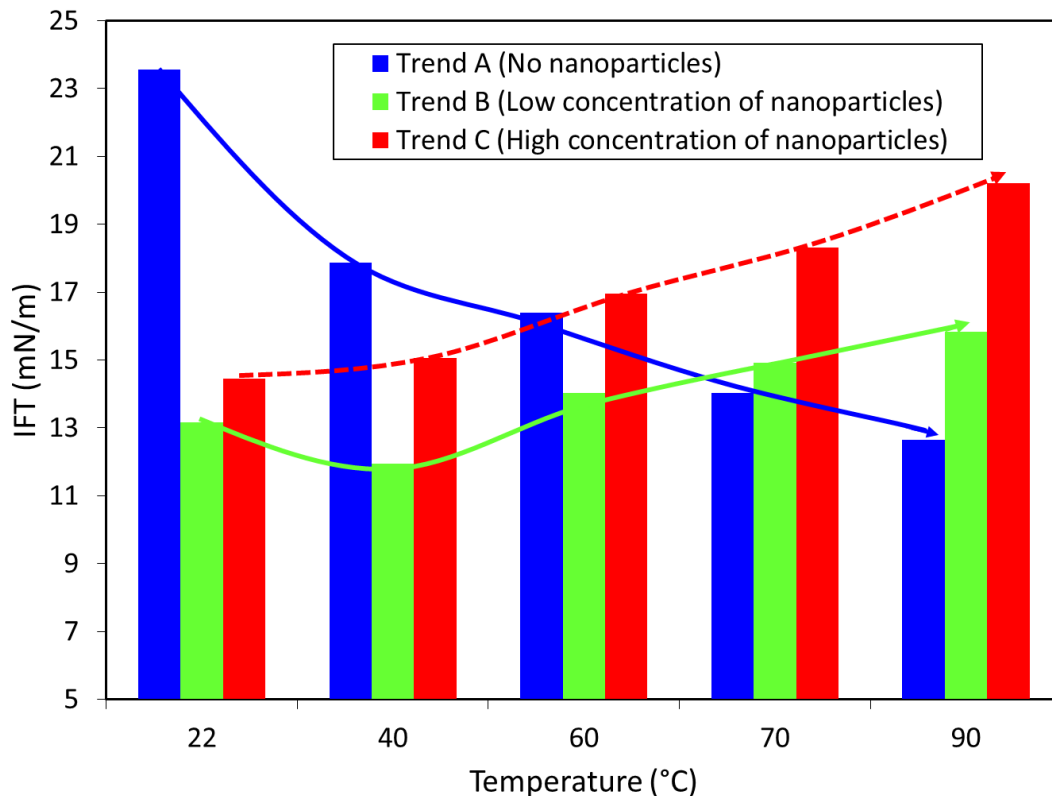
Figure 4-15: Three general trends of IFT change with increasing the temperature (Trend A: no nanoparticles, Trend B: low concentration of nanoparticles, Trend C: High concentration of nanoparticles)

103

In order to evaluate the effect of pressure on the oil-water interfacial tension in the presence of nanoparticles, the system's pressure is altered from ambient pressure to 500, 1000, 1500, 2000, 3000, 4000 and 5000 psia. The concentrations of HCl and silica nanoparticles are changed as in the previous section. IFT as a function of pressure and nanoparticle concentration is shown in Figure 4-16. The oil-water IFT decreases with increasing pressure. The trend of IFT decreases versus pressure is similar for both cases, with and without nanoparticles. Hence, it can be concluded that the reduction of the oil-water IFT is mostly related to the mechanism of interface compression with pressure and the presence of nanoparticles do not have a significant effect on the trend. Minimum IFT at the ambient conditions is obtained at nanoparticles concentration of 0.20 wt% for 0.025 wt% HCl solutions and 0.15 wt% for the solution containing 0.0076 wt% HCl. We observed the same trend in high pressure as well. Almost in all pressures, the minimum IFT value for solutions containing 0.025 wt% HCl is observed at 0.20 wt% nanoparticles concentration (Figure 4-16a) and for 0.0076 wt% HCl (Figure 4-16b), the minimum IFT in obtained for 0.15 wt% nanoparticle concentration. By further increasing the nanoparticle concentration in all pressures, the IFT value increases. As discussed in Figure 4-13, the IFT is mainly affected by the average size of nanoparticles in the solution. It appears that pressure does not have a significant effect on the stability (size) of nanoparticles in the H+ protected method. Since the size of nanoparticles is not affected by pressure, the IFT trend is also is similar in all pressures.
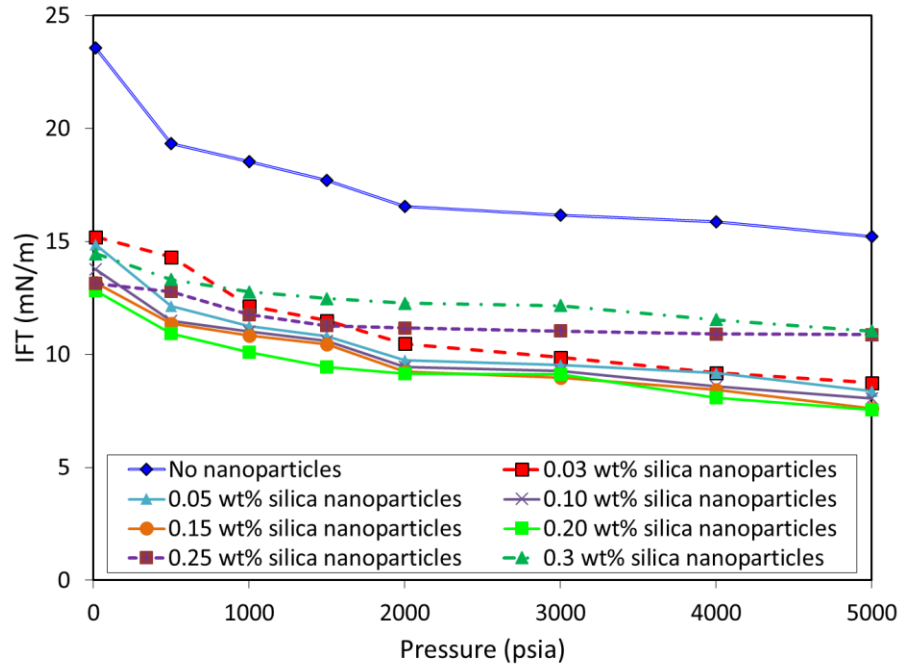
(a) Seawater containing 0.025 wt% HCl
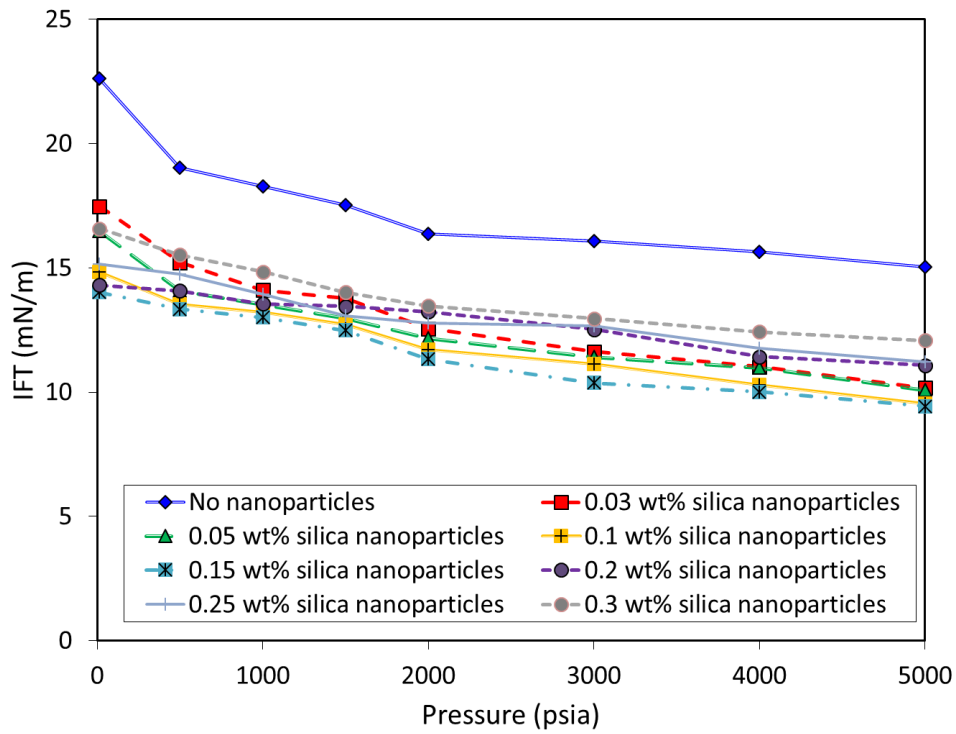
(b) Seawater containing 0.0076 wt% HCl

Figure 4-16: Effect of temperature on oil-water interfacial tension a) 0.025 wt% HCl and b) 0.0076 wt% HCl

4.4.5. Simulation study

The maximum reduction in oil-water interfacial value is obtained for 0.20 wt% of silica nanoparticles for solution containing 0.025 wt% HCl and 0.15 wt% nanoparticles for 0.0076 wt% HCl, where IFT value reduces from 23.56 ± 0.36 mN/m to 12.81 ± 0.77 mN/m and from 22.61 ± 0.41 mN/m to 14.01 ± 0.87 mN/m for 0.025 wt% HCl and 0.0076 wt% HCl, respectively. The question is does this amount of IFT reduction can have a remarkable effect on oil recovery? Can we consider IFT reduction as a possible mechanism for nanoparticle-EOR methods? Lower IFT value leads to higher capillary number and lower residual oil. Gray et al. [77] stated that two or three orders of magnitude IFT reduction is required to mobilize the oil. However, Rabiei et al. [78] showed that even less than 1 order of magnitude reduction in IFT value can have a significant effect on oil recovery. IFT alteration can affect the capillary curve [188] and oil-water relative permeability [81, 84]. Capillary pressure data for offshore NL oil and seawater is measured using centrifuge method and the capillary data was adjusted for the case of nanoparticles-solution using Leverett j-function [188].

$$\frac{(P_c)_1}{(P_c)_2} = \frac{(\gamma_{ow} \cos{(\theta_{ow})})_1}{(\gamma_{ow} \cos{(\theta_{ow})})_2} \tag{4-13}$$

where $(P_c)_1$ and $(P_c)_2$ are capillary pressures for oil-water system without and with nanoparticles, respectively. γ_{ow} is oil-water IFT and θ_{ow} is the contact angle between oil-water and rock. If we assume that IFT change is the only reason for oil recovery (it should be noted that in reality the θ_{ow} can also be affected by presence of nanoparticles), the capillary pressures can be corrected for nanoparticles-solution using the following equation:

$$\frac{(P_c)_1}{(P_c)_2} = \frac{(\gamma_{ow})_1}{(\gamma_{ow})_2} \tag{4-14}$$

Offshore NL oil-water relative permeability reported by Cao et al. [189] is used to develop the core-flooding model. The relative permeability correction for nanoparticles is quite complicated. In order to observe a remarkable change in the residual oil and irreducible water saturation, the capillary number should exceed the critical capillary number value. This critical capillary number is obtained for IFT values ranged from 0.1 to 0.01 mN/m in most studies which are far less than our IFT values [79, 81]. On the other hand, Shen et al. [85] stated that noticeable changes in the oil-water relative permeability only can be observed in the small IFT values (< 3 mN/m). If the IFT reduction is the only influence of nanoparticles on the system then no remarkable changes in the relative permeability should be expected. The oil-water relative permeability and the capillary pressure for the oil-water system without nanoparticles are summarized in Table 4-9.

Table 4-9: Relative permeability and capillary pressure data for seawater-oil without nanoparticles

Water Saturation	Water Relative Permeability (Krw)	Oil Relative Permeability (Kro)	Capillary Pressure (Drainage) (kPa)
0.35	0	0.78	766.13
0.4	0.01	0.60	96.93
0.45	0.03	0.44	51.81
0.5	0.06	0.29	36.77
0.55	0.08	0.16	29.25
0.6	0.11	0.15	21.73
0.65	0.14	0.06	0
0.69	0.16	0	0

The core-flooding experiments are simulated using CMG. A rectangular cube matrix with a square cross section of 3×3 cm and height of 10 cm is considered. As shown in Figure 4-17, the model is equally divided into 3 grids in x-direction, 3 grids in y-direction and 10 grids in z-direction. Porosity of all blocks is assigned as 0.20. Permeability in Z direction is considered as 100 mD but in X and Y direction 10 mD is allocated for blocks.
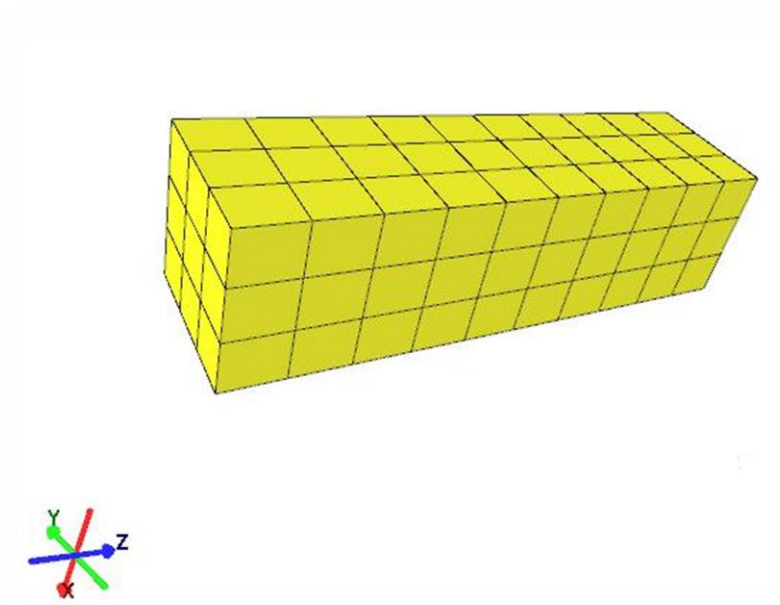
Figure 4-17: Schematic of core model used for simulation

Oil recovery in the cases with and without silica nanoparticles in seawater containing 0.025 wt% and 0.0076 wt% HCl are simulated and the results are shown in Figure 4-18. To validate the model, the simulation results for "without nanoparticles" is compared to core-flooding experiments conducted by Kim et al. [190] for offshore NL oil and seawater at ambient conditions. As illustrated in Figure 4-18, the ultimate recovery in the simulation data and the experiments are consistent. However, there are differences between experimental and simulation data in the first pore volume of injection. The standard deviations between simulation and experimental recovery for 0.5, 1.0, and 1.5 pore volumes of injection are 0.09, 0.03 and 0.01 respectively. The difference in the first pore volume of injection can be due to

the dead volume of core-flooding instrument, which, the injected aqueous phase displaced the oil from the core but there is a delay in the accumulation of oil in the graduated cylinders. By correcting the core-flooding data reported by Kim et al. [190] for dead volume, as shown in Figure 4-18, a better fit between the experimental and simulation data in the first pore volume of injection is obtained.. The simulation results reveal that IFT reduction cannot be the main mechanism for nanoparticle-EOR processes. Even with the maximum IFT reduction, 12.81 ± 0.77 mN/m and 14.01 ± 0.87 mN/m for 0.025 wt% HCl-seawater and 0.0076 wt%-seawater solutions, there is negligible difference in simulated oil recovery compared to water-flooding.

For 0.15 wt% silica nanoparticles in seawater containing 0.025 wt% HCl, we simulated the nanoparticle flooding considering a) only IFT reduction, and b) IFT reduction, wettability alteration, and relative permeability changes. As shown in Figure 4-18, considering the wettability alteration and relative permeability changes can significantly influence the simulated oil production from a model core sample. Experimentally, the wettability alteration data are obtained from [191] where for a Berea sandstone, the three-phase contact angle without nanoparticles and in the presence of silica nanoparticles (dispersed in seawater with 0.025 wt% HCl) is observed 51.7 ± 2.2 to 40.6 ± 1.4, respectively. Relative permeability data (Figure 4-19) is calculated from the unsteady-state core flooding data reported by Kim et al. [190] for 0.15 wt% silica nanoparticles dispersed in seawater containing 0.025 wt% HCl using JBN method [192]. The simulation results considering IFT reduction, wettability alteration, and relative permeability changes is consistent with the core-flooding data reported in [190] for the same conditions.
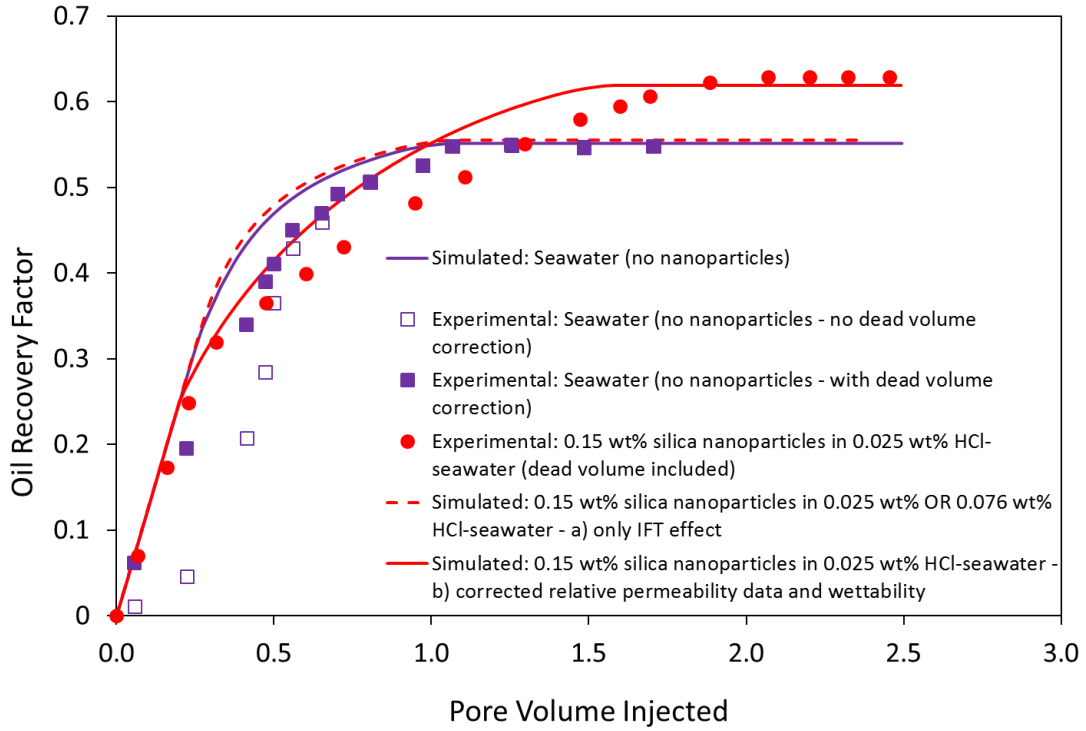
Figure 4-18: The effect of maximum IFT reduction on the oil recovery
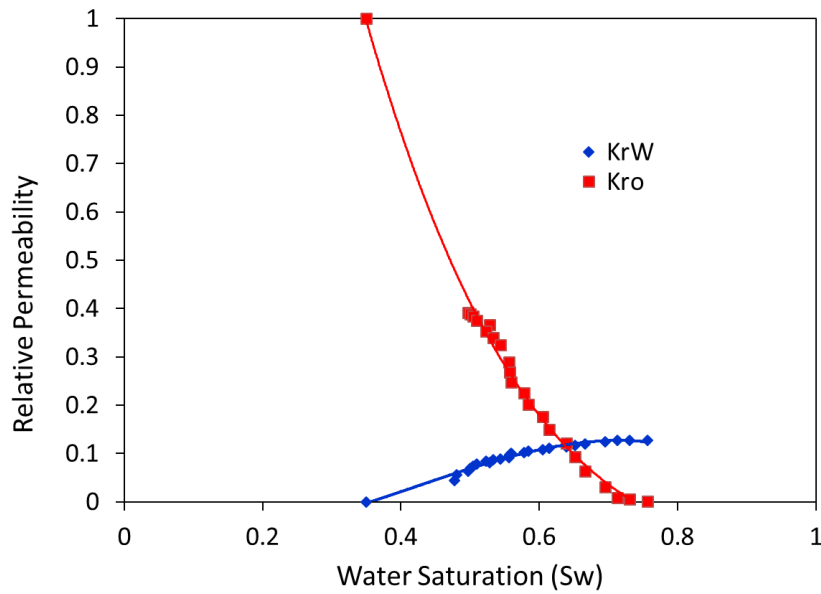
Figure 4-19: Oil and water relative permeability for H+ protected silica nanoparticles

4.5. Conclusion

In this paper, the mechanism and the conditions under which H^+-protected hydrophilic silica nanoparticles can reduce oil-water interfacial tension is experimentally investigated and the results compared with silica nanoparticles dispersed in the NaCl solutions. The major results are:

- H^+-protected hydrophilic silica nanoparticles can reduce oil-water IFT if the operating conditions and bulk properties are chosen appropriately. Maximum IFT reduction can be obtained for 0.20 wt% of silica nanoparticles for solution containing 0.025 wt% HCl and 0.15 wt% nanoparticles for 0.0076 wt% HCl, where IFT value reduces from 23.56 $\pm$ 0.36 mN/m to 12.81 $\pm$ 0.77 mN/m and from 22.61 $\pm$ 0.41 mN/m to 14.01 $\pm$ 0.87 mN/m for 0.025 wt% HCl and 0.0076 wt% HCl, respectively. Unlike silica nanoparticles dispersed in the NaCl solution, even a low concentrations of H^+-protected silica nanoparticles (0.03 wt%) can reduce oil-water IFT.

- The kinetic adsorption of H^+-protected silica nanoparticles and nanoparticles dispersed in a NaCl solution are quite similar. Three phases are observed in the kinetic adsorption of silica nanoparticles at the interface. At the early times (phase A), due to the absence of strong barriers to adsorption of nanoparticles, nanoparticles are rapidly adsorbed. At intermediate time periods (phase B), the presence of previously adsorbed nanoparticles at oil-water interface hampers further adsorption and reduces the adsorption rate. Hence, the rate in IFT reduction is not as pronounced. Finally, at late times (phase C), nanoparticle adsorption reaches a dynamic equilibrium with the desorption rate. The change in IFT during the rapid adsorption time (phase A) is much quicker for in seawater (around ten times faster in small concentrations, and

approximately double times in high concentrations). This is due to the reduction in the absolute zeta-potential of the oil-water interface and nanoparticles by adsorbed H^+ ions in their electrical double layer.

- By increasing the salt concentration of the solution, the zeta-potential of the nanoparticles decreases and the electrical double layer around the nanoparticle and oil-water interface compresses. Consequently, electrostatic barriers for adsorption of nanoparticles decrease and the repulsion between adsorbed nanoparticles at the interface decreases. Thus, a more compact monolayer can be formed at the oil-water interface and the IFT value decreases. Since the maximum compression of the electrical double layer occurs at critical salt concentration, the maximum IFT reduction is observed for this salt concentration for NaCl solutions.

- For H^+-protected silica nanoparticles, by increasing the concentration of silica nanoparticles, the oil-water interfacial tension decreases to reach a minimum value and then increases. The balance between the size of nanoparticles and the concentration of nanoparticles governs the maximum IFT reduction.

- For low concentrations of silica nanoparticles, the oil-water interfacial tension first decreases with increasing temperature and then the IFT increases. However, at high concentrations of nanoparticles, the IFT value increases with increasing temperature. Pressure does not have a significant effect on the performance of silica nanoparticles and the trend of decreasing oil-water interfacial tension is similar for the solutions with and without nanoparticles.

- IFT reduction cannot be the main mechanism for nanoparticle-EOR. Although nanoparticles can reduce the IFT value, its reduction is not sufficient to cause significant oil recovery.

5. CHAPTER FIVE

Toward A Mechanistic Understanding of Wettability Alteration in Reservoir Rocks Using Silica Nanoparticles (Paper 3, Published)

Abstract

Traditional concepts of simple liquid spreading may not apply to nanoparticle-fluids. Most investigations pertaining to the wettability alteration of solid surfaces due to the presence of nanoparticles in the fluid are oversimplified, i.e. nanoparticles dispersed in DI-water and smooth, homogeneous, and clean surfaces have been used. From a practical enhanced oil recovery (EOR) point of view, the nanoparticles must be dispersed in either seawater or high salinity formation water containing diverse types and concentrations of ions. These ions interact with the electrostatic properties of the nanoparticles. Likewise, the oil phase may contain many surface active components like asphaltene and naphthenic acids which can interact with nanoparticles at oil-water and oil-rock interface. In reality, the rock sample is a heterogeneous, non-smooth, mixed-wet substrate with a diverse mineralogical composition. The electrical charge of minerals can vary when contacted with an ionic fluid. This can alter the electrostatic repulsion between substrate and nanoparticles and consequently the substrate can either attract or repel charged particles, including nanoparticles. Hence, the role of nanoparticles must be evaluated considering multicomponent complex fluids and real formation rock.

Despite numerous reports regarding the wettability alteration of reservoir rock from oil-wet to water-wet by nanoparticles, some inherent limitations in the wettability alteration experiments prevent conclusions about the performance of nanoparticles in practical complex conditions. For instance, the wettability alteration by nanoparticles is often determined by contact angle measurements. In this method, the substrates are either aged with (immersed in) nanoparticle-fluids before conducting the experiments or contacted with nanoparticle-fluids before

attachment of the oil droplet on the rock surface. Hence, in both cases, before initiating the contact angle measurements, the nanoparticles would already exist at the oil-rock interface possibly giving inaccurate measurements.

The objective of this work is to investigate the mechanism of wettability alteration by silica nanoparticles pre-existing on the rock interface (conventional contact angle measurements) and using a new displacement contact angle method to better mimic the scenario of injecting a nanoparticle fluid into the reservoir already containing formation brine. The impact of pre-existing nanoparticles at the oil-rock interface (in the conventional contact angle measurements) on the contact angle measurements are examined for simple (n-decane, NaCl brine, and pure substrates) and complex (crude oil, seawater, and reservoir rock) systems on various wetting conditions of substrates (water-wet and oil-wet). The nanoparticles are dispersed in seawater using our H+ protected method [58]. Then, the effect of surface and nanoparticle charge on the contact angle is evaluated by adjusting the aqueous phase salinity. We also differentiate between the disjoining pressure mechanism and diffusion of silica nanoparticles through the oil phase by testing the attachment of nanoparticles on the rock surface.

5.1. Introduction

Utilizing a modified aqueous phase to remove and displace oil from a rock surface is one method to improve pore scale recovery during some chemical EOR methods such as smart water, low salinity water injection [193], surfactant flooding [194] , and potentially for nanoparticle enhanced water flooding [195]. This has led to a worldwide and still growing

interest in understanding mechanism of oil removal from a solid surface in the presence of an

aqueous solution containing micellar solutions [196, 197] and/or nanoparticles [119, 120, 198].

Kao et. al. [197] suggested the combination of "diffusion" and "roll-up" mechanisms to remove

oil from a solid surface in the presence of a micellar solution. They mentioned that the receding

of solid-oil-water contact angle is caused by the "roll-up" mechanism and the presence of the

second contact line is due to "diffusion". Roll-up, as shown in Figure 5-1a, can be simply

defined as the removal of an oil droplet from a rock surface due to the decrease in contact angle

between the aqueous phase and the substrate. Miller and Raney [199] presented the

"solubilization-emulsification" mechanism for oil removal from oily soils. In this mechanism,

as shown in Figure 5-1b, some portion of oil drop is detached from the surface by destabilizing

the oil-water interface (reducing oil-water interfacial tension).
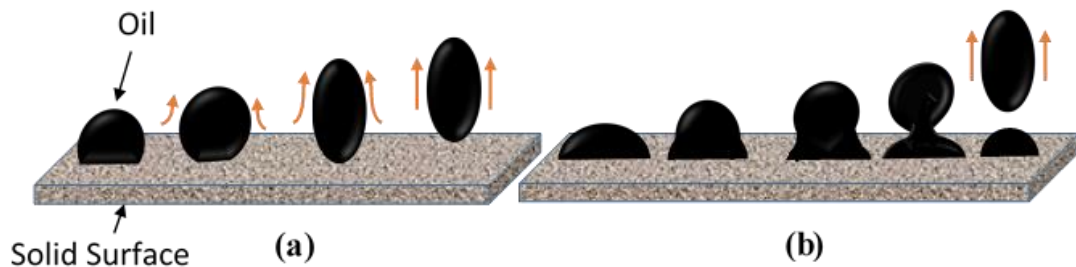
Figure 5-1: Mechanism of oil removal from a surface by a) roll-up, and b) emulsification (after [199])

Wettability alteration due to nanoparticles (nanoparticle-fluids) is complex. The conventional

concepts of simple liquid spreading [118], due to the complex interactions between the

nanoparticles and the solid surface at the three phase contact region, do not apply to

nanoparticle-fluids [119]. Kondiparty et al. [120] experimentally evaluated the dynamics of

nanoparticle-fluids spreading by directly observing the self-layering of nanoparticles. They

reached the conclusion that the three-phase contact line spontaneously decreases to reach an

equilibrium condition. Then, nanoparticles form ordered structures in the confinement of the three-phase contact region. This ordering in the wedge-like area causes an extra pressure in the film compared to bulk solution and separating oil drop from the surface, as illustrated in Figure 5-2. This pressure is known as "structural disjoining pressure". Sefiane et al. [121] reported that the change in the contact angle of oil, water, and rock surface can be due to combination of "structural disjoining pressure" and "adsorption" of nanoparticles on the rock's surface.
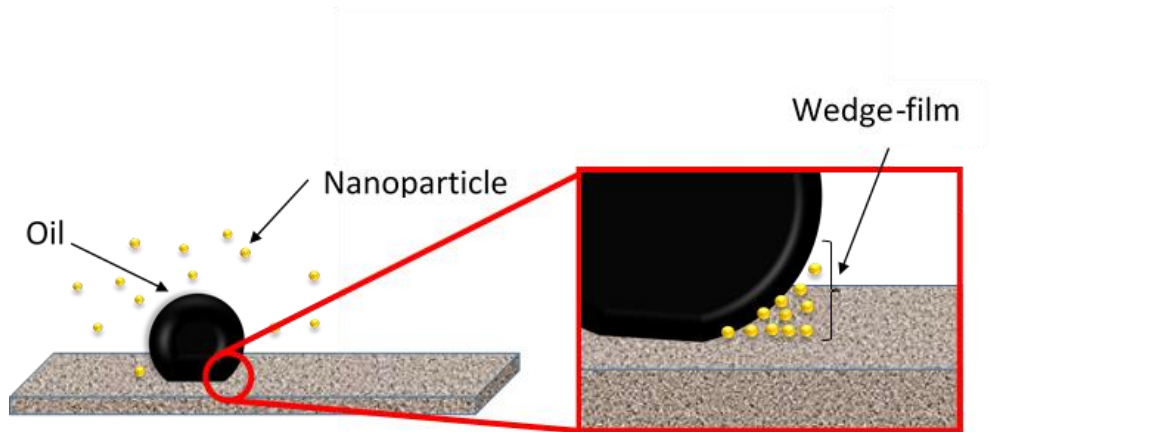
Figure 5-2: nanoparticle assembling is wedge film causes to structural disjoining pressure (After [122])

The wettability alteration of substrates using nanoparticle-fluids is sensitive to many factors including: nanoparticle size and concentration, initial contact angle [122], particle charge, surface wettability of nanoparticles [123], charge and roughness of the substrate surface, stabilizer concentration, type and concentrations of ions in the nanoparticle-fluids, bulk pressure and temperature, etc. Wasan et al. [122] tested canola oil drop spreading on a glass surface when surrounded by a silica nanoparticles-fluid. They pointed out that by increasing the concentration of nanoparticles, the structural disjoining pressure and spreading rate of the nanoparticles-fluid increases. They also noticed that the spreading rate of nanoparticles-fluid decreased with a decrease in the drop volume. Analyzing the effect of the contact angle on the shape of the meniscus profile illustrates that by altering the contact angle from 4° to 2.3° the

118

more pronounced nominal contact line displacement is observed, and the drop detached from the surface at 2.3°. They did not report the accuracy and precision of their experiments. Wang and Wu [123] examined the effect of particle charge and surface wettability of the nanoparticles on oil drop detachment from a surface by using molecular dynamic simulation. Their simulation showed that full detachment of oil droplet from a solid surface by nanoparticles is possible when the charge of particles exceeds a threshold value. They concluded that high charged hydrophobic nanoparticles have the best performance in oil detachment. Lim et al. [124] demonstrated that an oil drop detaches faster when the temperature and hydrophilicity of the substrate increases. In all these studies, the system was over simplified i.e. nanoparticles were dispersed in DI-water and the substrate was a smooth, clean and strongly hydrophilic surface. From an EOR point of view, wettability alteration of reservoir rock, and finally detachment of oil drop from a rock surface, is complex and oversimplified models may not fully mimic the practical EOR conditions. In the EOR processes, nanoparticles would be dispersed in either seawater or high salinity formation water containing diverse types and concentration of ions. The oil phase contains too many polar and nonpolar components which can affect the performance of nanoparticles. The substrate is a heterogeneous, non-smooth, mixed wet rock composed of various minerals. Further, the diverse minerals on the rock surface means that there are different electrostatic charges on the rock surface when contacted with an ionic solution.

Despite reports of wettability alteration of reservoir rock from oil-wet to water-wet by nanoparticles [17, 18, 200, 201], some inherent limitations in the contact angle measurements may prevent researchers from concluding about the performance and mechanism of wettability alteration by nanoparticles under realistic conditions. For instance, the wettability alteration of

nanoparticles is normally determined by apparent contact angle measurements. In this method, the substrates are either aged with (the substrate is submerged into the nanoparticles-fluid for couple hours [91] or couple days [103]) nanoparticle-fluids before conducting the experiments or it contacted with (the substrate is not aged in the nanoparticles-fluid, however, during the experiments the surface of substrate is exposed to the nanoparticle-fluid before attachment of oil droplet on the surface) nanoparticle-fluids before attachment of the oil droplet on the rock surface [90, 202-204]. In both cases as shown in Figure 5-3, in conventional contact angle measurements, the nanoparticles would already exist at the interfaces in both cases and possibly giving inaccurate measurements. However, under practical injection conditions, nanoparticles would not exist at the oil-rock interface before nanoparticle-fluids injection. Hence, the measured contact angles are not representative of practical injection conditions.
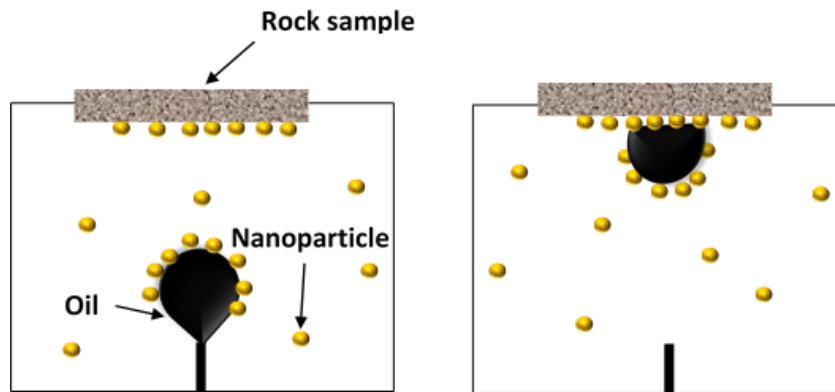
Figure 5-3: Nanoparticles at oil-rock interface during conventional contact angle measurements

In this study, the mechanism of wettability alteration by silica nanoparticles is investigated. The experiments are designed in a way to avoid inherent problems associated with conventional contact angle measurements. The effect of adsorbed nanoparticles at the oil-rock interface on the ultimate contact angle values in the simple (toluene, nanoparticles dispersed in 1 wt% NaCl, and pure minerals) and complex system (35°API offshore NL crude oil, H+ protected nanoparticles in seawater, and reservoir rocks) with various initial wetting conditions

(water-wet, and oil-wet) are examined. Then, the effect of nanoparticles and substrate charge on the wettability alteration performance of silica nanoparticles is investigated. Finally, the migration of silica nanoparticles through a continuous oil phase and its attachment at the rock surface is tested. Based on the results, the mechanism of wettability alteration by silica nanoparticles is discussed.

5.2. Materials and Methods

5.2.1. Materials

Nanoparticle-fluids: Amorphous hydrophilic silicon dioxide nanoparticles (SiO_2) (25 wt.% in deionized [DI] water) with the average diameter of 19.0 ± 0.8 nm and purity of greater than 99.9% were supplied by US Research Nanomaterial, Inc. Nanoparticle-fluids are prepared by dispersing 0.15 wt% of silica nanoparticles in either NaCl brine (simple system) or seawater using H+ protected method [58] (complex system). Based on this method, H+ ions prevent the multivalent ions in seawater to accumulate in the electrical double layer of silica nanoparticles by forming an H+ layer at electrical double layer and thus stabilizes them in seawater.

Oil phase: Decane (simple system) and 35ºAPI offshore NL crude oil (complex system) are used as the two oil phases.

Rock Samples: For the simple system, pure calcite, dolomite, and quartz are used as rock samples. For the complex system, chalk, carbonate rock and Berea sandstone are used. The size of the samples were approximately 1×1 cm^2. To obtain oil-wet samples, we aged the rocks in the crude oil at 60 ℃ for four weeks [205].

121

5.2.2. Methods

Contact angle measurements: As discussed before, the inherent limitations associated with conventional contact angle measurements can cause us to obtain misleading results. Hence, we modified the contact angle measurements in a way to have more consistency with practical EOR conditions. As shown in Figure 5-4, in real reservoir, first, the oil droplet is attached at the rock surface while formation water is surrounding that. Then, the formation water is displaced by nanoparticle-fluids. To mimic this condition in contact angle measurements, first the solid surface is contacted with a no nanoparticles aqueous phase and an oil drop (with the volume of 3-5 mm^3) is injected from the needle at the bottom of the cell. The drop is attached onto the rock surface and its side image is taken at a frequency of one image per second. After equilibrium (approximately 20 min after forming the drop based on dynamic contact angle measurements), the apparent contact angle (θ) is measured. This contact angle indicates the initial state of oil droplet in the reservoir. Then, the nanoparticles-fluid is injected very slowly into the measurement cell to displace the aqueous phase (displacement method). The water is displaced slow enough to not dislodge the oil droplet. To ensure that the aqueous phase is completely displaced with nanoparticles-fluid, the turbidity of outlet fluid is frequently measured and compared with the turbidity of the original nanoparticles-fluid. When the turbidity of the outlet fluid and the original nanoparticle-fluid are equal, we assume that the aqueous phase has been completely displaced by the nanoparticles-fluid. All experiments are conducted at ambient conditions. To check the repeatability of the measurements, three distinct measurements are performed, and the average is reported.
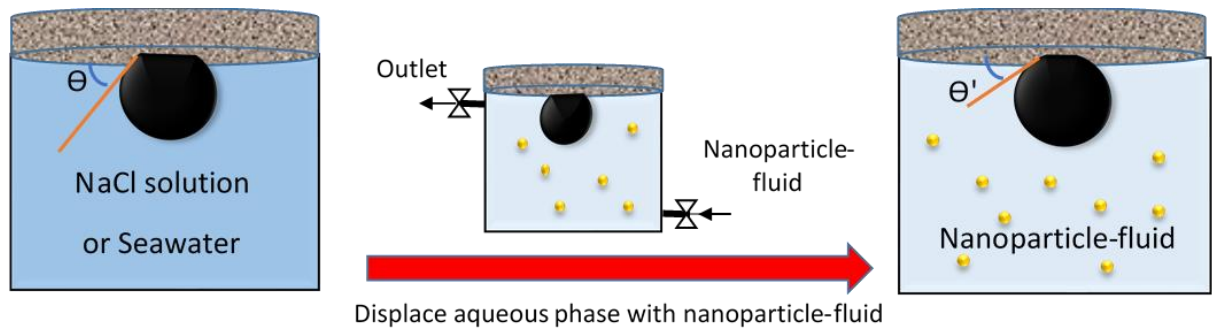
Figure 5-4: Schematic diagram of modified contact angle measurements procedure: a) measure contact angle of oil-water-substrate, b) displace aqueous phase with the nanoparticle-fluid, and c) measure the contact angle of oil-nanoparticle-fluid-substrate

Zeta-potential measurements: The zeta-potential of substrates and nanoparticles in various aqueous solutions are measured by a Malvern Zetasizer Nano Series ZS instrument. To measure the zeta-potential of rock surfaces, the rock samples are milled and 1 wt% of milled rocks are dispersed in aqueous solutions and mixed with magnetic mixer for 30 minutes. Then the zeta-potential of the samples are measured as described in [206].

Diffusivity experiments: A series of experiments are designed to detect the possible migration of silica nanoparticles through the oil phase. As shown in Figure 5-5, the rock sample is located at the top of the cell in contact with a layer of oil (the oil thickness is chosen arbitrarily as 1 mm) at ambient conditions. First, the cell is filled using a the aqueous phase (no nanoparticles) and after three weeks, the images of the substrate contacted with an oil phase are taken by scanning electron microscope (SEM). Then, the aqueous phase is replaced by the nanoparticle-fluid and after three weeks, another SEM image is taken from the same surface to detect possible nanoparticle attachments on the rock surface.
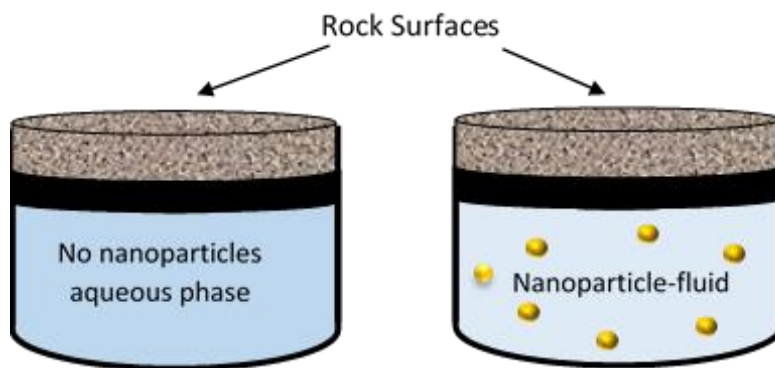
Figure 5-5: Schematic diagram of diffusivity detection cells

5.3. Results and Discussion

The impact of the experimental method on contact angle measurements for simple and complex systems is illustrated in Figure 5-6 and Figure 5-7, respectively. For each system, the apparent contact angle is measured for the three cases of no nanoparticles, with the new displacement method, and conventional method with nanoparticles. The initial conditions of the rocks are modified in a way to have an oil-wet and a water-wet surfaces for each rock types.

For water-wet simple system, as shown in Figure 5-6a, the initial contact angle (without nanoparticles) for dolomite, quartz and calcite are measured (in degrees) as 70.8 ± 1.5, 77.6 ± 1.8 and 55.6 ± 1.7, respectively.   By introducing silica nanoparticles in the system using the displacement method, the contact angles for three mentioned substrates decrease to 56.3 ± 1.7, 73.7 ± 1.8, and 47.4 ± 2.3, respectively. On the other hand, by adding nanoparticles using the conventional contact angle measurement method, the contact angles reduce to 47.5 ± 1.5, 64.5 ± 1.6, and 37.9 ± 2.0, respectively. The difference in the contact angle values obtained by the displacement and conventional methods illustrate the effect of already adsorbed nanoparticles at the oil-rock interface on the measurement of contact angles. The results show that more water-wet substrates are possible to obtain by nanoparticle-fluids. However, a substantial

124

portion of wettability alteration by nanoparticles in the water-wet rocks is solely due to the experimental artefacts (trapped nanoparticles in the oil-rock interface) which we would not have it in the realistic conditions. On the other hand, for oil-wet simple systems, as illustrated in Figure 5-6b, adding silica nanoparticles into the system by the displacement method had no significant change in contact angle.Whereas, the conventional method of contact angle measurements shows that nanoparticles can alter the wettability of the substrates from oil-wet to intermediate-wet condition. Obviously, the changes in the contact angle of the oil-wet conditions is due to experimental artefact, and nanoparticles does not have a significant effect on the wettability of oil-wet rocks.

(a) Water-wet condition   (b) Oil-wet condition
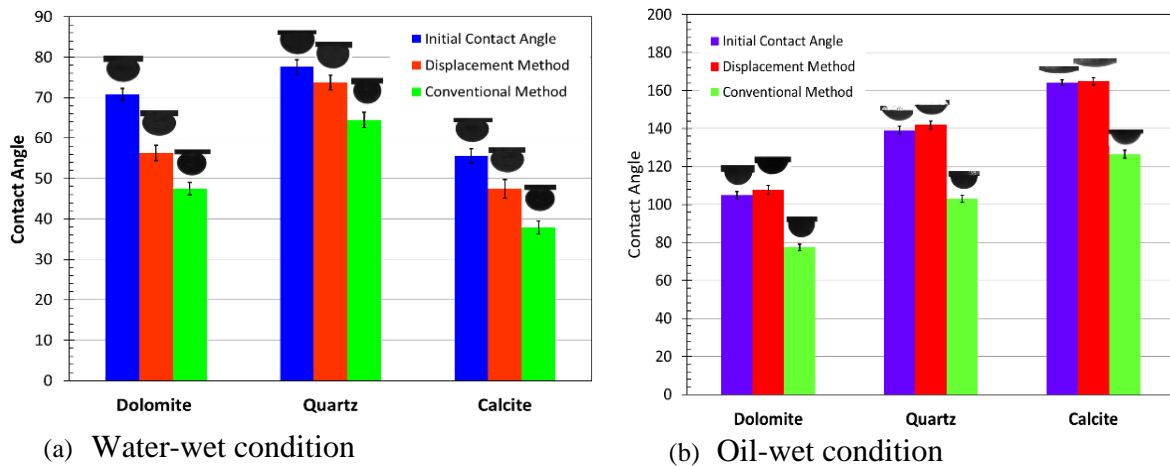
Figure 5-6: Wettability alteration due to the presence of silica nanoparticles in simple systems

Similar trends are also observed for complex systems. As shown in Figure 5-7a, for water-wet conditions, by introducing silica nanoparticles in the system using displacement method, the contact angle value decreases. However, the reduction in contact angle is far less than what is obtained using the conventional contact angle method. The contact angle measurements for oil-wet conditions in the complex system again show similar behaviour to the simple system. The displacement method results is no significant change in contact angle (as a slight increase)

while the contact angle decrease using the conventional method. The difference between conventional and displacement contact angle measurements is summarized in Table 5-1.

(a) Water-wet condition   (b) Oil-wet condition
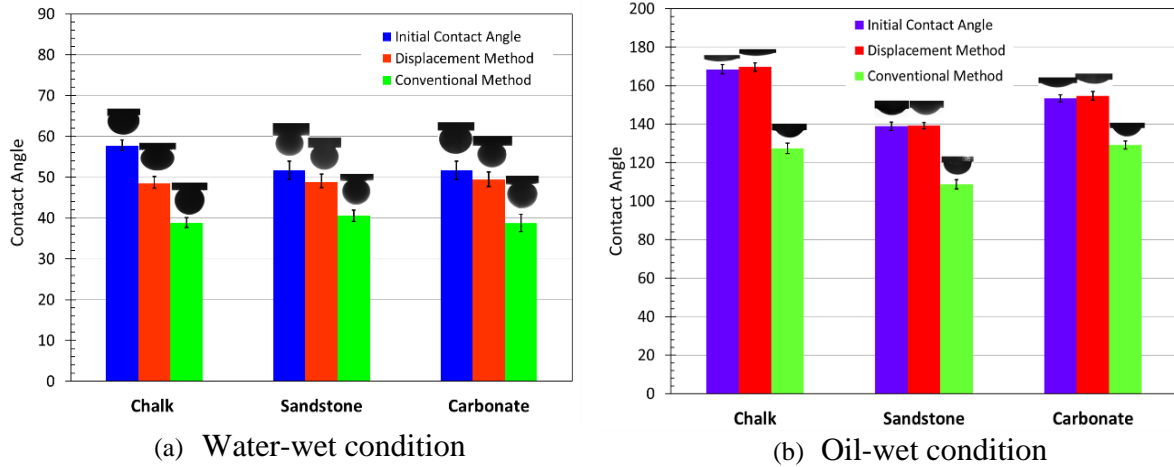
Figure 5-7: Wettability alteration due to the presence of silica nanoparticles in complex systems

Table 5-1: The difference between conventional and displacement contact angle measurements

Experiments Type	Rock Type	Oil Type	Initial Contact Angle	Difference between two measurements methods
Simple water-wet	Dolomite	Decane	70.8 ± 1.5	8.75 ± 1.9
	Quartz	Decane	77.6 ± 1.8	9.2 ± 1.9
	Calcite	Decane	55.6 ± 1.7	9.53 ± 2.3
Simple oil-wet	Dolomite	Decane	104.9 ± 1.8	30.4 ± 2.3
	Quartz	Decane	139.2 ± 2.0	39.0 ± 2.1
	Calcite	Decane	164.1 ± 1.4	38.3 ± 1.9
Complex water-wet	Chalk	Crude oil	57.8 ± 1.3	9.6 ± 1.7
	Sandstone	Crude oil	51.7 ± 2.2	8.2 ± 2.0
	Carbonate	Crude oil	51.7 ± 2.2	10.6 ± 1.9
Complex oil-wet	Chalk	Crude oil	168.5 ± 2.4	42.2 ± 2.7
	Sandstone	Crude oil	138.9 ± 2.1	30.5 ± 2.4
	Carbonate	Crude oil	153.4 ± 1.8	25.5 ± 2.3

In water-wet systems, the nanoparticles can interact at the three-phase interface in both the conventional and displacement methods since the surface is water-wet. The exaggerated reduction in contact angle using the conventional method is indicative of the nanoparticles pre-existing at the interface. The marked decrease in contact angles observed for the conventional contact angles measurements on an oil-wet surface indicates that the nanoparticles can interact

with the oil covered mineral and rock before an oil droplet is attached. Whereas in the displacement method, the nanoparticles have no way of forming a wedge since the oil droplet is in contact with the oil covered mineral or rock.

Based on the disjoining pressure theory for wettability alteration of nanoparticles, for nanoparticles to modify the oil-water-rock contact angle, the wedge-film must be formed in the three-phase interface. In the water-wet condition, as shown in Figure 5-8, there is a wedge-film, therefore, nanoparticles can accumulate in the confinement of oil-water-rock contact region and alter the contact angle by structural disjoining pressure. Furthermore, by introducing the nanoparticles in the system and their adsorption on the oil-water interface, the oil-water interfacial tension and subsequently the capillary pressure decreases. Decreasing the capillary pressure causes the wetting phase (here water) to spread more on the rock surface. Based on the capillary pressure equation ($P_c = P_{nw} - P_w$), the reduction in the capillary pressure means an increase in the pressure of the wetting phase, or decrease in the pressure of the non-wetting phase, or combination of both. In all cases, the equilibrium between the wetting and non-wetting phases on the rock surface collapses in the direction of excessive pressure from the wetting phase when nanoparticles are introduced compared to the previously equilibrated condition. Hence, as shown in Figure 5-8a, the capillary pressure and structural disjoining pressure affect the three-phase contact line in the same direction making the substrate more water-wet.

However, under oil-wet conditions, there is no wedge-film at the three-phase contact line. Hence, the nanoparticles cannot diffuse into the oil-rock interface to induce structural disjoining pressure. On the other hand, as shown in Figure 5-8b, the capillary pressure

reduction cause to more spreading of the oil phase on the rock surfaces (wetting phase) and consequently slightly shifting the rock surfaces toward oil-wet condition.
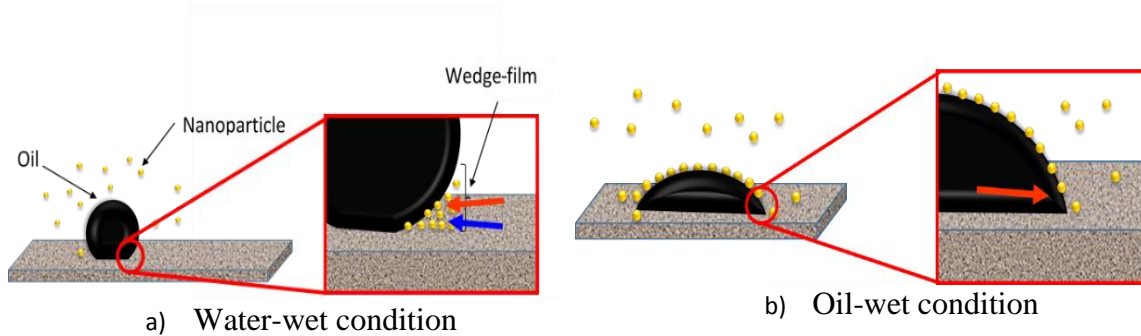
Figure 5-8: Mechanism of wettability alteration in a) water-wet and b) oil-wet conditions. Red arrow illustrates the forces due to capillary pressure reduction and blue arrow shows the forces due to disjointing pressure alteration

5.3.1. Effect of surface and nanoparticles' charge

The effect of substrate surface charge and nanoparticle's charge on the wettability alteration ability of silica nanoparticles is investigated. To accurately study the mechanism and avoid possible elaborations such as the effect of mineral variety of the rock surface, oil composition, and etc., a simple system of calcite, NaCl brine, and decane is employed. For NaCl brine concentrations of 0, 1, 2, and 5 wt%, the surface charge of calcite rock, initial contact angle (before introducing nanoparticles), ultimate contact angle (after nanoparticles are introduced with displacement method), and the charge of silica nanoparticles are measured, and the results are illustrated in Figure 5-9a. By increasing the NaCl concentration, the surface charge of calcite and silica nanoparticles move toward less negative or positive values. In other words, the absolute charge of calcite and silica nanoparticles decreases by increasing the salinity. On the other hand, the contact angle measurements reveal that by increasing the salinity, in both cases of with and without nanoparticles, more water-wet substrates can be achieved. However, as shown in Figure 5-9b, wettability alteration of calcite substrate due to the presence of nanoparticles decreases as salinity increases. By increasing the NaCl concentration, the

absolute charge of calcite surface and oil-water interface decreases. Hence, the electrostatic repulsion force between these two surfaces decreases and subsequently the disjoining pressure between the surface and the droplet increases. Furthermore, the excessive salinity compresses the electrical double layer of nanoparticles and consequently reduces the electrostatic repulsion between nanoparticles-nanoparticles and surfaces-nanoparticles. Hence, the extra pressure in the wedge-film (structural disjoining pressure) decreases. On the other hand, by increasing salinity, the absolute charge of nanoparticles reduces, and the number of adsorbed nanoparticles at the oil-water interface increases. Therefore, the IFT value and capillary pressure decreases. Capillary pressure reduction can lead to more spreading of wetting phase (water-wet condition). However, the impact of structural disjoining pressure outweighs the influence of capillary pressure. Hence, less pronounced wettability alteration is observed by increasing the salinity.
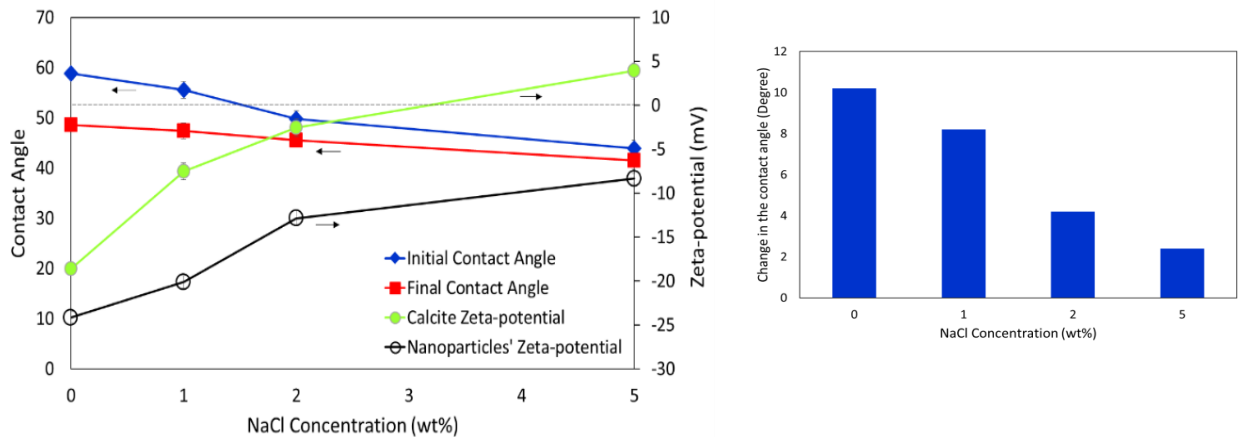
Figure 5-9: a) Effect of the nanoparticles' and calcite surface' charge on the wettability alteration ability of silica nanoparticles, b) Wettability alteration due to the presence of nanoparticles in various salinities

5.3.2. Migration of nanoparticles through the oil phase

The nanoparticles' possible migration through the oil phase and its attachment on the rock surface is another uncertainty in the mechanism of wettability alteration due to the presence of

nanoparticles. As shown in Figure 5-10, the primary evaluations with SEM images shows that there is no sign of silica nanoparticles agglomerations on the surface of pure calcite. However, the presence of an oil layer on the calcite surface limits the resolution of the SEM image to detect the single nanoparticles (not agglomerations of nanoparticles) on the calcite surface. Hence, more research is required to investigate the diffusion of nanoparticles through oil phase and evaluate the effect of pressure and temperature.
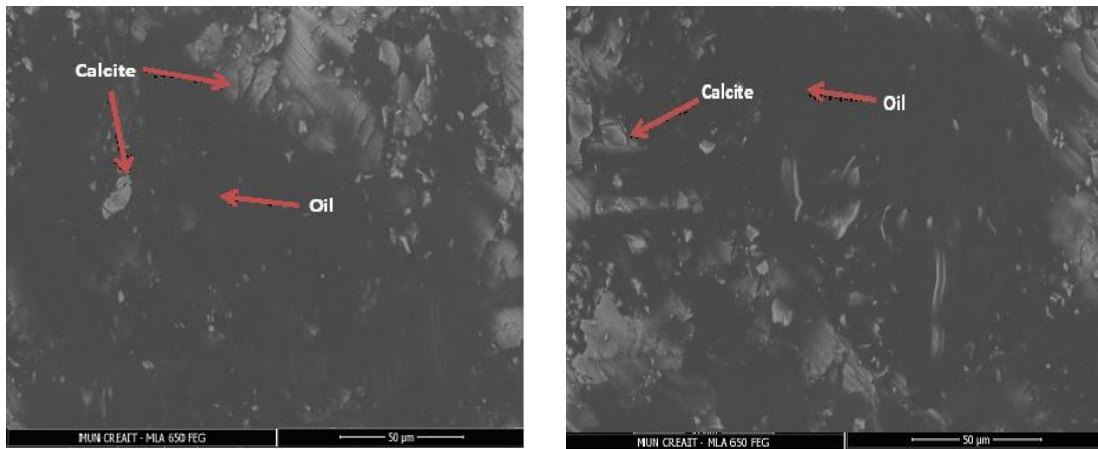
Figure 5-10: SEM image of calcite surface before (right) and after (left) contacting with an oil layer and nanoparticles

5.4. Conclusion

1. A large part of the wettability alteration ability of nanoparticles reported in the literature may be attributed to the method of measuring the contact angles where nanoparticles can adsorb on the rock surface before the introduction of the oil droplet. We show that the experimental methodology in how and when the nanoparticles and oil droplet are introduced is important in determining the wettability alteration capability of nanoparticles. If the nanoparticle fluid is in contact with the rock surface before the oil droplet is introduced, the reduction in contact angle may be skewed and overestimated compared to the more realistic situation of the nanoparticle-fluid being introduced into an already established three-phase equilibrium of oil-water-substrate.

2. Silica nanoparticles injected in an aqueous based nanoparticle-fluid are shown to reduce the contact angle (make the substrate more water-wet) only when the initial conditions are water-wet. Under oil-wet conditions, there is no significant change in wettability when a nanoparticle-fluid is injected.

3. Synergic effect of structural disjoining pressure and capillary pressure reduction is the mechanism of wettability alteration in the water-wet conditions. In the oil-wet conditions, the only possible mechanism is capillary pressure reduction.

4. The wettability alteration of calcite substrates in the presence of nanoparticles decreases with increasing salinity due to reduction of nanoparticle-nanoparticle and surface-nanoparticle electrostatic repulsion.

5. We did not observe nanoparticles diffusion through an oil film to attach to the rock surface. More investigation is required for conclusive results.

6.CHAPTER SIX

Summary and Recommendations for Future Work

Nanoparticles, due to their large surface area and small size, could be a promising water additive for EOR techniques. Previous literature illustrates the effectiveness of various nanoparticles in increasing oil production. Core-flooding and micromodel experiments revealed a significant extra oil production during nanoparticle enhanced water flooding. The EOR mechanism of nanoparticles is mainly attributed to the wettability alteration and IFT reduction, although other mechanisms such as in situ emulsification and water pathway alterations are also proposed. Despite efforts, there are many answers required before considering nanoparticles for EOR in the field.

Nanoparticles' stability in the aqueous phase is the first and foremost challenge. Nanoparticles are often dispersed in DI-water or low salinity NaCl brine in laboratory studies. Unlike nanoparticles' great stability in DI-water or low salinity NaCl brine, they are extremely unstable in high salinity diverse types of ionic solutions. Unstable nanoparticles can cause detrimental effects in oil reservoir through the aggregation of nanoparticles, plugging pore spaces, and consequently reducing permeability.

Another challenge of nanoparticle-EOR methods is the disparities of the laboratory experiments outcomes. The effects of nanoparticles on the IFT value, wettability alteration, and oil recovery from the sample reservoir cores are not conclusive. This is because many factors can affect the performance of nanoparticles in practical conditions and the presence or absence of one parameter can have a significant effect on the ultimate results. For instance, the performance of nanoparticles in IFT reduction, in addition to the nanoparticle's type and properties, can also be affected by the bulk properties of the aqueous solution (salinity, ion types and concentrations, and pH), oil phase characteristics (oil composition, concentration of natural surfactants such as asphaltene and resin), and operating conditions (temperature and

133

pressure). Hence, to evaluate the effect of nanoparticles on EOR, the mechanism of IFT reduction and wettability alteration by nanoparticles and the influence of various parameters must be precisely investigated.

The effect of nanoparticles on oil recovery is evaluated only in the laboratory scale by core-flooding, micromodel experiments, IFT measurements, and wettability alteration tests. The feasibility of upscaling these laboratory results to the real field scale is still unclear. In some cases, the experiments are oversimplified or the effect of some parameters are ignored. For instance, nanoparticles are dispersed in DI-water and smooth, homogeneous, and clean surfaces have been used. Furthermore, some laboratory experiments such as contact angle measurements are designed in a way that cannot mimic the real reservoir conditions.

In this thesis, some of these major challenges were addressed. After reviewing the literature about nanoparticle-EOR, the stability of nanoparticles in the aqueous solutions containing different types and concentrations of ions was discussed in chapter three. The mechanism of IFT reduction by nanoparticles and the effect of different parameters on the performance of nanoparticles was investigated in chapter four. In chapter five, the effect of pre-existing nanoparticles at the oil-rock interface on the wettability alteration capacity of nanoparticles was tested and the mechanism of wettability alteration by nanoparticles and the effect of different parameters was investigated.

6.1. Stability of nanoparticles

The main objective of this phase of the thesis was to find a method to stabilize silica nanoparticles in seawater. Since seawater is the main water resource for water enhanced nanoparticles flooding in offshore reservoirs, stabilizing silica nanoparticles in seawater is

extremely important. To this end, first, the stability of silica nanoparticles in the presence of different types and concentrations of ions is examined and the results are compared with the well-known DLVO theory. The results revealed that the presence of multivalent cation ions in the electrical double layer of silica nanoparticles destabilizes nanoparticles in seawater. Hence, to stabilize silica nanoparticles in seawater (or any ionic solution), the presence of multivalent ions in the electrical double layer of nanoparticles must be prevented. We proposed a novel method to stabilize silica nanoparticles in seawater (named the "H+ protected" method). In this method, the nanoparticles are first placed in an acidic solution to fill the electrical double layer of nanoparticles with H+ ions. Then, the prepared nanoparticle suspension is diluted by adding the desired amount of seawater. The presence of H+ ions prevents the multivalent ions in seawater from accumulating in the electrical double layer of silica nanoparticles by forming an H+ layer at the electrical double layer and thus stabilizes nanoparticles in seawater. The stability of silica nanoparticles using the H+ protection method was evaluated with different concentrations of nanoparticles and H+ ions.

6.2. IFT reduction

This phase of the study investigated the mechanism of oil-water interfacial tension reduction by nanoparticles. For nanoparticles to reduce the oil-water IFT, nanoparticles must self-assemble and form and sustain a monolayer at the interface. A tightly packed monolayer leads to lower IFT values. The adsorption of silica nanoparticles is energetically favoured (the attachment of nanoparticles at the interface reduces the energy of the interface) and DLVO calculations show that van der Waals attraction forces outweigh electrostatic repulsion forces. Hence, from the energy and force balance points of view, silica nanoparticles must self-assemble at the oil-water interface. However, energy reduction due to the adsorption of

nanoparticles at the interface is far less than the adsorption energy of micrometer particles; hence, it is possible that nanoparticles desorb from the interface due to thermal fluctuations. We observed three phases in the kinetic adsorption of silica nanoparticles at the interface. At the early times (phase A), due to the absence of strong barriers to the adsorption of nanoparticles, nanoparticles are rapidly adsorbed. At intermediate time periods (phase B), the presence of previously adsorbed nanoparticles at the oil-water interface hampers further adsorption and reduces the adsorption rate. Hence, the rate in IFT reduction is not as pronounced. Finally, at late times (phase C), nanoparticle adsorption reaches a dynamic equilibrium with the desorption rate. The change in IFT during the rapid adsorption time (phase A) is much quicker for in seawater (around ten times faster for small concentrations, and approximately double the time for high concentrations). This is due to the reduction in the absolute zeta-potential of the oil-water interface and nanoparticles by adsorbed H^+ ions in their electrical double layer.

Controlling parameters such as bulk solution properties (concentration of nanoparticles, the concentration of HCl, size, and charge of nanoparticles), and operating parameters (temperature and pressure) on the self-assembly of nanoparticles were also investigated. We observed that the balance between the size of nanoparticles and their concentration in the bulk solution governs the maximum IFT reduction. Increasing the concentration of nanoparticles in the solution causes achieving lower IFT values; however, the chance of collision between nanoparticles also increases with nanoparticle concentration; thus, the size of nanoparticles increases.

By increasing the salt concentration in the solution, the zeta-potential of nanoparticles decreases and the electrical double layer around the nanoparticle and oil-water interface

compresses. Consequently, electrostatic barriers for adsorption of nanoparticles and the repulsion between adsorbed nanoparticles at the interface decrease. Thus, a more compact monolayer can be formed at the oil-water interface and lower IFT values can be obtained. Since the maximum compression of the electrical double layer occurs at the critical salt concentration, the maximum IFT reduction is observed for this salt concentration for NaCl solutions.

We noticed that pressure has no significant impact on the performance of silica nanoparticles. Relatively similar trends of IFT reduction as a function of pressure were observed for the cases with and without nanoparticles. However, the presence of nanoparticles can alter the trend of IFT reduction by temperature for the no nanoparticles case. For low concentrations of silica nanoparticles, the oil-water IFT first decreases with increasing temperature and then increases. However, at the high concentrations of nanoparticles, the IFT value continuously increases with increasing temperature.

6.3. Wettability alteration

The aim of this phase of the study was to investigate the mechanism of wettability alteration by nanoparticles. First, the effect of pre-existing nanoparticles at the oil-rock interface during conventional contact angle measurements (experimental mistake) was evaluated. We observed that a large portion of the wettability alteration ability of nanoparticles reported in the literature may be attributed to the pre-existing nanoparticles at the oil-rock interface before conducting the contact angle measurements. Then, the effect of nanoparticles on the wettability alteration of different rock substrates with various initial wetting conditions was examined. The experimental results revealed that silica nanoparticles further reduce the contact angle (make the substrate more water-wet) only when we have a water-wet condition initially. Under oil-

wet conditions injecting, nanoparticles cause no significant change on the contact angle. A possible mechanism for wettability alteration by nanoparticles in water-wet conditions is the synergic effect of structural disjoining pressure and capillary pressure reduction. However, for oil-wet conditions, the only possible mechanism is capillary pressure reduction.   We noticed that increasing salinity weakens the ability of nanoparticles to alter the rock wettability due to the reduction of electrostatic repulsion between nanoparticles-nanoparticles and surfaces-nanoparticles in the wedge-film.

6.4. Recommendations for Future Work

IFT reduction and wettability alteration may not be the principle reason for nanoparticle-EOR. Hence, the mechanism of nanoparticle-EOR must be sought in other phenomena. The recommendations for future work based on the results of this thesis are summarized below:

- In the H+ protection method, four factors affect the stability of silica nanoparticles, the concentration of nanoparticles, the concentration of HCl, time, and temperature. We evaluated the effect of the first two parameters. The stability period of nanoparticles reduces at elevated temperature. Hence, there might be a relation between time and temperature for each nanoparticle/HCl ratio. It might be helpful to obtain this relation.

- The adsorption of nanoparticles at the oil-water interface reduces the IFT value. However, the magnitude of IFT reduction by silica nanoparticles is not sufficient to consider the IFT reduction as a mechanism of nanoparticle-EOR. The mechanism of IFT reduction by nanoparticles might be similar to that of surfactants. Presence of nanoparticles at the oil-water interface alters the force balance of interface molecules. Increase or decrease in the IFT value depends on the strength of molecular interactions between oil -nanoparticle molecules and water -nanoparticle molecules at the interface

138

compared to original oil-water molecular interactions. More strong interactions dictate lower IFT values. It is possible that nanoparticles are engineered in a way to achieve relatively less IFT value. More research is required to redesign the nanoparticles to obtain ultra-low IFT values.

- Nanoparticles have no significant effect on the wettability alteration of oil-wet substrates. They only can alter the wettability of water-wet rocks to more water-wet conditions. It is still unclear how nanoparticles increase oil recovery especially in the oil-wet systems.

- For nanoparticles to alter the rock wettability, they are required to reach the rock surface. However, in the oil reservoir, we normally have a layer of oil on the rock surface which prevents nanoparticles from direct contact with the rock surface. Hence, it is important to understand how nanoparticles migrate from an aqueous phase to the rock surface. SEM does not have enough resolution to detect the possible diffusion of nanoparticles through an oil phase and their attachment on the rock surface. Another method, such as atomic force microscopy (AFM), must be used to detect the possible migration of nanoparticles through an oil phase. The effects of oil layer thickness, temperature, pressure on the possible migration of nanoparticles must be evaluated to find the critical oil thickness in each operating condition (temperature, pressure); that would allow nanoparticles to reach the rock surface. Furthermore, the effect of the charge of the rock surface on the possible critical thickness must be investigated.

- Oil phase properties such as oil composition, concentration of natural surfactants, concentration of polar components, etc. can affect the performance of nanoparticles in IFT reduction and wettability alteration. More research is required to evaluate the effect

139

of the oil phase properties on IFT and wettability alteration with and without nanoparticles.

References

1. Petroleum, B., *BP energy outlook 2035*. BP stats, Jan, 2014.
2. Conti, J., et al., *International Energy Outlook 2016, With Projections to 2040. May 2016*. Washington, DC, USA: US Energy Information Administration (EIA). doi: DOE/EIA-0484, 2014.
3. Thomas, S., *Enhanced oil recovery-an overview*. Oil & Gas Science and Technology-Revue de l'IFP, 2008. **63**(1): p. 9-19.
4. Ayatollahi, S. and M.M. Zerafat. *Nanotechnology-assisted EOR techniques: New solutions to old challenges*. in *SPE International Oilfield Nanotechnology Conference and Exhibition*. 2012. Society of Petroleum Engineers.
5. Perez, J.M., *Iron oxide nanoparticles: hidden talent*. Nature nanotechnology, 2007. **2**(9): p. 535-536.
6. Munshi, A., et al., *Effect of nanoparticle size on sessile droplet contact angle*. Journal of Applied Physics, 2008. **103**(8): p. 084315.
7. Jafari, S., et al., *Experimental investigation of heavy oil recovery by continuous/WAG injection of CO2 saturated with silica nanoparticles*. International Journal of Oil, Gas and Coal Technology, 2015. **9**(2): p. 169-179.
8. Suleimanov, B., F. Ismailov, and E. Veliyev, *Nanofluid for enhanced oil recovery*. Journal of Petroleum Science and Engineering, 2011. **78**(2): p. 431-437.
9. Horikoshi, S. and N. Serpone, *Introduction to nanoparticles*. Microwaves in Nanoparticle Synthesis: Fundamentals and Applications, 2013: p. 1-24.
10. Bell, A.T., *The impact of nanoscience on heterogeneous catalysis*. Science, 2003. **299**(5613): p. 1688-1691.
11. Chávez-Miyauchi, T.s.E., A. Firoozabadi, and G.G. Fuller, *Nonmonotonic Elasticity of the Crude Oil–Brine Interface in Relation to Improved Oil Recovery*. Langmuir, 2016. **32**(9): p. 2192-2198.
12. Hendraningrat, L. and O. Torsæter, *Metal oxide-based nanoparticles: revealing their potential to enhance oil recovery in different wettability systems*. Applied Nanoscience, 2015. **5**(2): p. 181-199.
13. Zargartalebi, M., R. Kharrat, and N. Barati, *Enhancement of surfactant flooding performance by the use of silica nanoparticles*. Fuel, 2015. **143**: p. 21-27.
14. Hendraningrat, L., S. Li, and O. Torsæter, *A coreflood investigation of nanofluid enhanced oil recovery*. Journal of Petroleum Science and Engineering, 2013. **111**: p. 128-138.
15. Srivastava, A., et al., *Effects of silica nanoparticles and polymers on foam stability with sodium dodecylbenzene sulfonate in water–liquid paraffin oil emulsions at high temperatures*. Journal of Molecular Liquids, 2017. **241**: p. 1069-1078.
16. Maghzi, A., et al., *Monitoring wettability alteration by silica nanoparticles during water flooding to heavy oils in five-spot systems: A pore-level investigation*. Experimental Thermal and Fluid Science, 2012. **40**: p. 168-176.
17. Karimi, A., et al., *Wettability alteration in carbonates using zirconium oxide nanofluids: EOR implications*. Energy & Fuels, 2012. **26**(2): p. 1028-1036.
18. Giraldo, J., et al., *Wettability alteration of sandstone cores by alumina-based nanofluids*. Energy & Fuels, 2013. **27**(7): p. 3659-3665.

19. Gahrooei, H.R.E. and M.H. Ghazanfari, *Application of a water based nanofluid for wettability alteration of sandstone reservoir rocks to preferentially gas wetting condition.* Journal of Molecular Liquids, 2017. **232**: p. 351-360.

20. Austgen, D.M., et al., *Model of vapor-liquid equilibria for aqueous acid gas-alkanolamine systems using the electrolyte-NRTL equation.* Industrial & Engineering Chemistry Research, 1989. **28**(7): p. 1060-1073.

21. Fathi, S.J., T. Austad, and S. Strand, *Water-based enhanced oil recovery (EOR) by "smart water": Optimal ionic composition for EOR in carbonates.* Energy & fuels, 2011. **25**(11): p. 5173-5179.

22. Green, D.W. and G.P. Willhite, *Enhanced oil recovery.* Vol. 6. 1998: Henry L. Doherty Memorial Fund of AIME, Society of Petroleum Engineers Richardson, TX.

23. Khezrnejad, A., *Experimental investigation of nanoparticle enhanced oil recovery techniques using micromodels.* 2015, Memorial University of Newfoundland.

24. Esfandyari Bayat, A., et al., *Impact of metal oxide nanoparticles on enhanced oil recovery from limestone media at several temperatures.* Energy & Fuels, 2014. **28**(10): p. 6255-6266.

25. Onyekonwu, M.O. and N.A. Ogolo. *Investigating the use of nanoparticles in enhancing oil recovery.* in *Nigeria Annual international conference and exhibition.* 2010. Society of Petroleum Engineers.

26. Hendraningrat, L., S. Li, and O. Torsater. *A coreflood investigation of nanofluid enhanced oil recovery in low-medium permeability Berea sandstone.* in *SPE International Symposium on Oilfield Chemistry.* 2013. Society of Petroleum Engineers.

27. Nazari Moghaddam, R., et al., *Comparative study of using nanoparticles for enhanced oil recovery: wettability alteration of carbonate rocks.* Energy & Fuels, 2015. **29**(4): p. 2111-2119.

28. Ortega, D.J.S., et al. *The Effectiveness of Silicon Dioxide SiO 2 Nanoparticle as an Enhanced Oil Recovery Agent in Ben Nevis Formation, Hebron Field, Offshore Eastern Canada.* in *Abu Dhabi International Petroleum Exhibition & Conference.* 2016. Society of Petroleum Engineers.

29. Davies, R., et al., *Induced seismicity and hydraulic fracturing for the recovery of hydrocarbons.* Marine and Petroleum Geology, 2013. **45**: p. 171-185.

30. Rosen, M.J., et al., *Ultralow interfacial tension for enhanced oil recovery at very low surfactant concentrations.* Langmuir, 2005. **21**(9): p. 3749-3756.

31. Ahmadi, M.A. and S.R. Shadizadeh, *Adsorption of novel nonionic surfactant and particles mixture in carbonates: enhanced oil recovery implication.* Energy & Fuels, 2012. **26**(8): p. 4655-4663.

32. Al-Anssari, S., et al., *Effect of temperature and SiO 2 nanoparticle size on wettability alteration of oil-wet calcite.* Fuel, 2017. **206**: p. 34-42.

33. Molnes, S.N., et al., *Sandstone injectivity and salt stability of cellulose nanocrystals (CNC) dispersions—Premises for use of CNC in enhanced oil recovery.* Industrial Crops and Products, 2016. **93**: p. 152-160.

34. Hashemi, R., N.N. Nassar, and P. Pereira Almao, *Enhanced heavy oil recovery by in situ prepared ultradispersed multimetallic nanoparticles: A study of hot fluid flooding for Athabasca bitumen recovery.* Energy & Fuels, 2013. **27**(4): p. 2194-2201.

35. Li, S., L. Hendraningrat, and O. Torsaeter. *Improved oil recovery by hydrophilic silica nanoparticles suspension: 2 phase flow experimental studies*. in *IPTC 2013: International Petroleum Technology Conference*. 2013.

36. Tarboush, B.J.A. and M.M. Husein, *Adsorption of asphaltenes from heavy oil onto in situ prepared NiO nanoparticles*. Journal of colloid and interface science, 2012. **378**(1): p. 64-69.

37. Sun, X., et al., *Application of Nanoparticles in Enhanced Oil Recovery: A Critical Review of Recent Progress*. Energies, 2017. **10**(3): p. 345.

38. Somasundaran, P., et al., *Colloid systems and interfaces stability of dispersions through polymer and surfactant adsorption*. 2009: CRC Press, Boca Raton, FL.

39. Israelachvili, J.N., *Intermolecular and surface forces: revised third edition*. 2011: Academic press.

40. Sparreboom, W.v., A. Van Den Berg, and J. Eijkel, *Principles and applications of nanofluidic transport*. Nature nanotechnology, 2009. **4**(11): p. 713-720.

41. Saunders, S., et al., *Total interaction energy model to predict nanoparticle dispersability in CO2-expanded solvents*. Computer Aided Chemical Engineering, 2010. **28**: p. 1651-1656.

42. Metin, C.O., J.R. Baran, and Q.P. Nguyen, *Adsorption of surface functionalized silica nanoparticles onto mineral surfaces and decane/water interface*. Journal of Nanoparticle Research, 2012. **14**(11): p. 1246.

43. Dugyala, V.R., et al., *Role of electrostatic interactions in the adsorption kinetics of nanoparticles at fluid–fluid interfaces*. Physical Chemistry Chemical Physics, 2016. **18**(7): p. 5499-5508.

44. Hotze, E.M., T. Phenrat, and G.V. Lowry, *Nanoparticle aggregation: challenges to understanding transport and reactivity in the environment*. Journal of environmental quality, 2010. **39**(6): p. 1909-1924.

45. Eijkel, J.C. and A. Van Den Berg, *Nanofluidics: what is it and what can we expect from it?* Microfluidics and Nanofluidics, 2005. **1**(3): p. 249-267.

46. von Helmholtz, H., *Ueber einige Gesetze der Vertheilung elektrischer Ströme in körperlichen Leitern mit Anwendung auf die thierisch-elektrischen Versuche*. Ann. Phys. Chem, 1853. **89**: p. 211-233.

47. Gipson, K., et al., *The influence of synthesis parameters on particle size and photoluminescence characteristics of ligand capped Tb3+: LaF3*. Polymers, 2011. **3**(4): p. 2039-2052.

48. Gouy, G., *Constitution of the electric charge at the surface of an electrolyte*. J. phys, 1910. **9**(4): p. 457-467.

49. Napper, D.H., *Polymeric stabilization of colloidal dispersions*. Vol. 3. 1983: Academic Pr.

50. Zeng, Y., *Colloidal Dispersions Under Slit-pore Confinement*. 2012: Springer Science & Business Media.

51. Elimelech, M., J. Gregory, and X. Jia, *Particle deposition and aggregation: measurement, modelling and simulation*. 2013: Butterworth-Heinemann.

52. Lin, K.-W., et al., *Micro/Nano Lithography Sub-20nm node photomask cleaning enhanced by controlling zeta potential*.

53.   Hoek, E.M. and G.K. Agarwal, *Extended DLVO interactions between spherical particles and rough surfaces.* Journal of Colloid and Interface science, 2006. **298**(1): p. 50-58.

54.   Derjaguin, B. and L. Landau, *Theory of the stability of strongly charged lyophobic sols and of the adhesion of strongly charged particles in solutions of electrolytes.* Acta physicochim. URSS, 1941. **14**(6): p. 633-662.

55.   Verwey, E.J.W., J.T.G. Overbeek, and J.T.G. Overbeek, *Theory of the stability of lyophobic colloids.* 1999: Courier Corporation.

56.   Trefalt, G. and M. Borkovec, *Overview of DLVO theory.* Laboratory of Colloid and Surface Chemistry, University of Genebra, 2014.

57.   Behrens, S.H. and M. Borkovec, *Influence of the secondary interaction energy minimum on the early stages of colloidal aggregation.* Journal of colloid and interface science, 2000. **225**(2): p. 460-465.

58.   Sofla, S.J.D., L.A. James, and Y. Zhang, *Insight into the stability of hydrophilic silica nanoparticles in seawater for Enhanced oil recovery implications.* Fuel, 2018. **216**: p. 559-571.

59.   Metin, C.O., et al., *Stability of aqueous silica nanoparticle dispersions.* Journal of Nanoparticle Research, 2011. **13**(2): p. 839-850.

60.   Elimelech, M. and C.R. O'Melia, *Effect of particle size on collision efficiency in the deposition of Brownian particles with electrostatic energy barriers.* Langmuir, 1990. **6**(6): p. 1153-1163.

61.   Ortega-Vinuesa, J., A. Martın-Rodrıguez, and R. Hidalgo-Alvarez, *Colloidal stability of polymer colloids with different interfacial properties: mechanisms.* Journal of colloid and interface science, 1996. **184**(1): p. 259-267.

62.   Yotsumoto, H. and R.-H. Yoon, *Application of extended DLVO theory: I. Stability of rutile suspensions.* Journal of colloid and interface science, 1993. **157**(2): p. 426-433.

63.   Yotsumoto, H. and R.-H. Yoon, *Application of extended DLVO theory: II. Stability of silica suspensions.* Journal of Colloid and Interface Science, 1993. **157**(2): p. 434-441.

64.   Yoon, R.-H. and S. Ravishankar, *Application of extended DLVO theory: III. Effect of octanol on the long-range hydrophobic forces between dodecylamine-coated mica surfaces.* Journal of colloid and interface science, 1994. **166**(1): p. 215-224.

65.   Bizmark, N. and M.A. Ioannidis, *Effects of ionic strength on the colloidal stability and interfacial assembly of hydrophobic ethyl cellulose nanoparticles.* Langmuir, 2015. **31**(34): p. 9282-9289.

66.   Gilbert, T.R., R.V. Kirss, and N. Foster, *Chemistry: An Atoms-focused Approach.* 2013: WW Norton & Company.

67.   Somasundaran, P., et al., *Colloid systems and interfaces stability of dispersions through polymer and surfactant adsorption.* Handbook of surface and colloid chemistry, 2009. **1**.

68.   Swenson, J., M. Smalley, and H. Hatharasinghe, *Mechanism and strength of polymer bridging flocculation.* Physical review letters, 1998. **81**(26): p. 5840.

69.   Somasundaran, P., et al., *6 Colloid Systems and Interfaces Stability of Dispersions through Polymer and Surfactant Adsorption.* 2009.

70.   Besseling, N., *Theory of hydration forces between surfaces.* Langmuir, 1997. **13**(7): p. 2113-2122.

71. Ruths, M. and J.N. Israelachvili, *Surface forces and nanorheology of molecularly thin films*, in *Nanotribology and nanomechanics*. 2008, Springer. p. 417-515.

72. Kralchevsky, P.A., K.D. Danov, and E.S. Basheva, *Hydration force due to the reduced screening of the electrostatic repulsion in few-nanometer-thick films.* Current Opinion in Colloid & Interface Science, 2011. **16**(6): p. 517-524.

73. Brzozowska, A., et al., *On the stability of the polymer brushes formed by adsorption of ionomer complexes on hydrophilic and hydrophobic surfaces.* Journal of colloid and interface science, 2011. **353**(2): p. 380-391.

74. Kauzmann, W., *Some factors in the interpretation of protein denaturation.* Advances in protein chemistry, 1959. **14**: p. 1-63.

75. Rabinovich, Y.I. and B. Derjaguin, *Interaction of hydrophobized filaments in aqueous electrolyte solutions.* Colloids and Surfaces, 1988. **30**(3-4): p. 243-251.

76. Kronberg, B., K. Holmberg, and B. Lindman, *Surface chemistry of surfactants and polymers*. 2014: John Wiley & Sons.

77. Gray, M., et al. *Potential microbial enhanced oil recovery processes: a critical analysis*. in *SPE Annual Technical Conference and Exhibition*. 2008. Society of Petroleum Engineers.

78. Rabiei, A., et al., *Core flooding tests to investigate the effects of IFT reduction and wettability alteration on oil recovery during MEOR process in an Iranian oil reservoir.* Applied microbiology and biotechnology, 2013. **97**(13): p. 5979-5991.

79. Fulcher Jr, R.A., T. Ertekin, and C. Stahl, *Effect of capillary number and its constituents on two-phase relative permeability curves.* Journal of petroleum technology, 1985. **37**(02): p. 249-260.

80. Garnes, J., et al. *Capillary number relations for some North, Sea reservoir sandstones*. in *SPE/DOE Enhanced Oil Recovery Symposium*. 1990. Society of Petroleum Engineers.

81. Amaefule, J.O. and L.L. Handy, *The effect of interfacial tensions on relative oil/water permeabilities of consolidated porous media.* Society of Petroleum Engineers Journal, 1982. **22**(03): p. 371-381.

82. Guo, H., et al. *Review of capillary number in chemical enhanced oil recovery*. in *SPE Kuwait Oil and Gas Show and Conference*. 2015. Society of Petroleum Engineers.

83. Larry, W., *Lake. Enhanced oil recovery.* Prentice Hall, Englewood Cliffs, New Jersey, 1989. **7632**: p. 195-197.

84. Asar, H. and L.L. Handy, *Influence of interfacial tension on gas/oil relative permeability in a gas-condensate system.* SPE Reservoir Engineering, 1988. **3**(01): p. 257-264.

85. Shen, P., et al. *The Influence of Interfacial Tension on Water-Oil Two-Phase Relative Permeability*. in *SPE/DOE Symposium on Improved Oil Recovery*. 2006. Society of Petroleum Engineers.

86. Leverett, M.C., *Flow of oil-water mixtures through unconsolidated sands.* Transactions of the AIME, 1939. **132**(01): p. 149-171.

87. Wang, F., *Effect of wettability alteration on water/oil relative permeability, dispersion, and flowable saturation in porous media.* SPE reservoir engineering, 1988. **3**(02): p. 617-628.

88. Negin, C., S. Ali, and Q. Xie, *Most common surfactants employed in chemical enhanced oil recovery.* Petroleum, 2017. **3**(2): p. 197-211.

89. Rosen, M.J. and J.T. Kunjappu, *Reduction of surface and interfacial tension by surfactants.* Surfactants and Interfacial Phenomena, Fourth Edition, 2012: p. 235-271.

90. Roustaei, A., S. Saffarzadeh, and M. Mohammadi, *An evaluation of modified silica nanoparticles' efficiency in enhancing oil recovery of light and intermediate oil reservoirs.* Egyptian Journal of Petroleum, 2013. **22**(3): p. 427-433.

91. Joonaki, E. and S. Ghanaatian, *The application of nanofluids for enhanced oil recovery: effects on interfacial tension and coreflooding process.* Petroleum Science and Technology, 2014. **32**(21): p. 2599-2607.

92. Andreassen, L., *Nanoparticle effect on Interfacial Properties related to Enhanced Oil Recovery.* 2015, NTNU.

93. Ravera, F., et al., *Liquid–liquid interfacial properties of mixed nanoparticle–surfactant systems.* Colloids and Surfaces A: Physicochemical and Engineering Aspects, 2008. **323**(1): p. 99-108.

94. Ravera, F., et al., *Effect of nanoparticles on the interfacial properties of liquid/liquid and liquid/air surface layers.* The Journal of Physical Chemistry B, 2006. **110**(39): p. 19543-19551.

95. Metin, C.O. and Q.P. Nguyen, *The Retention of Silica Nanoparticles at Oil/Water Interface.*

96. Zargartalebi, M., N. Barati, and R. Kharrat, *Influences of hydrophilic and hydrophobic silica nanoparticles on anionic surfactant properties: Interfacial and adsorption behaviors.* Journal of Petroleum Science and Engineering, 2014. **119**: p. 36-43.

97. Ferdous, S., M.A. Ioannidis, and D.E. Henneke, *Effects of temperature, pH, and ionic strength on the adsorption of nanoparticles at liquid–liquid interfaces.* Journal of Nanoparticle Research, 2012. **14**(5): p. 850.

98. Lan, Q., et al., *Synergistic effect of silica nanoparticle and cetyltrimethyl ammonium bromide on the stabilization of O/W emulsions.* Colloids and Surfaces A: Physicochemical and Engineering Aspects, 2007. **302**(1): p. 126-135.

99. Salem Ragab, A.M. and A.E. Hannora. *A Comparative Investigation of Nano Particle Effects for Improved Oil Recovery–Experimental Work.* in *SPE Kuwait Oil and Gas Show and Conference.* 2015. Society of Petroleum Engineers.

100. Hendraningrat, L. and O. Torsæter, *Effects of the initial rock wettability on silica-based nanofluid-enhanced oil recovery processes at reservoir temperatures.* Energy & Fuels, 2014. **28**(10): p. 6228-6241.

101. Golshokooh, S., S. Ramazani, and M. Hekmatzadeh, *Investigating the effect of hybrid silica nanoparticles-copolymer on increasing oil recovery in a three dimensional porous media.* Scientia Iranica, 2017. **24**(6): p. 3466-3475.

102. Roustaei, A. and H. Bagherzadeh, *Experimental investigation of SiO 2 nanoparticles on enhanced oil recovery of carbonate reservoirs.* Journal of Petroleum Exploration and Production Technology, 2015. **5**(1): p. 27-33.

103. Moslan, M.S., et al. *Wettability Alteration of Dolomite Rock Using Nanofluids for Enhanced Oil Recovery.* in *Materials Science Forum.* 2016. Trans Tech Publ.

104. Saeed Jafari Daghlian Sofla, L.A.J., and Yahui Zhang, *nderstanding the behavior of H+-protected silica nanoparticles at oil-water interface for Enhanced Oil Recovery Implications.* Journal of Molecular Liquids, 2018.

105. Arab, D., A. Kantzas, and S.L. Bryant, *Nanoparticle stabilized oil in water emulsions: A critical review.* Journal of Petroleum Science and Engineering, 2018.

106. Lan, Q., et al., *Synergistic effect of silica nanoparticle and cetyltrimethyl ammonium bromide on the stabilization of O/W emulsions.* Colloids and Surfaces A: Physicochemical and Engineering Aspects, 2007. **302**(1-3): p. 126-135.

107. Moeini, F., et al., *Toward mechanistic understanding of heavy crude oil/brine interfacial tension: The roles of salinity, temperature and pressure.* Fluid phase equilibria, 2014. **375**: p. 191-200.

108. Lashkarbolooki, M., S. Ayatollahi, and M. Riazi, *The impacts of aqueous ions on interfacial tension and wettability of an asphaltenic–acidic crude oil reservoir during smart water injection.* Journal of Chemical & Engineering Data, 2014. **59**(11): p. 3624-3634.

109. Mittal, K.L., *Contact angle, wettability and adhesion.* Vol. 4. 2006: CRC Press.

110. Hirasaki, G., *Wettability: fundamentals and surface forces.* SPE Formation Evaluation, 1991. **6**(02): p. 217-226.

111. Anderson, W., *Literature survey. Part 2: wettability measurement.* J. Pet. Technol, 1986. **38**: p. 1246-1262.

112. Amott, E., *Observations relating to the wettability of porous rock.* 1959.

113. Donaldson, E.C., R.D. Thomas, and P.B. Lorenz, *Wettability determination and its effect on recovery efficiency.* Society of Petroleum Engineers Journal, 1969. **9**(01): p. 13-20.

114. Birkeland, M.Å., *Investigation of Nanoparticle Effect on Wettability and Interfacial tension: An Experimental Study of a Two-Phase System of Heavy Oil and Di Water.* 2013, Institutt for petroleumsteknologi og anvendt geofysikk.

115. Li, S., et al. *Effect of silica nanoparticles adsorption on the wettability index of Berea sandstone.* in *Paper SCA2013-059 presented at the international symposium of the society of core analysts held in Napa Valley, California, USA.* 2013.

116. Al-Anssari, S., et al., *Wettability alteration of oil-wet carbonate by silica nanofluid.* Journal of colloid and interface science, 2016. **461**: p. 435-442.

117. Ehtesabi, H., et al., *Enhanced heavy oil recovery in sandstone cores using TiO2 nanofluids.* Energy & Fuels, 2013. **28**(1): p. 423-430.

118. De Gennes, P.-G., *Wetting: statics and dynamics.* Reviews of modern physics, 1985. **57**(3): p. 827.

119. Wasan, D.T. and A.D. Nikolov, *Spreading of nanofluids on solids.* Nature, 2003. **423**(6936): p. 156.

120. Kondiparty, K., et al., *Dynamic spreading of nanofluids on solids. Part I: experimental.* Langmuir, 2012. **28**(41): p. 14618-14623.

121. Sefiane, K., J. Skilling, and J. MacGillivray, *Contact line motion and dynamic wetting of nanofluid solutions.* Advances in colloid and interface science, 2008. **138**(2): p. 101-120.

122. Kondiparty, K., et al., *Wetting and spreading of nanofluids on solid surfaces driven by the structural disjoining pressure: statics analysis and experiments.* Langmuir, 2011. **27**(7): p. 3324-3335.

123. Wang, F.-C. and H.-A. Wu, *Enhanced oil droplet detachment from solid surfaces in charged nanoparticle suspensions.* Soft Matter, 2013. **9**(33): p. 7974-7980.

124. Lim, S., et al., *The dynamic spreading of nanofluids on solid surfaces–Role of the nanofilm structural disjoining pressure.* Journal of colloid and interface science, 2016. **470**: p. 22-30.

125.   Fan, H. and A. Striolo, *Nanoparticle effects on the water-oil interfacial tension.* Physical Review E, 2012. **86**(5): p. 051610.

126.   Somasundaran, P., *Encyclopedia of surface and colloid science.* Vol. 2. 2006: CRC press.

127.   Zhang, H., A. Nikolov, and D. Wasan, *Enhanced oil recovery (EOR) using nanoparticle dispersions: Underlying mechanism and imbibition experiments.* Energy & Fuels, 2014. **28**(5): p. 3002-3009.

128.   Taborda, E.A., et al., *Effect of nanoparticles/nanofluids on the rheology of heavy crude oil and its mobility on porous media at reservoir conditions.* Fuel, 2016. **184**: p. 222-232.

129.   Ma, X., et al., *Preparation and characterization of silica/polyamide-imide nanocomposite thin films.* Nanoscale research letters, 2010. **5**(11): p. 1846-1851.

130.   Torsater, O., S. Li, and L. Hendraningrat. *A coreflood investigation of nanofluid enhanced oil recovery in low-medium permeability Berea sandstone.* in *SPE International Symposium on Oilfield Chemistry.* 2013. Society of Petroleum Engineers.

131.   Mohajeri, M., M. Hemmati, and A.S. Shekarabi, *An experimental study on using a nanosurfactant in an EOR process of heavy oil in a fractured micromodel.* Journal of Petroleum Science and Engineering, 2015. **126**: p. 162-173.

132.   Guo, F. and S. Aryana, *An experimental investigation of nanoparticle-stabilized CO 2 foam used in enhanced oil recovery.* Fuel, 2016. **186**: p. 430-442.

133.   Maghzi, A., et al., *The impact of silica nanoparticles on the performance of polymer solution in presence of salts in polymer flooding for heavy oil recovery.* Fuel, 2014. **123**: p. 123-132.

134.   Vasiliev, P.O., et al., *Colloidal aspects relating to direct incorporation of TiO 2 nanoparticles into mesoporous spheres by an aerosol-assisted process.* Journal of colloid and interface science, 2008. **319**(1): p. 144-151.

135.   Smith, A.M., A.A. Lee, and S. Perkin, *The electrostatic screening length in concentrated electrolytes increases with concentration.* The journal of physical chemistry letters, 2016. **7**(12): p. 2157-2163.

136.   Bukar, N., et al., *Influence of the Debye length on the interaction of a small molecule-modified Au nanoparticle with a surface-bound bioreceptor.* Chemical Communications, 2014. **50**(38): p. 4947-4950.

137.   French, R.A., et al., *Influence of ionic strength, pH, and cation valence on aggregation kinetics of titanium dioxide nanoparticles.* Environmental science & technology, 2009. **43**(5): p. 1354-1359.

138.   Hiemenz, P. and R. Rajagopalan, *Electrophoresis and other electrokinetic phenomena.* 1977, Marcel Dekker Inc., New York. p. 452-487.

139.   Birdi, K., *Handbook of surface and colloid chemistry.* 2015: CRC Press.

140.   Hunter, R.J., *Zeta potential in colloid science: principles and applications.* Vol. 2. 2013: Academic press.

141.   Barisik, M., et al., *Size dependent surface charge properties of silica nanoparticles.* The Journal of Physical Chemistry C, 2014. **118**(4): p. 1836-1842.

142.   Butt, H.-J., K. Graf, and M. Kappl, *Physics and chemistry of interfaces.* 2006: John Wiley & Sons.

143. Mandel, K., et al., *Surfactant free superparamagnetic iron oxide nanoparticles for stable ferrofluids in physiological solutions.* Chemical Communications, 2015. **51**(14): p. 2863-2866.

144. Choi, H.-H., J. Park, and R. Singh, *Nanosized CuO encapsulated silica particles using an electrochemical deposition coating.* Electrochemical and solid-state letters, 2004. **7**(1): p. C10-C12.

145. Ueno, K., et al., *Colloidal stability of bare and polymer-grafted silica nanoparticles in ionic liquids.* Langmuir, 2008. **24**(10): p. 5253-5259.

146. Molina-Bolivar, J. and J. Ortega-Vinuesa, *How proteins stabilize colloidal particles by means of hydration forces.* Langmuir, 1999. **15**(8): p. 2644-2653.

147. Szilagyi, I., A. Sadeghpour, and M. Borkovec, *Destabilization of colloidal suspensions by multivalent ions and polyelectrolytes: From screening to overcharging.* Langmuir, 2012. **28**(15): p. 6211-6215.

148. Bizmark, N., M.A. Ioannidis, and D.E. Henneke, *Irreversible adsorption-driven assembly of nanoparticles at fluid interfaces revealed by a dynamic surface tension probe.* Langmuir, 2014. **30**(3): p. 710-717.

149. Grasso, D., et al., *A review of non-DLVO interactions in environmental colloidal systems.* Reviews in Environmental Science and Biotechnology, 2002. **1**(1): p. 17-38.

150. Liu, H.H., et al., *Effect of hydration repulsion on nanoparticle agglomeration evaluated via a constant number Monte–Carlo simulation.* Nanotechnology, 2015. **26**(4): p. 045708.

151. Donaldson, E.C. and W. Alam, *Wettability*. 2013: Elsevier.

152. de Lara, L.S., V.A. Rigo, and C.R. Miranda, *The stability and interfacial properties of functionalized silica nanoparticles dispersed in brine studied by molecular dynamics.* Eur. Phys. J. B, 2015. **88**: p. 261.

153. Bagaria, H.G., et al., *Stabilization of iron oxide nanoparticles in high sodium and calcium brine at high temperatures with adsorbed sulfonated copolymers.* Langmuir, 2013. **29**(10): p. 3195-3206.

154. Nap, R.J., S.H. Park, and I. Szleifer, *On the stability of nanoparticles coated with polyelectrolytes in high salinity solutions.* Journal of Polymer Science Part B: Polymer Physics, 2014. **52**(24): p. 1689-1699.

155. Olajire, A.A., *Review of ASP EOR (alkaline surfactant polymer enhanced oil recovery) technology in the petroleum industry: Prospects and challenges.* Energy, 2014. **77**: p. 963-982.

156. Wang, D., et al., *Bridging interactions and selective nanoparticle aggregation mediated by monovalent cations.* ACS nano, 2010. **5**(1): p. 530-536.

157. Nelson, P.H., *Pore-throat sizes in sandstones, tight sandstones, and shales.* AAPG bulletin, 2009. **93**(3): p. 329-340.

158. Lindquist, W.B., et al., *Pore and throat size distributions measured from synchrotron X‐ray tomographic images of Fontainebleau sandstones.* Journal of Geophysical Research: Solid Earth, 2000. **105**(B9): p. 21509-21527.

159. Dominguez, G., *Carbonate reservoir characterization: a geologic-engineering analysis*. Vol. 30. 1992: Elsevier.

160. Ausbrooks, R., et al. *Pore-size distributions in vuggy carbonates from core images, NMR, and capillary pressure*. in *SPE annual technical conference and exhibition*. 1999. Society of Petroleum Engineers.

161. Peng, B., et al., *A review of nanomaterials for nanofluid enhanced oil recovery.* RSC Advances, 2017. **7**(51): p. 32246-32254.

162. Keller, A.A., et al., *Stability and aggregation of metal oxide nanoparticles in natural aqueous matrices.* Environ. Sci. Technol, 2010. **44**(6): p. 1962-1967.

163. Tombácz, E. and M. Szekeres, *Surface charge heterogeneity of kaolinite in aqueous suspension in comparison with montmorillonite.* Applied Clay Science, 2006. **34**(1): p. 105-124.

164. Korpany, K.V., et al., *Iron Oxide Surface Chemistry: Effect of Chemical Structure on Binding in Benzoic Acid and Catechol Derivatives.* Langmuir, 2017. **33**(12): p. 3000-3013.

165. Bai, M., et al., *Studies of injection parameters for chemical flooding in carbonate reservoirs.* Renewable and Sustainable Energy Reviews, 2017. **75**: p. 1464-1471.

166. Rezvani, H., et al., *How ZrO 2 nanoparticles improve the oil recovery by affecting the interfacial phenomena in the reservoir conditions?* Journal of Molecular Liquids, 2017.

167. Saien, J. and V. Fadaei, *The study of interfacial tension of kerosene-water under influence of CTAB surfactant and different size silica nanoparticles.* Journal of Molecular Liquids, 2018. **255**: p. 439-446.

168. Rezaei, A., et al., *Using surface modified clay nanoparticles to improve rheological behavior of Hydrolized Polyacrylamid (HPAM) solution for enhanced oil recovery with polymer flooding.* Journal of Molecular Liquids, 2016. **222**: p. 1148-1156.

169. Saien, J. and M. Bahrami, *Understanding the effect of different size silica nanoparticles and SDS surfactant mixtures on interfacial tension of n-hexane–water.* Journal of Molecular Liquids, 2016. **224**: p. 158-164.

170. Liz-Marzán, L.M. and I. Lado-Touriño, *Reduction and stabilization of silver nanoparticles in ethanol by nonionic surfactants.* Langmuir, 1996. **12**(15): p. 3585-3589.

171. Napper, D., *Polymeric stabilization of colloidal dispersions.* Department of Physical Chemistry, University of Sydney, Australia, 1988.

172. Rogalska, E., et al., *Formation and properties of Langmuir and Gibbs monolayers: a comparative study using hydrogenated and partially fluorinated amphiphilic derivatives of mannitol.* Chemistry and physics of lipids, 2000. **105**(1): p. 71-91.

173. Garbin, V., J.C. Crocker, and K.J. Stebe, *Nanoparticles at fluid interfaces: Exploiting capping ligands to control adsorption, stability and dynamics.* Journal of colloid and interface science, 2012. **387**(1): p. 1-11.

174. Nelson, A., et al., *A multiscale approach to the adsorption of core–shell nanoparticles at fluid interfaces.* Soft matter, 2015. **11**(1): p. 118-129.

175. Lyklema, J., *Fundamentals of interface and colloid science.* Kolloidnyi Zhurnal, 1994. **56**(2): p. 303-398.

176. Binks, B.P. and S. Lumsdon, *Influence of particle wettability on the type and stability of surfactant-free emulsions.* Langmuir, 2000. **16**(23): p. 8622-8631.

177. Poulichet, V. and V. Garbin, *Ultrafast desorption of colloidal particles from fluid interfaces.* Proceedings of the National Academy of Sciences, 2015. **112**(19): p. 5932-5937.

178. Stocco, A., et al., *Aqueous foams stabilized solely by particles.* Soft Matter, 2011. **7**(4): p. 1260-1267.

179. Paunov, V.N., *Novel method for determining the three-phase contact angle of colloid particles adsorbed at air− water and oil− water interfaces.* Langmuir, 2003. **19**(19): p. 7970-7976.

180. Du, K., et al., *Adsorption energy of nano-and microparticles at liquid− liquid interfaces.* Langmuir, 2010. **26**(15): p. 12518-12522.

181. Schwenke, K., L. Isa, and E. Del Gado, *Assembly of nanoparticles at liquid interfaces: crowding and ordering.* Langmuir, 2014. **30**(11): p. 3069-3074.

182. Danov, K., et al., *Particle− Interface Interaction across a Nonpolar Medium in Relation to the Production of Particle-Stabilized Emulsions.* Langmuir, 2006. **22**(1): p. 106-115.

183. Bizmark, N. and M. Ioannidis, *Ethyl cellulose nanoparticles at the alkane-water interface and the making of Pickering emulsions.* Langmuir, 2017.

184. Retsch, M., et al., *Fabrication of Large‐Area, Transferable Colloidal Monolayers Utilizing Self‐Assembly at the Air/Water Interface.* Macromolecular Chemistry and Physics, 2009. **210**(3‐4): p. 230-241.

185. Han, Y., et al., *Dynamics of ethyl cellulose nanoparticle self-assembly at the interface of a nematic liquid crystal droplet.* Physical Chemistry Chemical Physics, 2017. **19**(36): p. 24955-24960.

186. Reincke, F., et al., *Understanding the self-assembly of charged nanoparticles at the water/oil interface.* Physical Chemistry Chemical Physics, 2006. **8**(33): p. 3828-3835.

187. Marinova, K., et al., *Charging of oil− water interfaces due to spontaneous adsorption of hydroxyl ions.* Langmuir, 1996. **12**(8): p. 2045-2051.

188. Leverett, M., *Capillary behavior in porous solids.* Transactions of the AIME, 1941. **142**(01): p. 152-169.

189. Cao, J., L.A. James, and T.E. Johansen. *Determination of two phase relative permeability from core floods with constant pressure boundaries*. in *Society of Core Analysis Symposium, Avignon, France*. 2014.

190. Kim, H., et al. *Experimental Investigation of EOR by Injecting SiO2 Nanoparticles as Water Additive with Application to the Hebron Field*. in *IOR 2017-19th European Symposium on Improved Oil Recovery*. 2017.

191. Saeed Jafari Daghlian Sofla, L.A.J., Yahui Zhang, *TOWARD A MECHANISTIC UNDERSTANDING OF WETTABILITY ALTERATION IN RESERVOIR ROCKS USING SILICA NANOPARTICLES.* International Symposium of the Society of Core Analysts 2018.

192. Tao, T. and A. Watson, *Accuracy of JBN estimates of relative permeability: part 1-error analysis.* Society of Petroleum Engineers Journal, 1984. **24**(02): p. 209-214.

193. Sheng, J., *Critical review of low-salinity waterflooding.* Journal of Petroleum Science and Engineering, 2014. **120**: p. 216-224.

194. Sofla, S.J.D., M. Sharifi, and A.H. Sarapardeh, *Toward mechanistic understanding of natural surfactant flooding in enhanced oil recovery processes: the role of salinity, surfactant concentration and rock type.* Journal of Molecular Liquids, 2016. **222**: p. 632-639.

195. Khezrnejad, A., L. James, and T. Johansen. *Water enhancement using nanoparticles in water alternating gas (WAG) micromodel experiments*. in *SPE Annual Technical Conference and Exhibition*. 2014. Society of Petroleum Engineers.

196.   Rowe, A., et al., *Oil detachment from solid surfaces in aqueous surfactant solutions as a function of pH.* Industrial & engineering chemistry research, 2002. **41**(7): p. 1787-1795.

197.   Kao, R., et al., *Mechanisms of oil removal from a solid surface in the presence of anionic micellar solutions.* Colloids and Surfaces, 1988. **34**(4): p. 389-398.

198.   Chengara, A., et al., *Spreading of nanofluids driven by the structural disjoining pressure gradient.* Journal of colloid and interface science, 2004. **280**(1): p. 192-201.

199.   Miller, C.A. and K.H. Raney, *Solubilization—emulsification mechanisms of detergency.* Colloids and Surfaces A: Physicochemical and Engineering Aspects, 1993. **74**(2-3): p. 169-215.

200.   Dai, C., et al., *Spontaneous Imbibition Investigation of Self-Dispersing Silica Nanofluids for Enhanced Oil Recovery in Low-Permeability Cores.* Energy & Fuels, 2017. **31**(3): p. 2663-2668.

201.   Ahmadi, M.A. and S.R. Shadizadeh, *Induced effect of adding nano silica on adsorption of a natural surfactant onto sandstone rock: experimental and theoretical study.* Journal of Petroleum Science and Engineering, 2013. **112**: p. 239-247.

202.   Dehghan Monfared, A., et al., *Potential Application of Silica Nanoparticles for Wettability Alteration of Oil–Wet Calcite: A Mechanistic Study.* Energy & Fuels, 2016. **30**(5): p. 3947-3961.

203.   Al-Anssari, S., et al., *Wettability alteration of oil-wet carbonate by silica nanofluid.* Journal of colloid and interface science, 2016. **461**: p. 435-442.

204.   Lim, S., et al., *Nanofluids alter the surface wettability of solids.* Langmuir, 2015. **31**(21): p. 5827-5835.

205.   Sripal, E. and L. James, *Application of an Optimization Method for the Restoration of Core Samples for SCAL Experiments.* Petrophysics, 2018. **59**(01): p. 72-81.

206.   Saeed Jafari Daghlian Sofla, L.A.J., Yahui Zhang, *Understanding the behavior of H+ protected silica nanoparticles at oil-water interface for Enhanced Oil Recovery Implications*   Journal of Molecular Liquids 2018.

Appendix

NOMENCLATURES

Variables/Parameters	Description
λ_i	Effective permeability of ith phase
μ	Viscosity
M	Mobility ratio
E_{vdw}	Van der Waals forces
A	Hamaker constant
K	Debye Length
$\rho\infty_i$	Number density of ith ion in the solution
T	Temperature
ε_r	Relative permittivity of the solution
e	Elementary charge of an electron
$\varepsilon_\circ$	Absolute permittivity
K_B	Boltzmann's constant
ψ_0	Surface charge of particles
γ	Reduced surface potential
ψ_s	Surface potential
E_{EL}	Electrostatic repulsion forces
E_h	Hydrophobic forces
N_c	Capillary number
v	Darcy velocity
θ	Contact angle between the oil-water-rock interface
P_C	Capillary pressure
N_A	Avogadro's number
C_0	Molar bulk concentration
K_1	Dimensionless adsorption parameter
K_a	Adsorption constant
$\emptyset_\infty$	Fractional coverage of the interface at steady state condition
ΔE	Adsorption energy